A GTO-based Scheme for Small Power Tapping from HVDC Transmission Systems

By:

Mohammad R. Agha Ebrahimi

A Thesis

Submitted to the Faculty of Graduate Studies

in Partial Fulfillment of the requirements

for the Degree of

Doctor of Philosophy

Department of Electrical and Computer Engineering

The University of Manitoba

Winnipeg, Manitoba, Canada.

THE UNIVERSITY OF MANITOBA

FACULTY OF GRADUATE STUDIES

*****

COPYRIGHT PERMISSION PAGE

A GTO-BASED SCHEME FOR SMALL POWER TAPPING FROM HVDC TRANSMISSION SYSTEMS

BY

MOHAMMAD R. AGHA EBRAHIMI

A Thesis/Practicum submitted to the Faculty of Graduate Studies of The University of Manitoba in partial fulfillment of the requirements of the degree of

DOCTOR OF PHILOSOPHY

بسم‌ا..الرحمن الرحیم

تقدیم به میهن عزیزم ایران.

آنجا که نخلهای سرافراز و معطرش ایستاده مرده‌اند ، باشد که ما زندگان به ذلت درنغلتیم!

و به یاد شهید سید محمود فیاض و هزاران عاشق بیقراری که حیات کوتاه اما پربارشان یادآور آن بود که:

"هر شب ستاره‌ای به زمین می‌کشند و باز

این آسمان غمزده غرق ستاره است".

To my beloved motherland, Iran. And to her fallen defenders.

Acknowledgment

The author would like to express deep gratitude and appreciation to his thesis advisor, Dr. R. W. Menzies, for suggesting the thesis topic, and for his continuous guidance, encouragement, and support throughout the course of this project. Indeed, the author is extremely satisfied that what he has learned from Dr. Menzies is not limited to a number of formulas and techniques, but also shows him how to be a better human being and a caring friend.

Thanks are also due to the members of the author's Advisory Committee, Drs. A. Gole, M. Rashwan, and S. Balakrishnan, for their useful suggestions and comments through the regular annual meetings. Also, the author would like to thank Dr. M. R. Iravani of the University of Toronto for accepting to be the author's External Examiner.

The author's graduate studies at the University of Manitoba have been made possible by the support of the Iranian Ministry of Culture and Higher Education (MCHE), through a 2-year scholarship for his Master's program, and a 4-year scholarship for his Ph.D. program. For this, the author is greatly indebted to the MCHE.

This project was also financially supported by Manitoba HVDC Research Centre. Their invaluable support is greatly appreciated.

Last, but not least, the author must express his endless thanks to his loving wife, Farideh, who while being a very busy graduate student herself and a caring mother, never failed to be a committed and supporting wife too. Indeed, it was her sacrifice and hard work at home which enabled the author to achieve his goals at the school.

Abstract

Ever since the High Voltage Direct Current (HVDC) Transmission Systems were developed and utilized in power systems, power tapping from these transmission systems, be it for supplying isolated communities and/or loads in the vicinity of the transmission system, or to pick up dispersed generation, has presented formidable technical, as well as economical challenges to power system designers. As the size of the intermediate load, or local generation, has decreased, the severity of these challenges has increased. During the years different methods to achieve tapping have been proposed and studied. To this date, however, no practical small tapping station has been commissioned in any HVDC transmission system.

The current study, deals with this problem by paying special attention to the new semi-conductor technologies available on the market, which have made the production of powerful thyristors with turn off capability, i.e. Gate Turn Off Thyristors, or GTO thyristors, possible.

A tapping scheme, using GTO thyristor switches, is proposed, and using the PSCAD/ EMTDC digital simulation software package, the operation of the proposed scheme is studied.

Simulation results prove the practicality of the proposed scheme and the quality of the power being tapped into a small local load is within the acceptable limits. The performance of the control systems, have been studied and found to be satisfactory. Also, the use of a customized air-core transformer, with a diameter of 5 m, to feed loads of up to 600 kW is shown to be possible.

The tapping station is found to be unable to impose any significant negative effect on the performance of the main HVDC system.

Table of Contents

Chapter One
Introduction to HVDC Transmission Systems

In this chapter, a brief review of HVDC Transmission Systems, including the historical review and the principles of operation, is presented.

1.1. HVDC versus HVAC: A Historical Review

In the last few decades of the nineteenth century, when the commercial use of electric energy began, the first commercial generators were of the direct current (DC) type, and thus, the early distribution systems were DC, as well. Because of the low levels of voltage used in the distribution systems, transmission distances were necessarily short. The potential benefits of electric energy were powerful motivations behind a variety of works undertaken in Europe and America to improve the existing transmission systems.

In 1883, the 10-years long work done by Nicola Tesla bore fruit, and he was granted patents for the invention of polyphase alternating current (AC) systems. Elimination of commutators

made generators simpler, and the use of transformers allowed voltages to be changed easily. Consequently, the use of higher voltages became practical, and this made transmission over long distances feasible. The subsequent exploitation of hydroelectric potentials far away from the main load centers, resulted in more expansion in AC transmission systems.

Regardless of the fast growth in the utilization of the AC systems, electrical engineers continued to look for effective ways to use DC transmission at high voltages. They had realized that the cost of overhead lines and cables for high voltage direct current (HVDC) could be considerably lower than AC at the same power. The only obstacle to be overcome, was to develop adequate converters, suitable for very large transmission systems. This obstacle was finally removed by successful use of large mercury arc valves in the early years of the HVDC era, and later, by the use of thyristor valves, capable of carrying large amounts of currents, and withstanding high voltages.

The first commercial HVDC scheme was a submarine cable link, connecting two AC systems of the Swedish mainland, and the island of Gotland. The scheme was rated for 20 MW at 100 kV, and was commissioned in 1953. Since then, more than 80 HVDC schemes, totalling nearly 58,230 MW of capacity, have been installed and commissioned around the world. Currently, at least 26 other HVDC schemes with a total capacity of around 27,440 MW are being designed, or are under construction in different corners of the globe. Among the schemes in operation, the largest long-distance overhead-line HVDC transmission system is the 6300 MW Itaipu scheme in Brazil, consisting of two biploes each rated at +/- 600 kV, and with a length of around 800 km. The largest HVDC submarine cable scheme is the 2000 MW link between France and England [1],[2].

1.2. HVDC Transmission Systems: Principles of Operation

Fig. 1.1 shows a typical HVDC transmission system, connecting two AC systems A and B together. The system has two poles, one positive and one negative, and thus, is called a biploe.

Specific details of the scheme, such as DC line resistance, AC and DC filters, smoothing reactors, compensating capacitors, etc., are omitted for the sake of brevity. Also, it is assumed that the system uses six-pulse configuration, while most modern HVDC schemes use twelve-pulse configuration instead.

An HVDC system, principally, converts the AC power to DC power by the rectifier operation, transmits it to the inverter location, and converts it back to AC power, where it can be used by regular power system customers. The DC voltage at the rectifier, V_{Rec}, is maintained at the desired level by means of controlling the value of the firing angle, based on the following relationship:

$$V_{Rec} = \frac{3\sqrt{2}}{\pi} \times V_{L-L} \cos\alpha_1 - \frac{3}{\pi} \times X_c I_{dc}, \qquad (1.1)$$

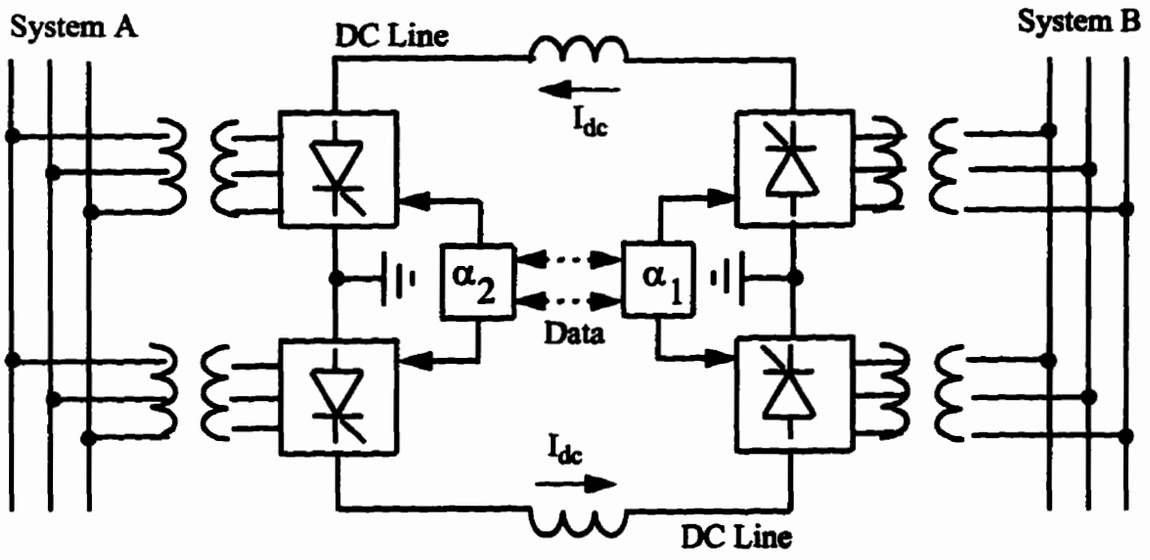

Fig. 1.1 - A Bipole HVDC Transmission System

where V_{L-L} is the AC side voltage, X_c is the commutating reactance, α_1 is the firing angle issued to the rectifier by the control system, and finally, I_{dc} is the DC current in the transmission line. The second part of equation (1.1) accounts for the voltage drop on the DC side, resulting from the overlap phenomenon in the rectifier.

Similarly, the DC voltage at the inverter can be maintained at the desired level by controlling the firing angle issued to the inverter, i.e. α_2. The relationship between the DC voltage at the rectifier and the voltage at the inverter is based on the following simple equation:

$$V_{Rec} = V_{Inv} + R_{dc} \times I_{dc}, \tag{1.2}$$

where R_{dc} is the line's DC resistance.

The DC power at the rectifier site is equal to:

$$P_{Rec} = V_{Rec} \times I_{dc}, \tag{1.3}$$

which is equal to the power being fed into the AC system by the inverter, plus ohmic losses in the transmission line (converter losses are being neglected), or:

$$P_{Rec} = P_{Inv} + R_{dc} \times I_{dc}^{2}. \tag{1.4}$$

It is evident that by selecting proper values for the firing angles issued to the converters, the polarity of the DC voltage, the voltage magnitude, and thus the current magnitude can be chosen at will. This means that the flow of the DC power in the transmission line, both in terms of direction and magnitude, is easily controllable by simple control actions. This fact makes the HVDC systems one of the most advantageous means of controlling the exchange of power between two AC systems.

Detailed discussions regarding the operation and design of HVDC systems can be found in the literature, for example in [1] and [3].

1.3. HVDC or HVAC: The Choice

In order to be able to make a proper choice between an HVDC system and a similar HVAC system, both the advantages and disadvantages of the HVDC system must be considered. The choice, then, will be clear, once one outweighs the other.

1.3.1. Advantages

The advantages of an HVDC transmission system over an AC system transmitting the same amount of power, briefly, can be summarized as follows [3]:

- Greater power transmission capacity per conductor, which means less costs for lines, cables, and right of way,

- Simpler line and tower construction,

- Ground return can be used, so each conductor can be operated as an independent circuit during emergencies or line repairs, etc.,

- There is no charging current, or skin effect,

- Line power factor is always unity, so there is no need for reactive compensation,

- Synchronous operation is not required, therefore the transmission distance is not limited by stability factors,

- The two AC frequencies can be different,

- The short circuit current on the DC line is low, and does not contribute to the fault current on the AC side; and,

- The power in the tie-line, both in magnitude and direction, can be easily controlled.

1.3.2. Disadvantages

The above advantages are gained at the expense of the following disadvantages [3]:

- AC/DC/AC converters are expensive,

- Converters require additional capacitors/synchronous condensers to provide large amounts of reactive power,

- Converters generate harmonics, therefore they require both AC and DC filters,

- Converters have little overload capability; and,

- The fact that there is no HVDC circuit breaker at present, is an obstacle in the way of multi-terminal operation, tapping, or network operation.

1.3.3. Selection Criteria

A comparison between the above advantages and disadvantages clearly shows that an HVDC system can be chosen over a similar AC system, if and when:

- The length of the system is long enough, so that the savings made in the costs of lines, cables, towers, and right of way, more than covers for the costs of additional installations like converters, filters, etc.; and/or,

- The specific connection between two AC systems can not be achieved by an AC tie-line, for various reasons like different frequencies, long submarine cables, asynchronous operation of the two systems or connection of a weak AC system to a strong AC system.

1.4. Objectives of the Thesis

As mentioned in Section 1.3.2, one of the disadvantages of HVDC transmission systems is the fact that these system can not be easily tapped to feed small isolated loads located in their vicinity. The objective of this study, therefore, is to propose a practical scheme for small power

tapping from HVDC systems, and to study different operational aspects of the proposed scheme.Throughout the study, attention is paid solely to the solid state devices currently available on the market, as well as the real power supply levels needed by isolated communities. It is hoped that establishing practical tapping schemes will lead to even more attractiveness of HVDC systems, as well as improving the living conditions and economic growth of the small isolated communities who live close to these systems.

1.5. Summary of the Chapter

In this chapter, a brief historic review of HVDC Transmission Systems was presented. Principles of operation of these systems were introduced, and the criterion for selection between the HVDC and HVAC system, based on the advantages and disadvantages of HVDC systems, was discussed. Finally, the objective of the thesis, i.e. finding a practical solution for the problem of small power taping from HVDC transmission systems, was stated.

Chapter Two

Small Power Tapping from HVDC Transmission Systems

Although the HVDC transmission systems, if proved to be superior to AC transmission for a specific case, present notable economical, as well as technical advantages, these systems are usually designed on a point-to-point basis. As some of these HVDC transmission systems pass over relatively small communities with no connection to major power transmission systems, it is most desirable to find methods for economically connecting these communities to the HVDC system. Examples of such isolated communities can be found in Northern Canada, where electric rates are as high as 14 times those in the southern region, and service is often limited to a few household appliances like light bulbs and radios. These constraints bar any serious social and economic development [4]. Another classic example is the case of the Brazilian indigenous tribes who live close to the huge Itaipu HVDC system, but are deprived from the amenities provided by the electric energy [5]. The possibility of connecting such communities to existing

HVDC systems, if established, makes HVDC transmission even more attractive. There are also considerations in political decision-making centers which may lead to making the availability of the power to the people around large transmission systems mandatory.

2.1. Isolated Loads in Canada

A survey was done by the Manitoba HVDC Research Center for GEC-Alsthom during 1991 and 1992, to get a complete set of information about the Canadian communities which are not connected to the electric grids, and are served by diesel-electric generators. Four provinces of Manitoba, British Columbia, Alberta, and Ontario, as well as the Yukon Territory participated in the survey and provided the Center with information about 50 isolated communities, out of a probable 80 communities throughout the country. Table 2.1, used with written permission of GEC-Alsthom, shows the peak demand of these communities at the time of the survey [6].

Table 2.1 - The Number of Isolated Communities Within a Range of Peak Demand (kW)

Province/Territory	26 < P. D. < 600	720 < P. D. < 784	980 < P. D.
Manitoba	6	0	0
Yukon	5	0	0
British Columbia	1	1	5
Alberta	8	0	2
Ontario	19	2	1

The results show that in 78% of the cases the demand is below 600 kW, for 6% of the cases the demand is between 600 kW and 800 kW, and the remaining 16% need supplies of above 800 kW. Throughout the current study, these numbers serve to prove the adequacy of the tapping scheme, to be proposed and studied later, for the majority of the isolated communities in Canada.

It seems reasonable to expect that the isolated communities in other parts of the industrial world, as well as the developing world, require similar levels of power supply.

2.2. Series and Parallel Taps

Generally, tapping stations can be divided into two categories. These categories are series and parallel taps. Each category has its special characteristics, and is suitable for a certain range of power rating [5].

2.2.1. Series Tap

Fig. 2.1 shows a series tap. The series tap is a single-phase, full-wave bridge, connected in series with the transmission line. The current passing through the tap is the line's DC current, and therefore, the tap has to be rated for the full line current.

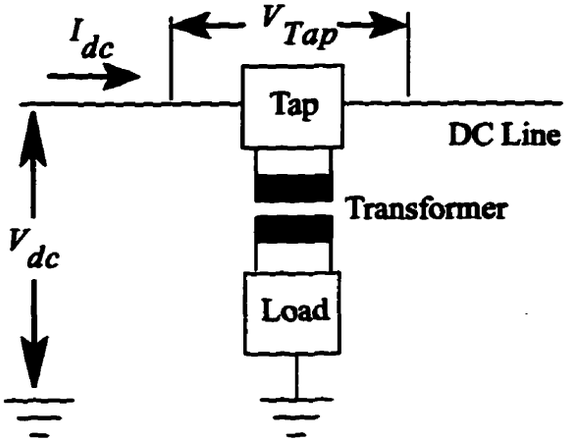

Fig. 2.1 - A Series Tap

This tap is a current-source converter, and the power being tapped from the HVDC system to the local load is:

$$P_{Tap} = V_{Tap} \times I_{dc}. \qquad (2.1)$$

It is evident that the tapped power varies with the amount of the DC current in the transmission line. Therefore the control over the amount of the tapped power is done through the control of the tap voltage, by a combination of firing angle control and/or transformer tap changer position.

The series tap, because of its negligible impact on the amount of the DC current in the transmission line, is best suited for small loads, i.e. loads with ratings less than 10% that of the main terminals. Also, its control can be totally local without any need for an integrated control system throughout the whole HVDC system, thus avoiding high costs of communication.

2.2.2. Parallel Tap

Fig. 2.2shows a parallel tap. The parallel tap is a three-phase inverter, connected between the transmission line and the ground, and thus, operating at the full mono-polar DC voltage. The tap, diverts a fraction of the line's DC current, into the local load, and therefore its current rating is determined by the local load's rating.

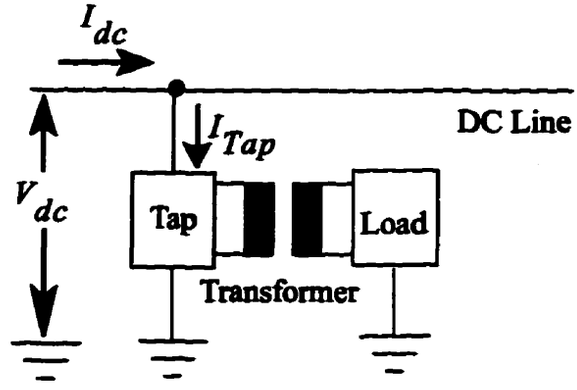

Fig. 2.2 - A Parallel Tap

This tap is a voltage-source converter, and the power being tapped from the HVDC system and to the local load is:

$$P_{Tap} = V_{dc} \times I_{Tap} . \qquad (2.2)$$

The fact that the DC current in the line is partially diverted by the tap necessitates the utilization of an integrated control regime throughout the system, by which the sum of current settings in all rectifiers is set equal to the sum of current settings in all inverters, on a per pole basis. This means more hardware and communication costs, which in turn, makes the parallel tap economically non-feasible for small loads. Failure to achieve this will result in the flow of current through the ground return, or metallic neutral. Another limitation in the use of parallel taps for small loads is the fact that the combination of high voltage and low current ratings will result in a high installation cost per kW [5].

The parallel tap, because of the above mentioned reservations, thus, is most suitable for tapping relatively larger amounts of power (compared with the main terminal's rating), and for the multi-terminal operation of HVDC systems.

2.3. Previous Work in Power Tapping from HVDC Transmission Systems

For large loads, i.e. loads which are in the same order as the whole system's capacity, multiterminal schemes have been designed and commissioned. The first multiterminal HVDC system to be commissioned was the tapping of the monopolar Sardinia to Italy HVDC link on Corsica. The tap's rating is 50 MW, while the main terminal's capacity is 200 MW. The system was not initially designed as a multiterminal system, and the tapping was added to the original system by adding a parallel converter at Corsica [7]. The first HVDC system to be initially designed as a multiterminal system, was the Quebec-New England DC link, with a 2140 MW parallel tap at the Nicolet Station [5].

For small taps, i.e. taps with ratings less than 10 percent of the main terminal rating, however, the economical competitiveness compared with other supply alternatives (e.g. local generation),

as well as technical reservations have to be well fulfilled. Amongst the main requirements of a small tapping station, one can point to the following [8-10]:

a) The per unit cost of the tap must be strongly constrained, i.e., the fixed cost must be kept as low as possible,

b) The tap must have a negligible impact on the reliability of the main HVDC system. This implies that any fault in the tap must not be able to shut the whole system down; and,

c) The tap control should not interfere with the main system control, i.e., the tap control system has to be strictly local. Failure to achieve this means more complex control systems and higher costs in hardware for communication and control.

In the past, a number of schemes have been proposed for small power tapping from HVDC systems. The majority of those schemes propose the use of force-commutated or line-commutated inverters to tap the power off from the HVDC system. These schemes, inherently, require additional commutation circuitry or local generation capacity, which in turn, lead to high costs of installation and/or operation of such tap stations. Amongst the studies done in this regard, one can point to those of: Turanli, Menzies and Woodford, which uses a capacitor-commutated inverter, employing two six-pulse thyristor- bridges in series with the DC line [11], and Bowles, Nakra and Turner, in which a two-part scheme is proposed. The first part consists of two conventional converter bridges connected in series with the line, the output of which goes to a DYy three-phase transformer, and the second part is a synchronous machine which provides the commutation voltages for the bridges, as well as part of the total reactive requirement [12].

The fast development of new semiconductor devices having turn-off capabilities, i.e. GTO thyristors, has brought about new ideas about designing small tapping stations. Amongst the

most recent proposed schemes, are those proposed by Ekstrom and Lamell [13], and by Zhao and Iravani [14].The proposed scheme by Ekstrom and Lamell is based on a current-source line-commutated single-phase thyristor bridge, connected in series with DC line, and dependent on locally provided DC voltage for starting the tap operation.

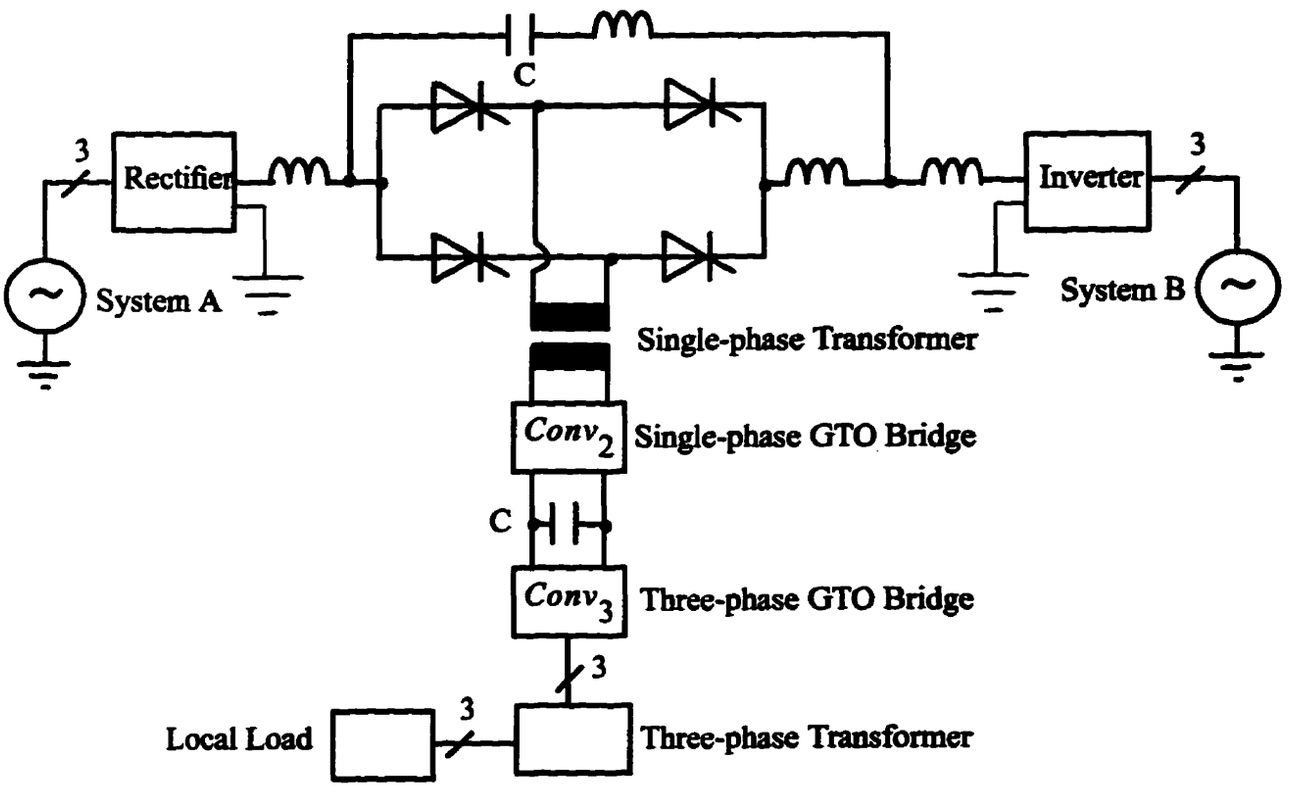

Fig. 2.3 - The Scheme Proposed by Ekstrom and Lammel

Fig. 2.3 shows the schematic of their proposed scheme. According to Ekstrom and Lamell, this scheme, which works in two steps, eliminates the need of a three-phase transformer between the DC line and the ground potential by using a single-phase transformer. From the results of the EMTP simulations made on the scheme, they expect their proposed scheme to yield good dynamic results [13].

2.4. Summary of the Chapter

In this chapter, the problems associated with small power tapping from HVDC transmission systems, as well as the motivation behind the study of small power tapping were briefly discussed. Next, the results of a survey with regard to the Canadian communities which are isolated from the electric grids were presented. Then, the two main kinds of tapping schemes, i.e. series and parallel taps, were considered. The main economical and technical requirements for a small tapping station, too, were studied. And finally, the previous work done in this field was introduced.

Chapter Three

The Proposed Scheme

Based on the previous discussions about the need to tap power from HVDC transmission systems, and in accordance with the requirements outlined for a small tapping station, a novel method is introduced which is technically feasible and also economical. The scheme is inspired by the availability of GTO thyristors on the market, having peak repetitive voltage ratings of up to 4.5 kV, DC current capabilities of up to 1 kA, and controllable current ratings of up to 3 kA [15]. The scheme presented here, is meant to minimize the number of elements required and eliminate the need to locally provide DC voltage (apart from a small control supply) and the need for commutating circuitry/machines, while meeting all the requirements outlined earlier for a small tapping station.

In this Chapter, the proposed tapping scheme will be introduced, and its performance will be digitally simulated with the results being presented in Chapter Four and Chapter Five. For each

part of the scheme, different possible control regimes will be introduced and studied. It will be shown that some of these control regimes are more advantageous compared to the others. Also, it will be shown in Chapter Five that with this specific scheme, and certain modes of operation, ordinary thyristors are capable of replacing the GTO thyristors in the series tap, without decreasing its abilities.

3.1. The Proposed Scheme

The proposed scheme uses a series tap consisting of 4 GTO thyristors, two capacitors, a single-phase transformer (possibly air core), and a single-phase to three-phase converter feeding the local load. Its control regime is completely local. Fig. 3.1 shows the proposed scheme and Table 3.1 presents a quantitative comparison between this scheme and the one proposed in [13]:

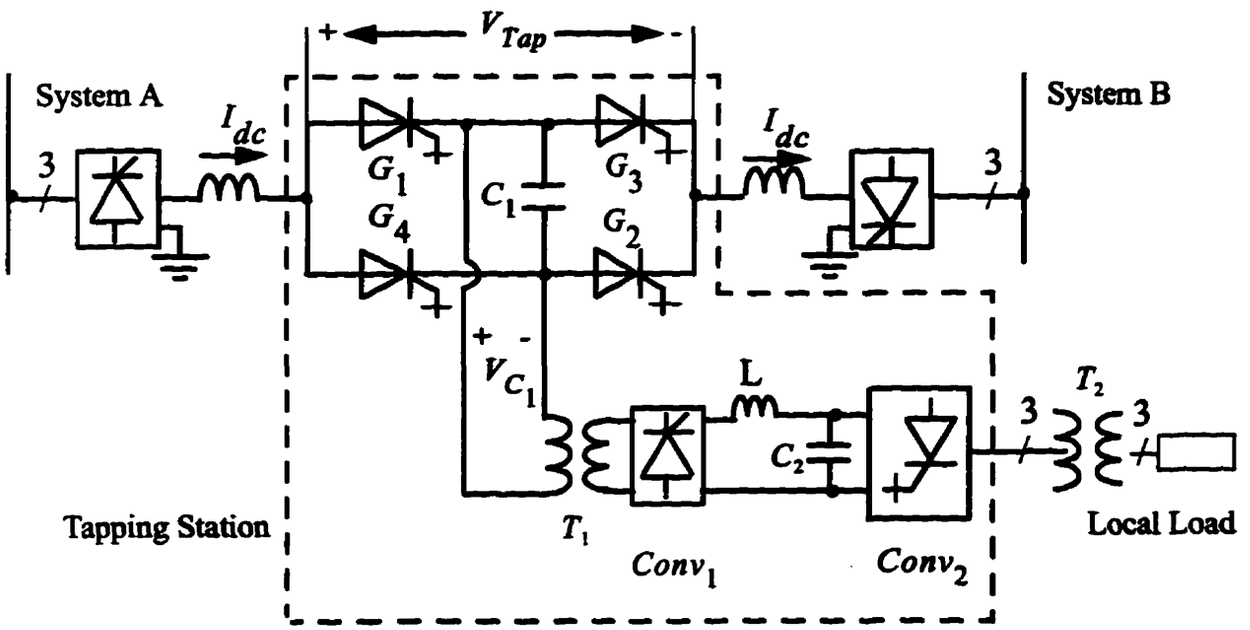

$Conv_1$ = Single-phase Rectifier T_1 = Single-phase transformer

$Conv_2$ = Three-phase GTO Inverter T_2 = Three-phase transformer

Fig. 3.1 - The Proposed Tapping Scheme

Table 3.1 - Comparative Data

Item	Ekstrom's Scheme	Proposed Scheme
GTO Thyristors	10	10
Thyristors	4	2
Diodes	-	2
Capacitors	2	2
Reactors	2	1
Three-phase Transformer	1	1
Single-phase Transformer	1	1
Air-core Transformer Possible?	No	Yes
Local DC Voltage Needed?	Yes	No

3.2. Air-Core Transformer

One major potential advantage of the proposed scheme is the possibility of using an air core single-phase transformer to achieve insolation between the line potential and the ground potential. The idea of using air-core transformer was proposed in an internal report regarding small power tapping, prepared for Manitoba HVDC Research Centre by Mr. G. D. Irwin.

An air core transformer is far less costly compared to a similar conventional transformer. It provides insulation by simply separating the two windings in the air, and does not need complex insulation, protection, and cooling peripheral devices/systems. It is also very light in weight, thereby making the whole tapping assembly lighter in weight and easier to install.

Looking at the scheme proposed by Ekstrom (page 15), it is evident that the commutation on the tap thyristors is provided by the DC voltage across the intermediate capacitor, through the action of the single-phase GTO thyristor bridge $Conv_2$. The commutation voltage is transformed to the line potential by the single-phase transformer. This necessitates the

deployment of a robust, low-leakage transformer, with a very good voltage regulation, an aspect non-existent in any air core transformer. In the proposed scheme, however, there is no need to have a commutation voltage on the tap GTO thyristors. A high-leakage transformer, moreover, does not contribute to system losses or weak performance. Therefore it seems quite plausible to use an air core transformer in the tapping scheme, with results as good as those anticipated from a small tapping station.

As for the possibility of producing such an air core transformer, there seemingly exists no major obstacle. Dry-type reactor technology which had its beginning in the early 1900's can be used in manufacturing the air core transformer. Because of their design features and their cost effectiveness, air core reactors employing dry type technology have become the technology of choice for many applications. This is the situation for HVDC projects, which typically require a high number of reactors, such as smoothing reactors, harmonic and radio interference filter reactors. Dry-type technology has been applied for over 25 years on HVDC projects around the world [16].

To estimate the range of voltages that can be applied on the air-core reactors, a practical case in which such a reactor can be used as an smoothing reactor is being considered.

Bipole One of the Manitoba Hydro's Nelson River HVDC System has three six-pulse bridges connected in series. Each bridge has a DC voltage of 157 kV, a line-to-line AC voltage of 134 kV, a reactance, X_c, of 10.53 Ω (0.2. p.u.), and a maximum DC current of 1.8 kA. From the following equation [3]:

$$V_{dc} = \frac{3\sqrt{2}}{\pi} \times V_{L-L} \cos\alpha - \frac{3}{\pi} \times X_c I_{dc} \quad , \qquad (3.1)$$

and at the full load, the firing angle, α, is found to be equal to 15 degrees. Also, from the following equation [3]:

$$I_{dc} = \frac{V_{L-L}}{\sqrt{2}.X_c}[\cos\alpha - \cos(\alpha + \mu)] \qquad (3.2)$$

the overlap angle, μ, is found to be equal to 25 degrees. Using these values, and from Fig. 4.5 in page 314 of [3], the ratio of the first significant voltage harmonic, i.e. the sixth harmonic, to the DC voltage is:

$$\frac{V_6}{V_{d0}} = 0.07 \qquad (3.3)$$

Considering the total DC voltage of 450 kV, the peak sixth harmonic voltage is equal to 31.5 kV. If only a V_6/V_{d0} of 2% is allowed on the HVDC line, it means that a sixth harmonic voltage of 22.5 kV has to be absorbed by (dropped across) the smoothing reactor. Therefore, the air-core reactors currently on the market, seem capable of withstanding the kind of AC voltages to be seen later during the analysis of the proposed scheme. As for the DC currents allowed through these reactors, there shouldn't be any problem with currents of up to 2 kA, which is the typical DC current passing through most of the smoothing reactors.

Chapter Six of this thesis is completely devoted to the analytical study of the air core transformer, its digital simulation, and its performance in conjunction with the proposed tapping scheme.

3.3. Operation of the Proposed Scheme

The idea in the proposed scheme is as follows. The DC current in the main line passes through the capacitor C_1 by firing the GTO thyristors G_1 and G_2. Assuming a zero initial voltage for the capacitor, the current charges the capacitor to a voltage level, proportional to the time current is flowing in it, as equation (3.4) shows:

$$V_{C_1}(t) = \frac{1}{C_1} \times \int_0^t I_{C_1} dt \,, \qquad (3.4)$$

in which I_{C_1} is the total capacitor current and t is the time duration for which the current has been passing through the capacitor.

This voltage is directly applied across the non-conducting GTO thyristors, as well as the primary winding of the single-phase transformer. When the voltage reaches to the maximum bearable voltage for the non-conducting GTO thyristors, which currently is about 4.5 kV for the most powerful GTO thyristors available on the market, G_1 and G_2 are turned off and G_3 and G_4 are turned on. Reversing the direction of the DC current in the capacitor, brings the capacitor's voltage to zero and further charges it in the opposite direction. Again, when the voltage reaches its maximum allowable level in the negative half-cycle, the conducting GTO thyristors are turned off and the other two are turned on. Alternate repetition of this process creates a saw-tooth voltage in the capacitor, which is transformed by the single-phase transformer to the ground potential. The single-phase voltage created in this manner, then, can be converted to a three-phase voltage, using a single-phase to three-phase converter, and supplied to the local load, via a three-phase transformer.

The following case illustrates the proposed idea. If a DC current of 2 kA is flowing in the HVDC line, and if a 125 μF capacitor is to be used in the series tap, it takes 0.25 ms for the capacitor to be charged from zero voltage to 4 kV. If the current is reversed at this moment, it takes another 0.5 ms for the voltage to reach -4 kV. Therefore, while the current will have a square-wave form with a frequency of 1 kHz, the voltage is expected to have a saw-tooth shape, with the same frequency, and a peak magnitude of 4 kV. Fig. 3.2 shows the square-wave capacitor current in this case.

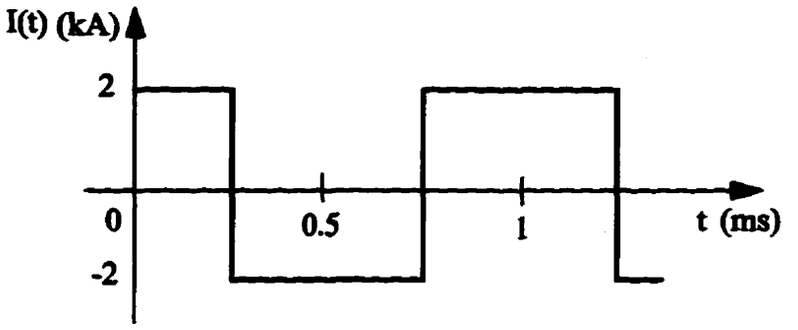

Fig. 3.2 - Square-wave Capacitor Current

It can be shown that the above square-wave current is represented by the following Fourier series [17]:

$$I(t) = 2\sum_{n=0}^{\infty}\frac{4}{\pi}\frac{(-1)^n}{(2n+1)}\cos(2n+1)\omega t \quad \text{(kA)}, \tag{3.5}$$

in which $\omega = 2\pi(1000)$ rad/s. Using equation (3.4), and integrating equation (3.5) from *0* to *t*, it can be shown that the resulting voltage is represented by the following Fourier series:

$$V(t) = 2.546\sum_{n=0}^{\infty}\frac{4}{\pi}\frac{(-1)^n}{(2n+1)^2}\sin(2n+1)\omega t \quad \text{(kV)}. \tag{3.6}$$

Using the MATLAB software package, and taking into consideration only the first 50 terms, the waveforms resulting from the Fourier series (3.5) and (3.6) are shown in Fig. 3.3.

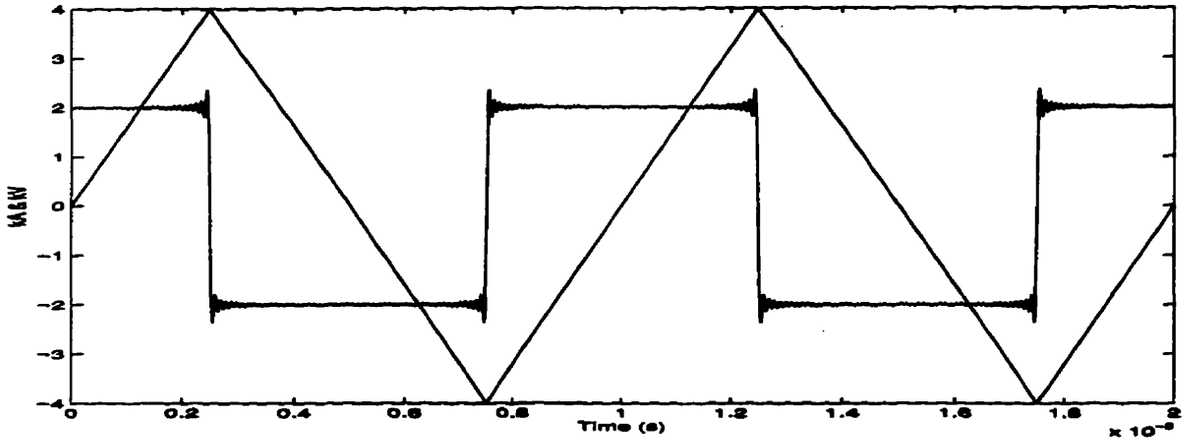

Fig. 3.3 -Capacitor's Square-wave Current and Saw-tooth Voltage

The reason behind choosing such high frequencies is the fact that this will decrease the size of the capacitor drastically, typical values being between 100-200 μF, and thus makes the tapping station less expensive. As the iron losses increase drastically at higher frequencies, the air core single-phase transformer will have the additional advantage of avoiding high iron losses. And finally, a higher frequency means that the harmonics imposed on the DC line are higher compared with the AC system frequency, and thus, easier to filter through the DC filters.

This analysis shows that with a proper control regime, a saw-tooth voltage can be generated, the peak magnitude of which is dependent on the DC line current. However, since the power being tapped from the DC line is dependent on the generated AC voltage, it is necessary to keep the peak AC voltage constant, or as close to a constant value as possible. Achieving this goal requires control regimes which, through changing the firing frequency of the tap switches or similar means, can keep the voltage constant for different values of the DC line current within its normal operational range. Moreover, the conditions assumed in the above are those of a no-load situation, in which the only current passing through the capacitor is the DC line current. In a practical situation, the primary current of the single-phase transformer also flows through the capacitor and its effect on the capacitor voltage has to be taken into consideration by the control regime.

To examine the effects of loading on the capacitor voltage, it is assumed that the capacitor is paralleled with a R-L branch. The R-L branch values are chosen in a way that under a saw-tooth voltage with a peak magnitude of 4 kV, a power of 1.23 MVA with a lagging power factor of 0.707 is absorbed by the branch, representing the local load and the single-phase transformer. This is very close to a typical isolated load, with an air-core single-phase transformer in the tapping scheme. As the rms value of the voltage is equal to $4/(\sqrt{3})$ kV, the values for R and L are found to be 3.06 Ω and 487 μH, respectively. The current injected into the two branches

is a square-wave current with a frequency of 1000 Hz, and a peak magnitude of 2 kA. Fig. 3.4 shows the simplified configuration for the tapping station under the load conditions.

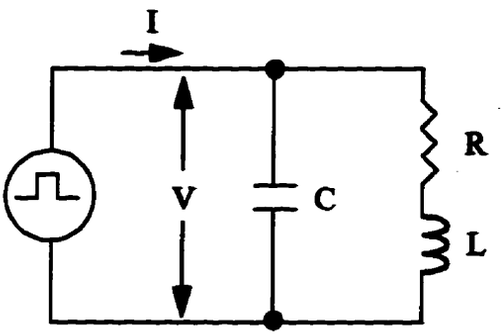

Fig. 3.4 - Simplified Loaded Tap

Using the Fourier series (3.5), the current is assumed to be a summation of 50 sinusoidal currents with different frequencies, $I(n\omega)$. At each harmonic frequency, the equivalent impedance, $Z(n\omega)$, is calculated and all harmonic voltages, i.e. the phasors $I(n\omega)$ $*Z(n\omega)$, are added together to get the total voltage. Fig. 3.5 shows the resulting voltage, derived by MATLAB software package.

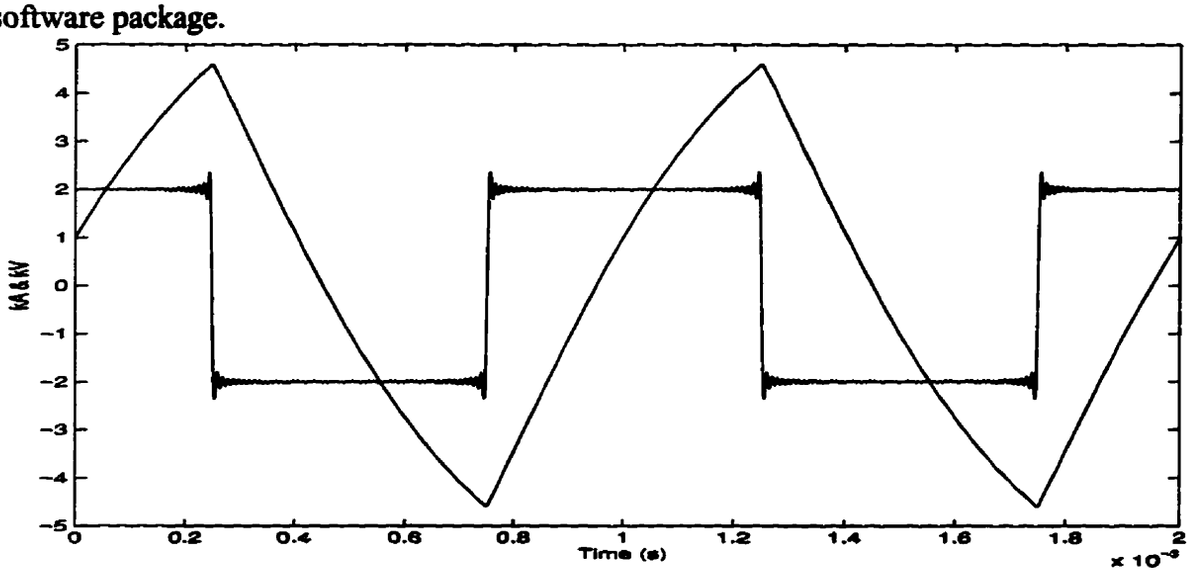

Fig. 3.5 - Current and Voltage for the Loaded Conditions @ 1000 Hz

It is evident that, unlike the no-load conditions shown in Fig. 3.3, the peak voltage has increased to about 4.7 kV. This is because of the current in the parallel branch, as mentioned earlier.

If the frequency of the injected current is increased from its original value of 1000 Hz, the peak magnitude of the voltage is expected to drop, because of the fact that the equivalent impedance will decrease accordingly (at higher frequencies, C is the decisive part of the impedance).

Fig. 3.6 shows the voltage across the capacitor for a frequency of 1150 Hz.

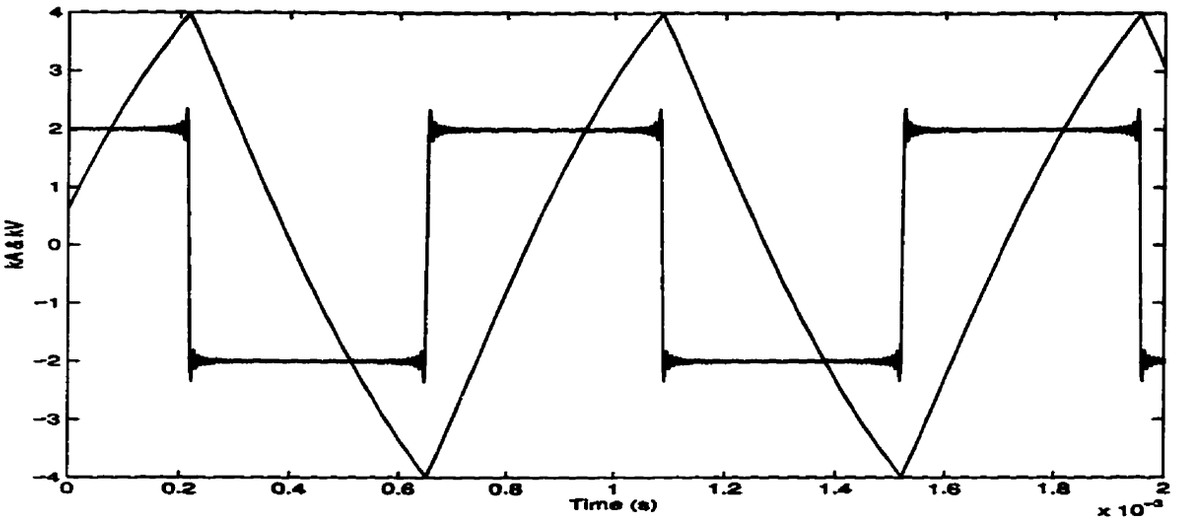

Fig. 3.6 - Current and Voltage for the Loaded Conditions @ 1150 Hz

The 15% increase in the frequency of the square-wave current has resulted in a drop in the voltage's peak magnitude, sufficient to keep it within ±4 kV.

In the following Section, a number of alternative control regimes for three different parts of the tapping scheme are presented and studied.

3.4. Control Regimes for the Proposed Scheme

In order to control the quality of the power being tapped from the HVDC system, and also to protect the tapping station's various elements, several parameters must be closely monitored and kept within acceptable margins. These parameters include tap's AC voltage V_{C_1}, the load AC voltage, and load frequency. These parameters are being controlled, directly or indirectly,

through the control regimes presented in the following for each of the three converters in the tapping scheme.

3.4.1. Controls for the Series Tap

The AC voltage created by the series tap (across the capacitor C_1) can be controlled through a number of different control strategies. Three possible methods are considered in the current study, and are as follows:

1. Bang-Bang Method: The alternate switching on and off of the two pairs of GTO thyristors, initially, was believed to be possible by using a simple bang-bang control regime which works exactly in the manner explained in Section 3.3. The voltage across the capacitor is monitored, and when it reaches the set maximum (in both positive and negative half-cycles), firing signals are issued to the non-conducting switches to turn on, and to the conducting switches to turn off. During the simulation of the proposed scheme, however, it was realized that switching the conducting GTO thyristors off at a moment when the alternating voltage has reached its maximum allowable value, will not stop the voltage from further increasing beyond its maximum level. This is because of the fact that although the DC line current, because of its path being reversed, will flow through the capacitor in the opposite direction, the current in the single-phase transformer's primary winding will continue to flow through the capacitor in the same direction for a while, because of the inductance in the transformer winding, and this current can increase the alternating saw-tooth voltage even further. This situation is especially serious when the peak current in the transformer primary winding is comparable to or even higher than the DC line current, for example during low-level DC power transmission and high local demand, where the reversal of the DC current will not reverse the flow of the total current in the capacitor, i.e. I_{C_1}.

In addition to the above disadvantage, it was realized that firing the switches in the series tap solely based on the shape of the AC voltage will result in the collapse of the AC voltage, and thus a halt in the power tapping, for specific levels of DC current. This situation is illustrated through the following example.

The series tap has a 125 μF capacitor, and the single-phase transformer and the local load together are represented by an R-L branch paralleled with the capacitor. The resistance is selected to be equal to 3.06 Ω, and the inductance is equal to 487 μH. At a frequency of 1000 Hz, and with a peak saw-tooth voltage of 4 kV, this translates to a local load of about 1.23 MVA with a lagging power factor of 0.707, which is reasonably similar to a typical local load with an air-core transformer in the tapping scheme. At the start of the system operation, a DC current of 2 kA is passing through the series tap, and the bang-bang control system is set to limit the peak voltage to 4 kV. The operation of the system is simulated by PSCAD/EMTDC digital simulation software package [18] and is shown in Fig. 3.7.

At t=0.05 seconds, the DC current is reduced to 1.5 kA, because of which, the frequency of the saw-tooth voltage is reduced by the control system in order to keep the peak voltage at the pre-set level. At t=0.01 seconds, the current is reduced to 1.2 kA, but the AC voltage has collapsed and the capacitor voltage stays constant at 3.672 kV. During the same period, the load current is exactly equal to 1.2 kA DC, which when multiplied by the 3.06 Ω load resistance, gives a DC load voltage of 3.672 kV. This means that at a moment, when the DC voltage across the resistance is equal to the DC voltage across the capacitor, the flow of current into the capacitor will stop, and all the DC current will pass through the load branch, thus stopping the capacitor voltage from changing in both directions. Consequently, the bang-bang control system, naturally, will not change the conducting switches because the pre-set limit will not be reached, and the AC voltage will collapse. In reality, however, as soon as the AC voltage collapses, the

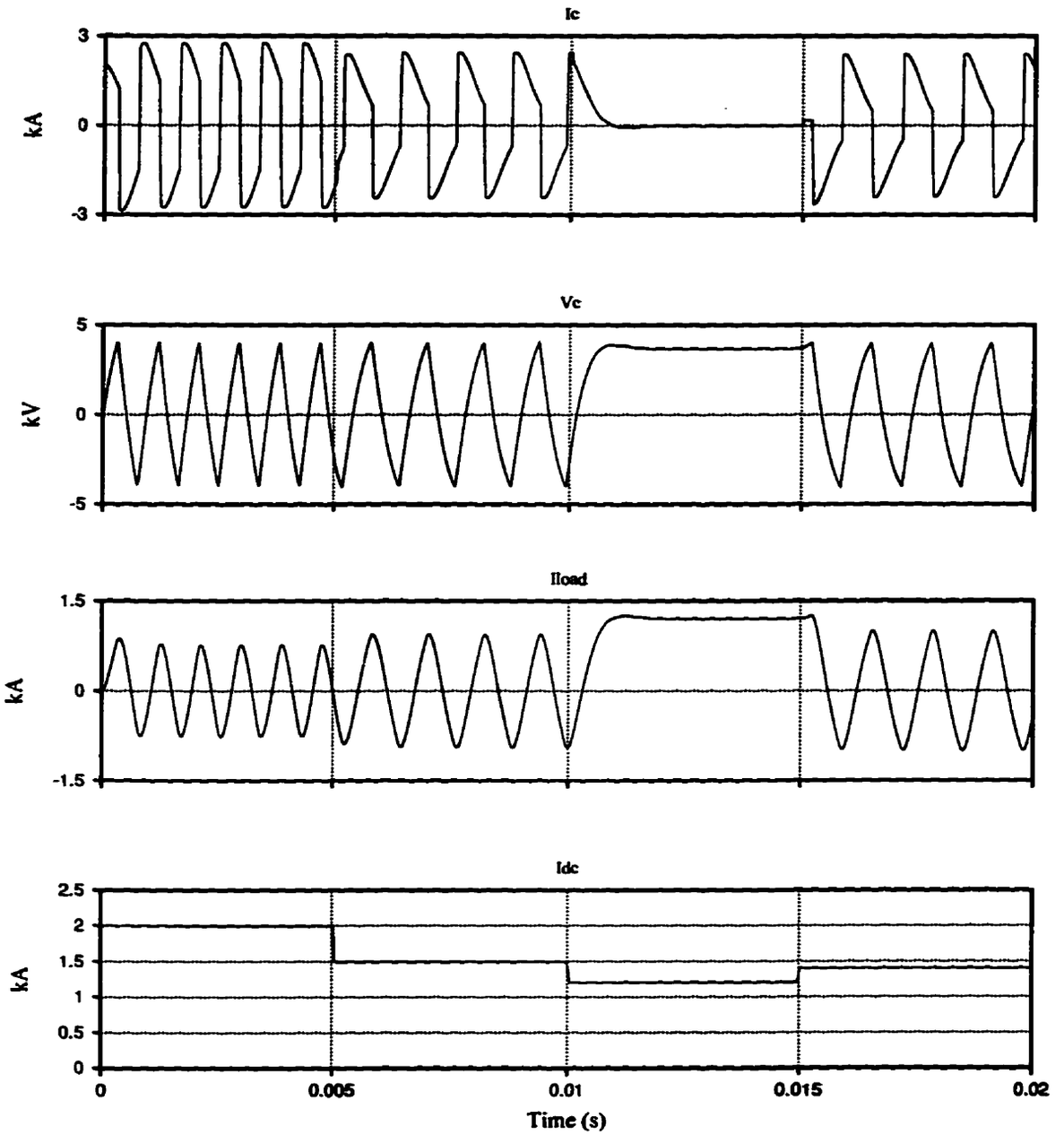

Fig. 3.7 - Operation of the Tapping System with Bang-bang Control

local load will not be represented in the primary of the single-phase transformer anymore, and thus the actual resistance will be the small primary winding resistance. The capacitor voltage, in the absence of any flow of DC current through it, will gradually decrease (discharge in the

parallel branch) to a small level equal to that of the ohmic voltage drop across the primary winding, which by now, carries all the DC line current. Since each GTO thyristor is supposed to carry the DC current for half of each cycle, the average current ability will be chosen to be equal to 1 kA, which is also currently the maximum available on the market. Uninterrupted flow of DC current through only two of the GTO thyristors, thus, will eventually result in their overcurrent damage. In the impractical situation, where the DC current is increased so that the ohmic voltage drop is larger than the pre-set limit, the bang-bang control system, once again, is able to switch off the conducting GTO thyristors, and switch on the non-conducting ones, and consequently, re-establish the saw-tooth voltage. This, however, will not happen in a practical situation.

For the above reasons, the bang-bang control strategy proved impractical and, therefore, is not employed in the study of the tapping scheme's operation.

2. Variable-Frequency Strategy: It is evident from the previous explanation about the operation of the proposed scheme that the firing frequency of GTO thyristors for a given capacitance is dependent on the amount of the DC current passing through the main line, plus the current passing through the transformer's primary winding. For this reason, a variable frequency PI-controller (Proportional-Integral) system, as shown in Fig. 3.8, is used, where the frequency can vary between 200 Hz and 1500 Hz, the maximum frequency allowable for the currently available GTO thyristors on the market [15]:

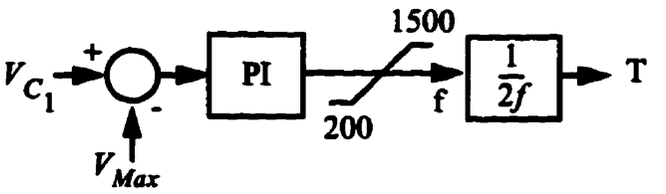

Fig. 3.8 - Firing Frequency Controller

The controller ensures that the peak voltage (in both positive and negative directions) does not exceed 4.5 kV. The feedback to the PI-controller is the rms value of the capacitor voltage, while the reference value, i.e. V_{Max}, is the maximum peak voltage divided by $\sqrt{3}$. At no-load condition, the AC voltage is completely in a saw-tooth shape and its rms can be shown to be equal to its peak value divided by $\sqrt{3}$. As the load is increased on the tap, the AC voltage becomes more similar to a sinusoidal waveform as shown in Fig. 3.7, and in an ideal situation, where it assumes a complete sinusoidal form, its peak magnitude is only $\sqrt{2}$ times its rms value. For this reason, the division of the maximum voltage by $\sqrt{3}$ provides a reasonable safety margin for the switches.

This control strategy, because of its relative independence from the voltage shape, and because of the fact that it issues the firing signals based on the frequency, and not the peak of the voltage, is capable of maintaining the AC voltage for a wide range of DC current in the line. This will be shown in Chapter Four.

3. Constant-Frequency Strategy: This is an alternative control strategy, and similar to the variable-frequency strategy, issues the firing signals in a quasi-feedforward mode, without being totally dependent on the peak of the AC voltage. The idea in this control strategy is as follows.

A constant frequency is selected for the operation of the tapping scheme. The capacitance is chosen in a way that at minimum capacitor current, a complete saw-tooth voltage is generated. As the current increases above the minimum limit, the current is allowed to go through the capacitor for only a fraction of a half-cycle, long enough to charge the capacitor to the set maximum value. As soon as the maximum level is achieved, the conducting GTO thyristor on the right-hand-side of the series tap in Fig. 3.1 is turned off, and the non-conducting switch on the same side is turned on. This provides a direct path for the DC line, bypassing the capacitor.

At the end of the half-cycle, the conducting GTO on the left-hand-side will be turned off, and the non-conducting switch on the same side is turned on, allowing the DC current to flow through the capacitor in the opposite direction, compared to the previous half-cycle.

If the working frequency is selected to be equal to 200 Hz, and if the minimum and the maximum peak currents through the capacitor are to be equal to 0.5 kA and 2.5 kA respectively, the capacitance needs to be, based on the equation (3.4), equal to 156.25 μF, if the maximum voltage is to be 4 kV. Fig. 3.9shows the resulting voltage for four different values of peak capacitor current.

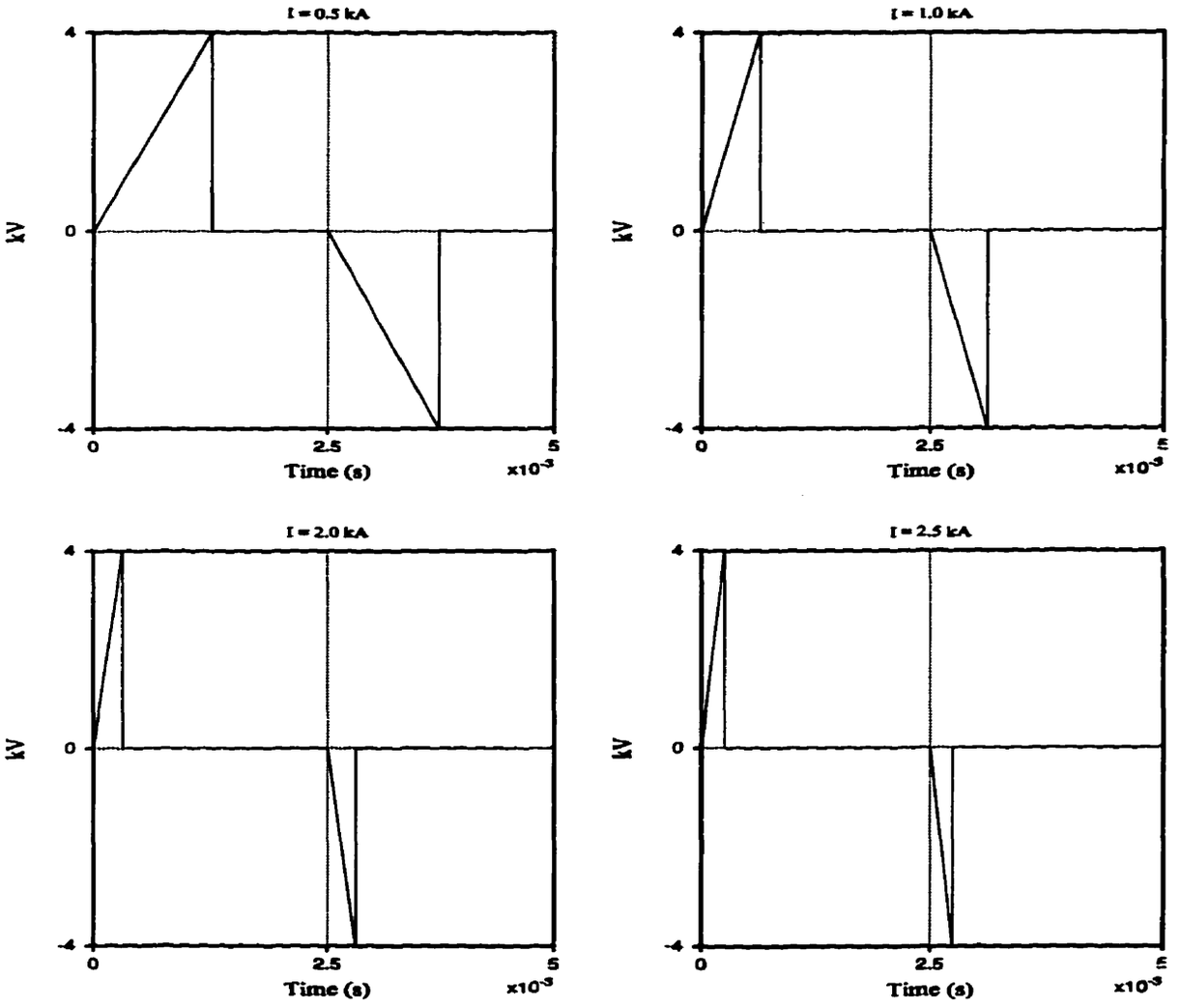

Fig. 3.9 - Constant Frequency Voltage for Different Capacitor Currents

It must be clarified that the voltages shown in Fig. 3.9 are the AC voltages imposed on the HVDC line. The AC voltage seen by the primary winding of the single-phase transformer, however, will not include the sudden jumps to zero, because the capacitor voltage, which is applied on this winding, will not be discharged instantaneously. Fig. 3.10 shows a typical voltage expected to be applied on the single-phase transformer.

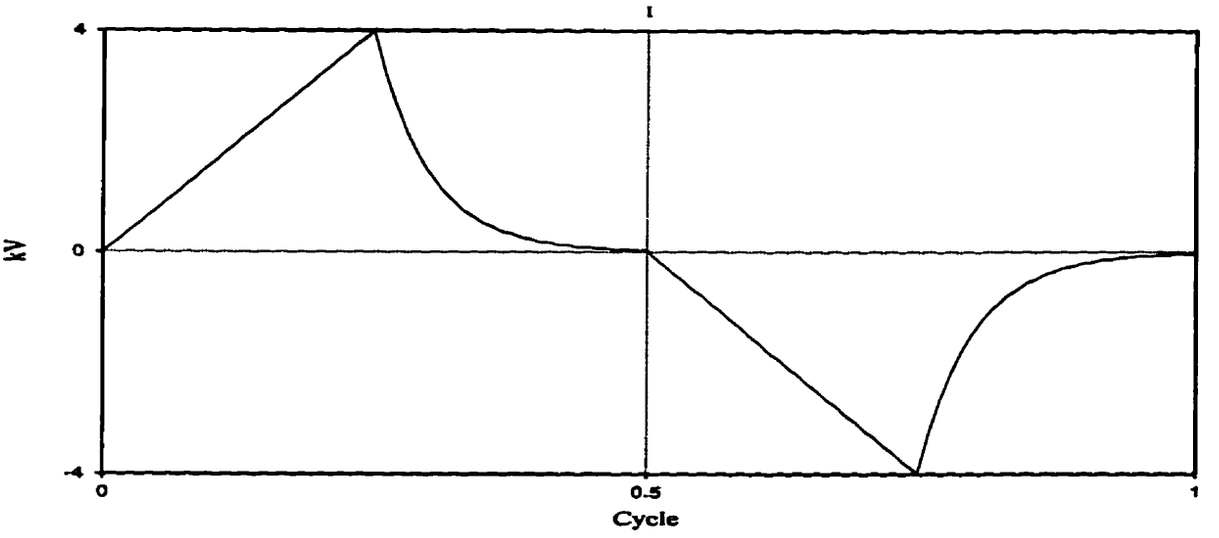

Fig. 3.10 - Expected AC Voltage Applied on the Transformer's Primary Winding

The constant frequency regime is more advantageous, compared to the variable-frequency regime, if instead of the air-core transformer a conventional iron-core transformer is to be used. This is because of the fact that the iron losses increase drastically at high frequencies, and also because of the fact that it is very difficult to design an iron-core transformer which can provide a good degree of voltage regulation over a wide range of frequencies. The disadvantage of this method, compared to the variable-frequency method, however, is that only GTO thyristors can be used in the series tap, while as it will be shown in Chapter Five, with the variable-frequency method, ordinary thyristors can replace the GTO thyristors.

The results of the study of the system operation using the constant-frequency controller will be presented in Chapter Five.

3.4.2. Controls for the Single-phase Rectifier

As mentioned earlier, the high frequency single-phase voltage created on the capacitor C_1 is transformed to the ground potential by the single-phase transformer T_1, and is then rectified by the single-phase bridge in order to charge the DC link capacitor C_2. The DC link voltage is the source for the three-phase voltage-source inverter, and therefore, it is necessary to control this DC voltage in order to maintain a constant load voltage. There are two possible choices for the configuration of the single-phase bridge, which are as follows:

1. Half-Wave Bridge: In this configuration, the single-phase bridge consists of two thyristors in the upper half of the bridge, and two diodes in the lower half. A PI-controller, along with a Phase Locked Loop (PLL), controls the firing angle issued to the thyristors, in order to maintain a constant DC voltage across the DC link capacitor C_2. This kind of control over the DC link voltage is necessary if the Programmed Pulse Width Modulation (PPWM), to be introduced in the next Section is to be employed for controlling the three-phase inverter.

It is noteworthy that a full-wave bridge is not necessary, because the DC link voltage is always positive. Fig. 3.11 shows the control regime for the half-wave configuration, in which V_{ac} is the single-phase transformer's secondary voltage.

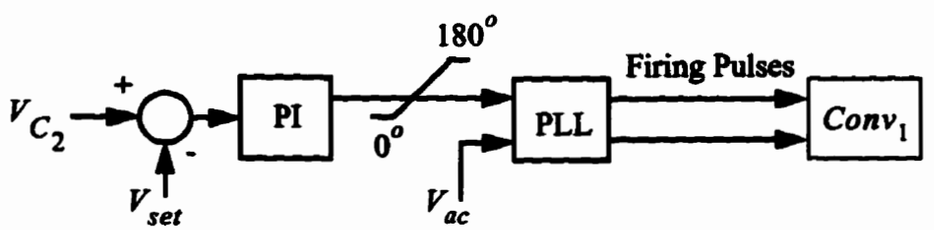

Fig. 3.11 - DC Link Voltage Controller

In ordinary cases, where the input to the single-phase bridge is a sinusoidal waveform the DC output can be controlled by the firing angles, based on the following relationship [19]:

$$V_{dc} = \frac{V_m}{\pi}(\cos\alpha + 1) \ , \qquad (3.7)$$

in which V_m is the peak AC voltage. In the present case, in which the AC voltage is not a perfect sinusoidal waveform, however, the PLL may not be able to perform as expected. The performance of the system with a half-wave single-phase bridge will be studied in Chapter Four.

2. Uncontrolled Bridge: In this method, the single-phase bridge is a simple diode bridge, providing a variable DC link voltage. The bridge has no specific controls, and the control employed in the three-phase inverter must be capable of handling variable DC voltage. It will be shown in Chapter Five that a Sinewave Pulse Width Modulation technique for the three-phase inverter will be necessary/adequate to control the load voltage along with an uncontrolled single-phase bridge.

3.4.3. Controls for the Three-phase Voltage-source Inverter

As the last stage of the tapping process, the voltage-source GTO inverter, $Conv_2$, converts the DC voltage across the DC link capacitor C_2 to a three-phase AC voltage. As the inverter is from the voltage-source family, the techniques of Pulse Width Modulation are suitable for controlling the inverter. However, based on the control chosen for the single-phase bridge, at least two possible methods exist, and are as follows:

1. Programmed Pulse Width Modulation (PPWM): This technique, briefly, uses a number of pre-calculated angles for firing the GTO thyristors in the inverter, and can optimize a number of quantities, like the magnitude of the fundamental frequency component, and the first significant harmonic present in the AC voltage [20]. Firing the GTO thyristors at these angles

changes the square DC voltage to a two-level line-to-neutral alternating voltage, as shown in Fig. 3.12, consisting of a wide spectrum of harmonics.

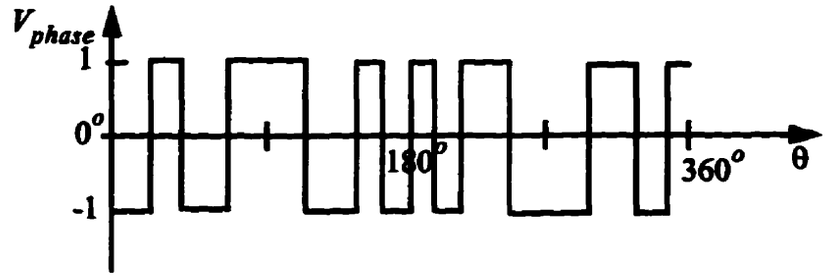

Fig. 3.12 - Line-to-neutral PWM Waveform

The resulting waveform shown in Fig. 3.12, can be expressed by the following Fourier series:

$$V_{phase} = \sum_{n=1}^{\infty} a_n \cdot \sin(n\theta) + b_n \cdot \cos(n\theta), \tag{3.8}$$

in which:

$$b_n = 0, \tag{3.9}$$

and:

$$a_n = \frac{4}{n\pi} \times \left[-1 - 2 \bullet \sum_{k=1}^{N} (-1)^k \cos(n\alpha_k) \right]. \tag{3.10}$$

The system of non-linear equations generated by equation (3.10) has N variables (α_1 to α_N) and a set of solutions is obtainable by equating N-1 harmonics to zero, and assigning a specific value to the fundamental magnitude, a_1. Therefore, for each properly calculated number of angles, say k, k-1 odd harmonics will be absent in the AC voltage's harmonic spectrum. The remaining harmonics, because of their high order nature, can be easily filtered by a single high pass filter. The outcome is a nearly perfect sinusoidal AC voltage, fed to the local load. The PPWM not only controls the magnitude of the load voltage, it is also the only criterion by which

the frequency of the voltage fed to the local load is controlled, and has proved to be quite effective, as will be shown in Chapter Four.

To find the appropriate PPWM firing angles for the proposed scheme, a fundamental magnitude of 1.0 p.u. is chosen. Also, it is desired to eliminate the first 10 harmonics in the spectrum of the load voltage. So, using the n-dimensional Newton-Raphson algorithm [24], a total of 11 firing angles, (α_1 to α_{11}) were calculated and are shown in Table 3.2.

Table 3.2: Firing Angles

Firing angle (Alpha)	Degrees
1	6.715
2	15.206
3	20.181
4	30.381
5	33.746
6	45.491
7	47.471
8	60.494
9	61.404
10	75.346
11	75.758

Note that with this number of firings per cycle, the converter switching frequency, f_c, found by the following equation [20]:

$$f_c = (2n+1)f \tag{3.11}$$

and for a load frequency, f, of 60 Hz will be equal to 1380 Hz, which is within the capabilities of the available GTO thyristors on the market [15].

The above firing angles have been calculated based on the assumption of a constant DC link voltage. Otherwise, if the DC link voltage is to be varied, the firing angles, too, need to vary to keep the fundamental component at the desired level, and to keep the first significant harmonic the same as expected. This means that the PPWM has to be either employed in conjunction with the half-wave bridge which can offer a constant DC link voltage, or else, the firing angles have to be constantly read from a look-up table, based on the new DC link voltage. Alternatively, several new methods for on-line calculation of the firing angles have been recently proposed. One example of such methods is the work done by Mohaddes et. al. at the University of Manitoba in which switching angles are controlled by a feedforward artificial neural network[21] and the controller is capable of maintaining constant load voltage with a variable DC link voltage.

Also, it is noteworthy that in the above analysis, for the sake of generality, the 11 firing angles are chosen in a way that all of the first 10 harmonics, i.e. 3, 5, 7,..., 21 are eliminated, and the first significant harmonic is the 23rd. This is specially useful, when the load is directly connected to the voltage-source inverter, and when significant unbalances are expected in the load. However, in the majority of the practical cases, where the inverter is connected to the load through a three-phase delta-wye transformer (or ungrounded wye, balanced load), tripplen harmonics, i.e. 3, 9, 15 and so on, do not need to be eliminated by the PPWM action, because they will be automatically eliminated in the delta winding of the transformer and will not appear in the load voltage. Removing the tripplen harmonics from the PPWM elimination process, moreover, has two additional advantages which, briefly, are as follows:

1. Based on the equation (3.11), the maximum number of firing angles is 12, if the frequency of the load voltage is equal to 60 Hz, and if the GTO thyristors can be fired at a maximum of 1500 Hz frequency[15]. Leaving the tripplen harmonics intact in the voltage spectrum and devoting the 12 allowed firing angles to eliminating the first 11 non-tripplen harmonics means

that the first significant harmonic will be the 37th, which is higher in nature, compared to the 23rd or 25th harmonic, and therefore, easier to filter through a high-pass filter.

2. Based on Parseval's formula [22], and for the specific square-wave voltage obtained from the PPWM action in the inverter, the sum of the harmonics is always equal to a constant value, or:

$$\sum_{n=1}^{\infty} a_n^2 = \int_0^{2\pi} f(\theta)^2 d\theta = \int_0^{2\pi} V_{DC}^2 d\theta = 2\pi V_{DC}^2 \ . \qquad (3.12)$$

This means that the existence of the tripplen harmonics in the inverter output, which are going to be eliminated automatically by the three-phase transformer, makes the magnitude of the non-tripplen harmonics even smaller.

The end result of the above two facts is a much more sinusoidal load voltage.

2. Sinusoidal Pulse Width Modulation (SPWM): An alternative method for controlling the voltage-source inverter is the Sinusoidal Pulse Width Modulation [23]. In this method the intersections of a triangular waveform and a reference sinewave are used as the firing instances in the inverter. The triangular waveform has a magnitude of 1, and a frequency of p times that of the load frequency. The reference sinewave, has a frequency equal to the load frequency, in this case 60 Hz, and its magnitude varies between zero and one. The load voltage obtained through this method will have a fundamental frequency of 60 Hz, and the per unit magnitude of the fundamental component will be equal to that of the reference sinewave. Because of the PWM action, the harmonic of the order p will be dominant. If p is chosen as a multiple of 3, in the present case 9, the dominant harmonic will be automatically eliminated in the delta winding of the three-phase transformer, and the rest of the harmonics can be filtered by a high-pass filter. Fig. 3.13 shows the PWM waveforms and the resulting phase voltage.

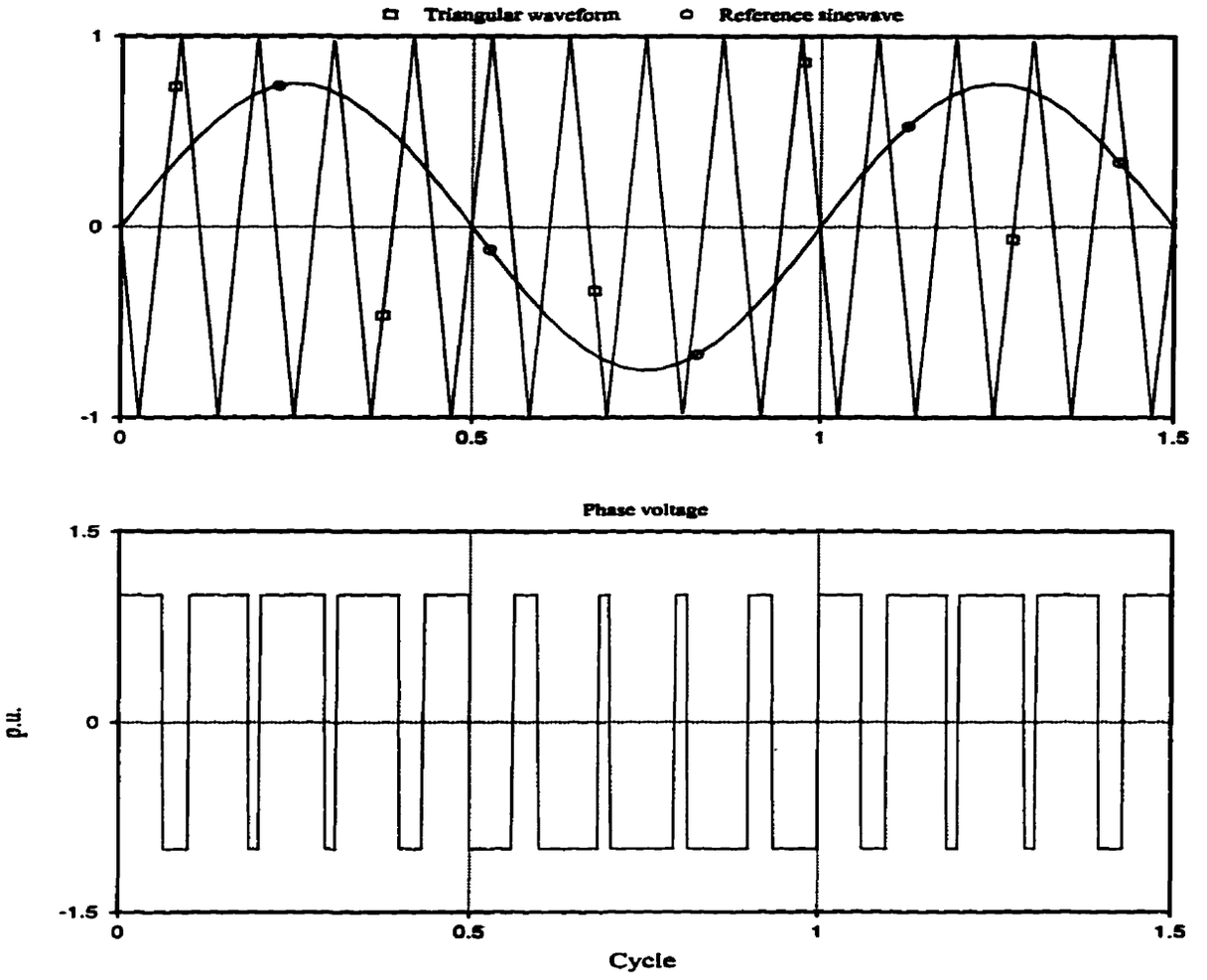

Fig. 3.13 - PWM Waveforms and the Phase Voltage

Fig. 3.14 shows the result of a Fourier analysis on the phase voltage in Fig. 3.13.

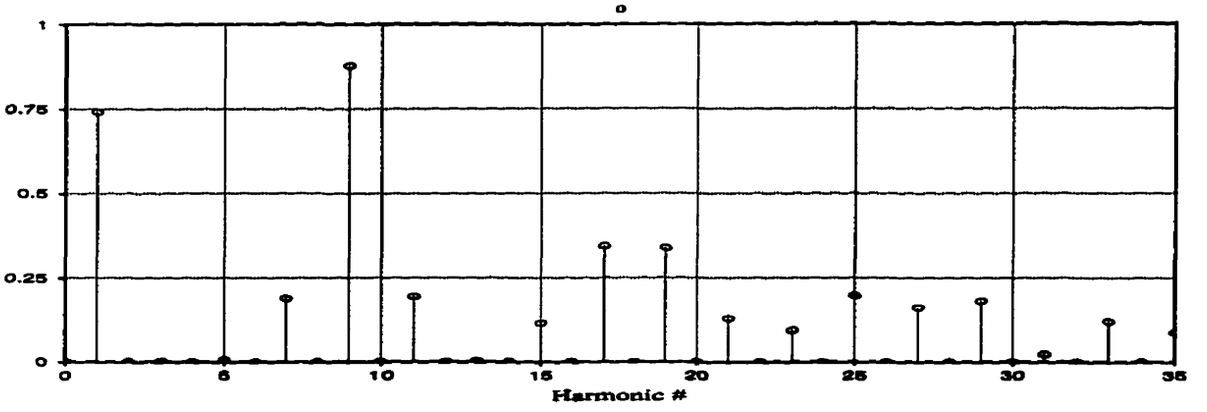

Fig. 3.14 - Harmonic Spectrum of the Phase Voltage

The dominant harmonic, as expected, is the 9th. And the magnitude of the fundamental component is equal to that of the reference sinewave, i.e. 0.75 p.u.

The ratio of the reference sinewave peak magnitude to the peak magnitude of the triangular waveform is called the modulation index, and it can be changed by a control system, in order to maintain a constant value for the fundamental component when the DC link voltage varies. This concept is used in the control system shown in Fig. 3.15, whereby the load rms voltage is protected against the fluctuations in the DC link voltage, through a variable modulation index, denoted by m here.

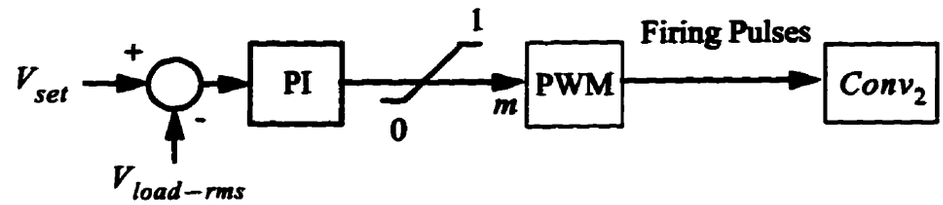

Fig. 3.15 - Load RMS Voltage Control

3.5. Summary of the Chapter

In this chapter, a practical solution for small power tapping from HVDC transmission systems was proposed. Details of the proposed scheme, including the possibility of using a single-phase air-core transformer in it, were discussed. Also, different control regimes for the three converters were proposed and studied.

Chapter Four

Feasibility Studies of the Proposed Scheme

In order to examine the feasibility of the proposed scheme, and to observe the performance of the control systems, the digital simulation software package PSCAD/EMTDC was used [18]. This package is an electromagnetic transients simulation program, with a graphical user interface, that can simulate power systems as well as power electronic components. The simulation was done in two stages. The first stage was to examine the general feasibility of the tapping scheme, and the second stage dealt with more detailed operation of the system, in the face of varying DC current in the transmission line, as well as variations in the local load. The results of these two stages of simulation are presented here.

In both stages of the digital simulation, the air core transformer was simulated using the conventional single-phase transformer model existing in PSCAD/EMTDC. The only difference was that the air core nature of the transformer was modelled by a 0.3 per unit leakage reactance,

as well as a 30% magnetizing current in the model. More accurate representation of the air-core transformer is to be presented in Chapters Six.

4.1. General Operation of the Tapping Scheme

In order to study the tap's general operation, and at the first stage, the variable-frequency control regime (Fig. 3.8) was chosen for the series tap. An uncontrolled (diode) configuration was selected for the single-phase bridge, $Conv_1$, so no control is applied on the DC link voltage. And finally, the voltage-source inverter, $Conv_2$, was controlled by the PPWM technique.

I it was assumed that the DC current in the main DC line is 2 kA, and the local load is a 1.25 MVA impedance load with a lagging power factor of 0.8. For the PPWM technique in the three-phase inverter, since no three-phase transformer was employed in the load,11 angles α_1 to α_{11} were calculated, in anticipation of having the output voltage free from the first 10 odd harmonics, i.e. harmonic numbers 3,5,..., 21. The system was started at Time=0 s. and the local load was applied on the inverter at time=0.1 s.

Fig. 4.1 shows the positive and negative envelopes of the capacitor C_1 voltage, as well as its rms value, set to be equal to 2.5 kV by the control system. It is clear that the voltage does not exceed the maximum allowable value of 4.5 kV.

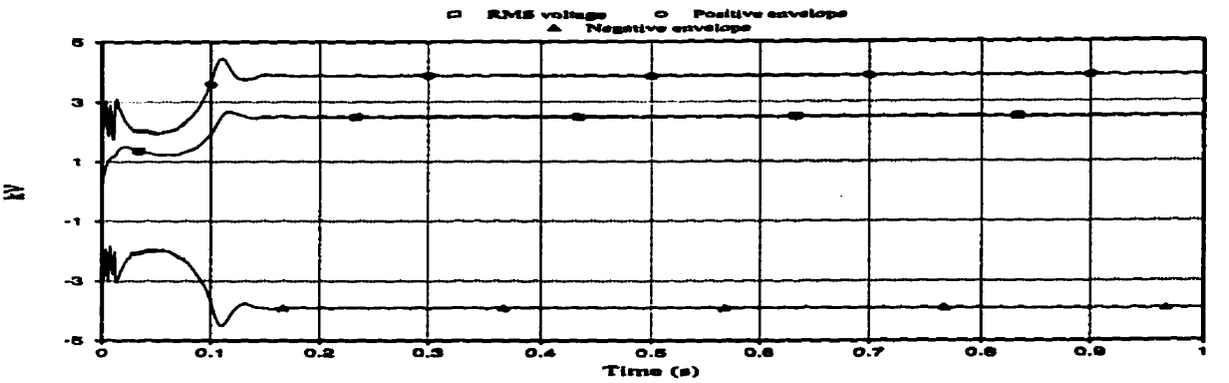

Fig. 4.1 - Capacitor C1 Voltage

Fig. 4.2 shows the saw-tooth voltage across the capacitor C_1 in the steady state. The voltage is close to what was expected. The deviation from the perfect saw-tooth shape is because of the single-phase transformer's primary current passing through the tap capacitor.

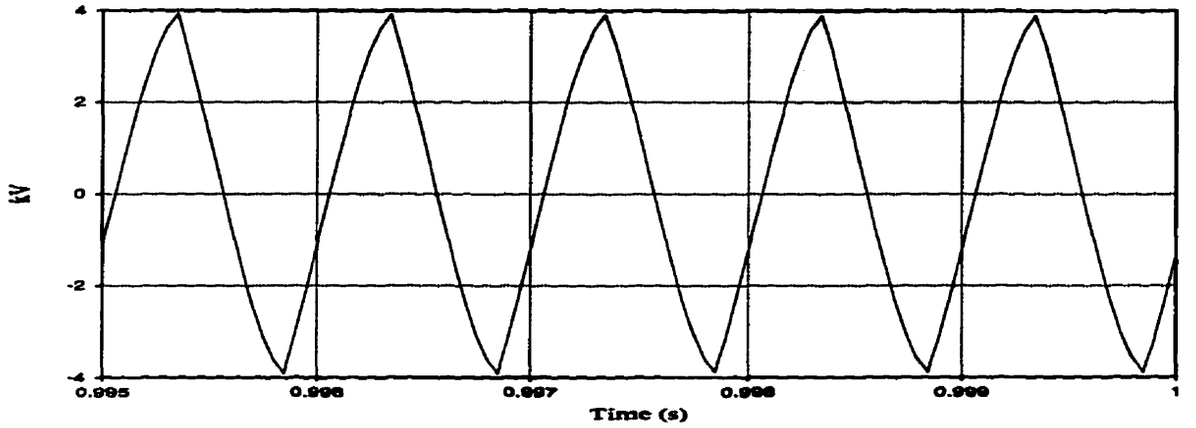

Fig. 4.2 - Tap's Capacitor Voltage

Fig. 4.3 shows the firing frequency of the series tap. The frequency, in the steady state, is about 1 kHz, which is equal to the value chosen in the design of the system. The input voltage to the controller, Vmax, is ramped at the beginning, and since the capacitor voltage is higher than the input voltage (still lower than the maximum value), the frequency reaches its upper limit, but as soon as the capacitor voltage drops below the input value, the frequency is decreased to keep the voltage at the desired level. As soon as the load is applied on the system, the frequency is slightly increased.

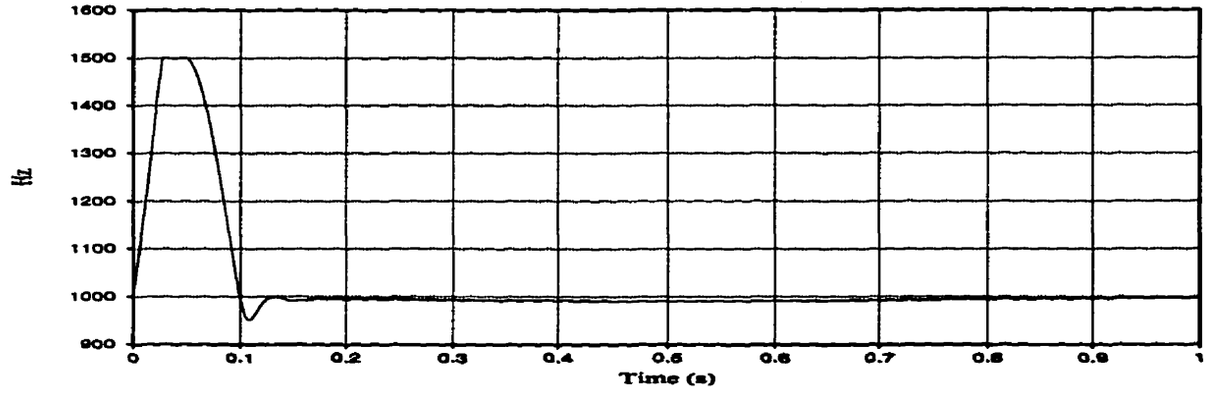

Fig. 4.3 - Tap's Firing Frequency

Fig. 4.4 shows the voltage of the intermediate capacitor, C_2. As mentioned earlier, the voltage control for the intermediate DC link capacitor was not used in the first stage and instead, a diode bridge was used to rectify the single-phase transformer's secondary voltage. The resulting DC voltage, nevertheless, is quite satisfactory.

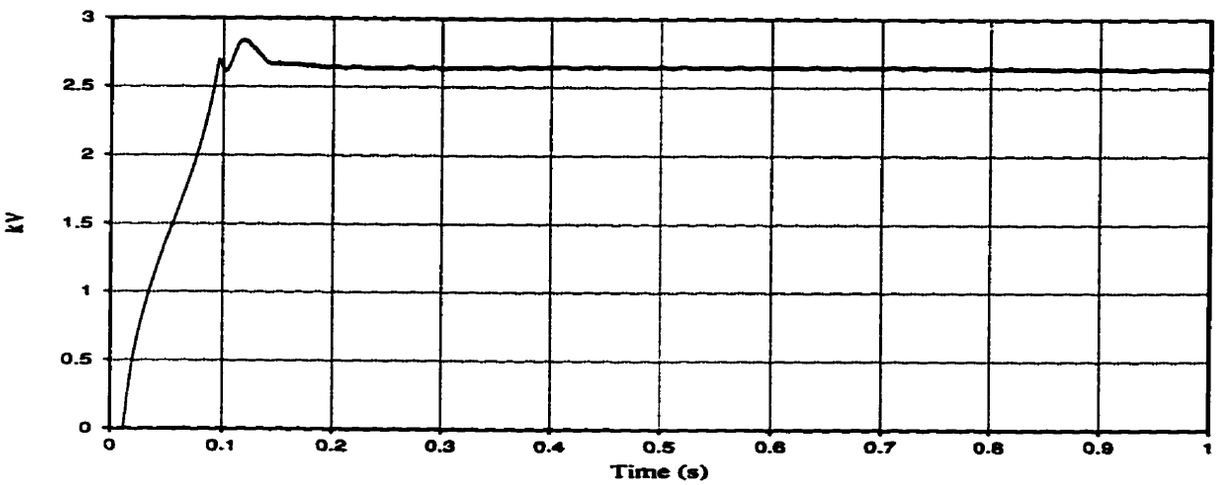

Fig. 4.4 - Intermediate Capacitor (C2) Voltage

In Fig. 4.5, the output of the three-phase voltage-source inverter, i.e. the line-to-line voltage between phases a and b, V_{ab}, is shown. The PWM angles used in the inverter, as well as the fundamental frequency component (60 Hz) are clearly shown.

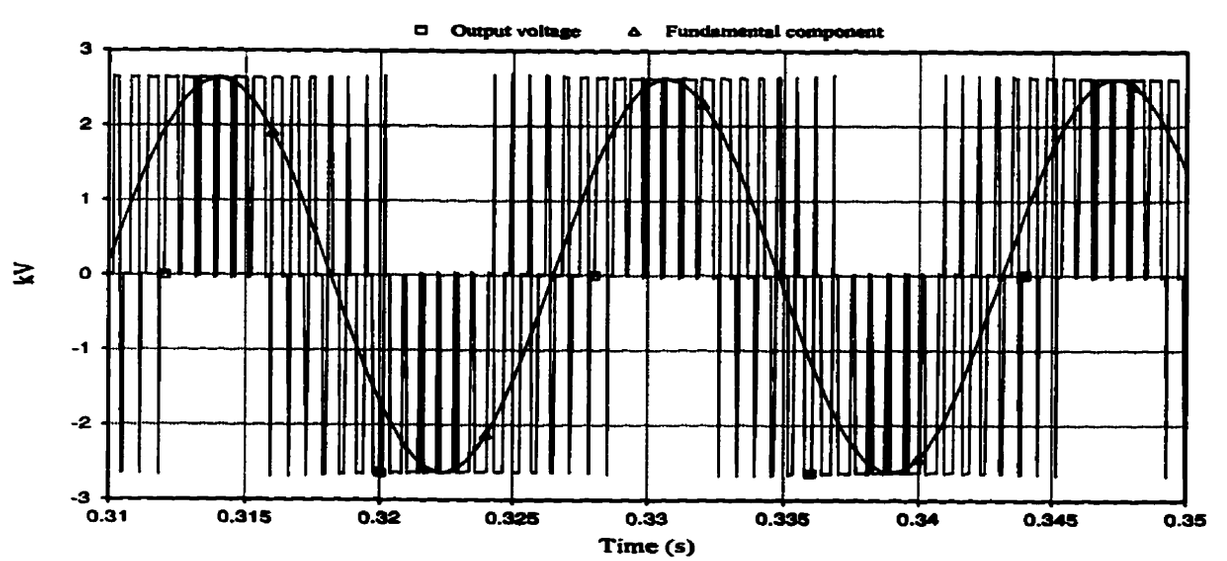

Fig. 4.5 - Load's Line Voltage, Vab

A Fourier analysis was performed on the output voltage to determine the harmonic content of the voltage. The resulting harmonic spectrum of the load's voltage is shown in Fig. 4.6. It is evident that the first significant harmonic is the 23rd, as anticipated from the selected PWM angles. The peak value of the fundamental component is about 2.3 kV, which is close to the sought value of 1.0 p.u. For the voltage, the Total Harmonic Distortion (THD) is equal to 82.3% which indicates the need for installation of harmonic filters on the load side.

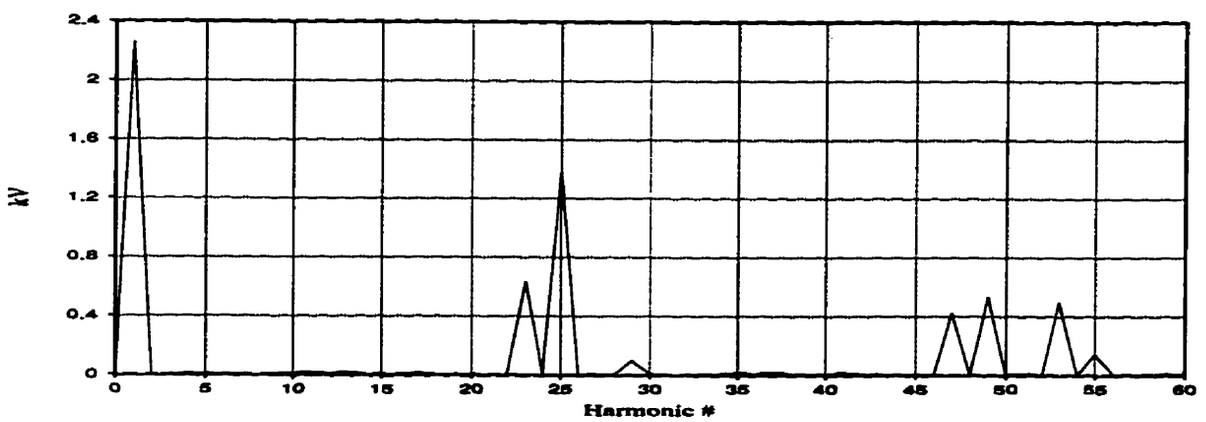

Fig. 4.6 - Vab Harmonic Spectrum

Fig. 4.7 shows the three line currents of I_a, I_b, and I_c, being fed to the load. The sinusoidal nature of the currents is evident, even in the absence of filtering devices. This is due to the inductive nature of the load.

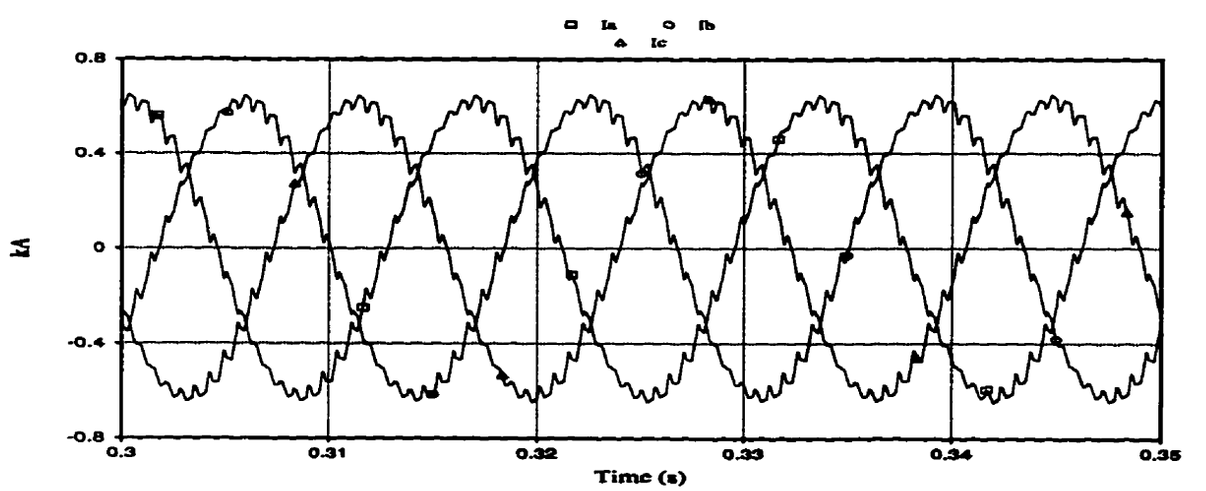

Fig. 4.7 - Load Line Currents

Further Fourier analysis was conducted on the current waveforms. The result is shown in Fig. 4.8. Again, the first significant harmonic is the 23rd, although in the case of current, of a much lower value, as pointed out earlier. The THD for the current is only 4.8%.

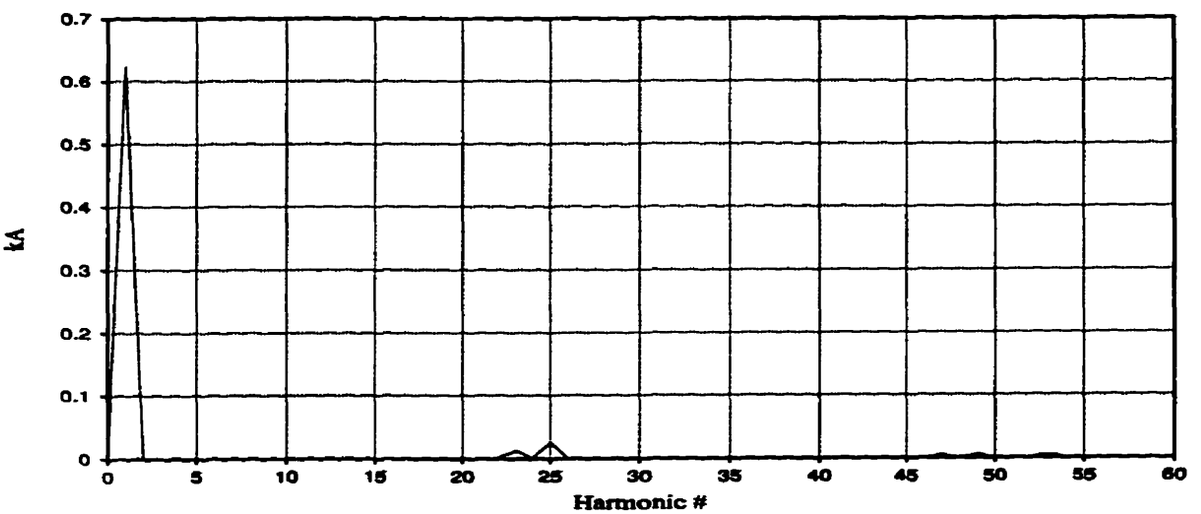

Fig. 4.8 - Ia Harmonic Spectrum

And finally, Fig. 4.9, shows the real and reactive powers, P and Q, tapped from the HVDC system into the local load. The total power is slightly less than 1.25 MVA, because of the voltage drop in the intermediate DC link.

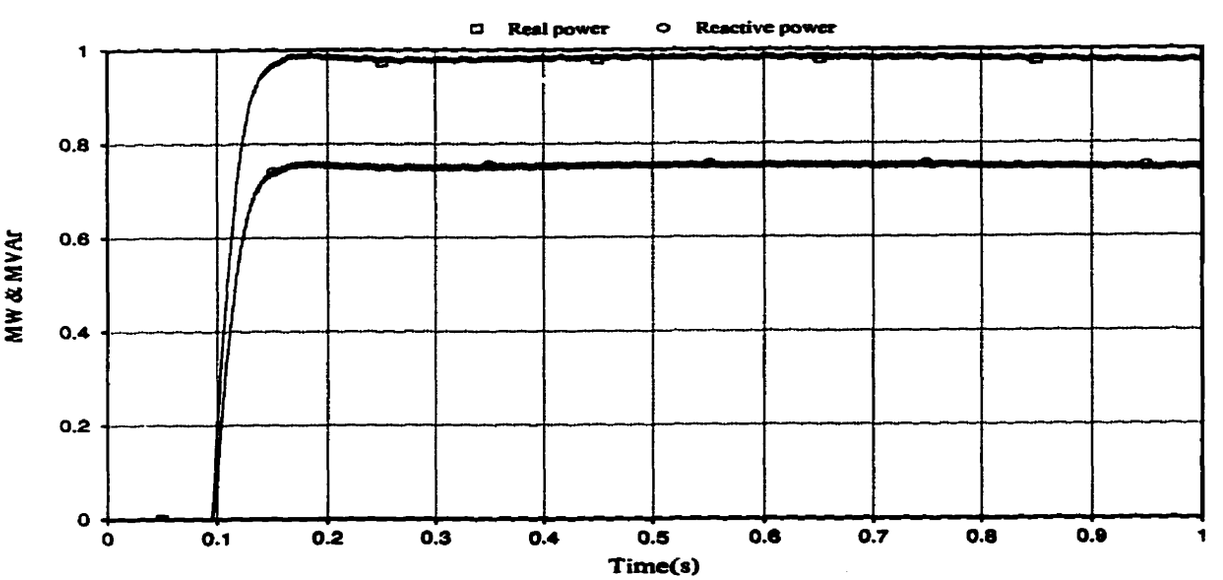

Fig. 4.9 - Laod's Real and Reactive Powers

The simulation results shown in the above serve to verify the feasibility of the scheme, within reasonable operating standards. Also, the 1 MW tapped power is more than enough for most of the isolated loads, as discussed earlier in Section 2.1.

4.2. Detailed Operation of the Tapping Scheme

After establishing the feasibility of the scheme, the operation of the system under variable line current and different load conditions was simulated. In this stage, the half-wave single-phase rectifier, along with its voltage control regime (Fig. 3.11) were incorporated into the single-phase to three-phase converter.As well, the local load was isolated from the single-phase to three-phase converter through a three-phase transformer. The voltage-source inverter is still controlled by PPWM technique, and the firing angles remain the same as before, despite the presence of the three-phase transformer in the load configuration. In a practical case, however, the removal of tripplen harmonics can be done by the transformer, as mentioned in Section 3.4.3.

It was assumed that the DC current in the main DC line is 2 kA at the beginning of the tap start-up. A local load of 1.0 MVA, with a lagging power factor of 0.8, was chosen to represent the peak load. The firing angles in the PPWM technique were calculated and chosen in anticipation of having the output voltage free from the first 10 harmonics, i.e. harmonics number 3,5,...21.

The system was started at Time=0 s. At Time=0.2 s., when the tap capacitor C_1 has reached at steady state operation, the single-phase rectifier is activated and the DC link capacitor begins to charge. At Time=3.5 s., 40% of the load is applied on the inverter. At Time=5 s., the load is increased to 70% of the maximum load, and finally, at Time=6.5 s. the load reaches its peak of 1 MVA. At Time=8 s., the DC current in the main DC line, starts to vary from 1.0 p.u. to 0.5 p.u. and again to its rated value of 2 kA. For convenience, the variations in the DC current have

been applied by a sinusoidal waveform. The results of the first 10 seconds of the simulation are presented here.

Fig. 4.10 shows the DC current in the main DC line.

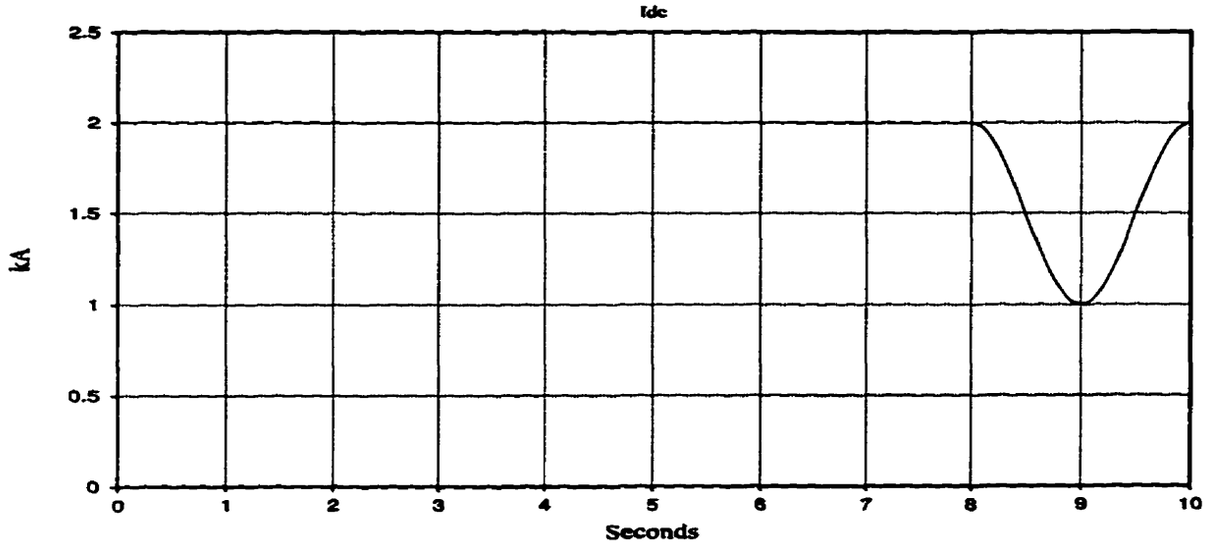

Fig. 4.10 - Current in the DC Line

Fig. 4.11 shows the output of the firing frequency controller. The frequency is about 800 Hz at no-load, and is increased as the load increases. The variations of the frequency in response to the changes in the DC line current are evident.

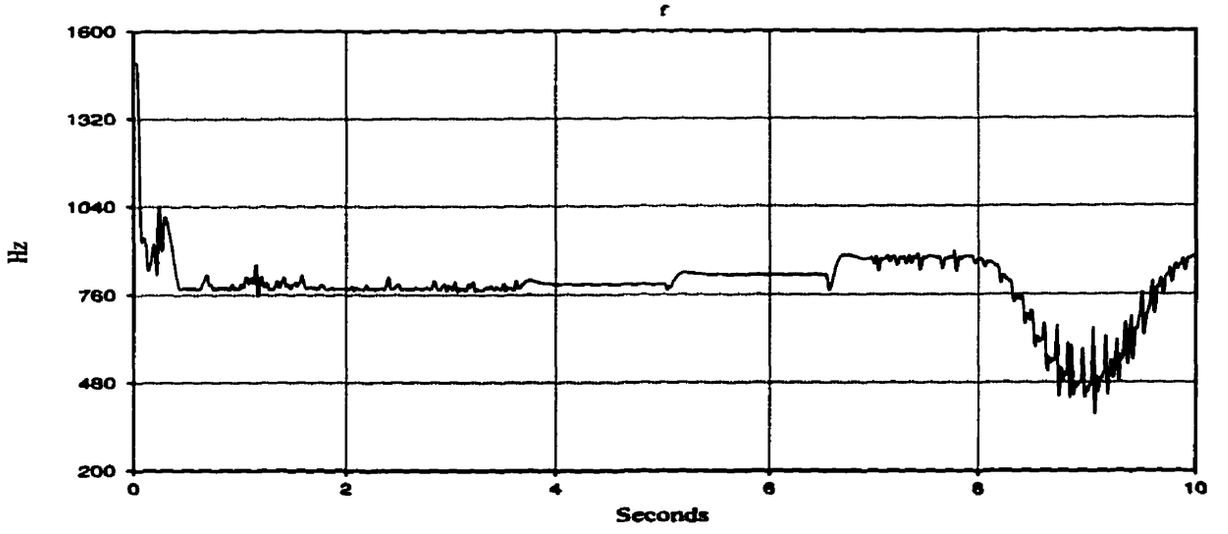

Fig. 4.11 - Tap's Firing Frequency

Fig. 4.12 shows the positive and negative envelopes of the capacitor C_1 voltage.The peak voltage, most of the time, does not exceed the set limit of 4.5 kV, but during some transients, the voltage may exceed the limit temporarily. For this reason, it is necessary to set the voltage limit slightly below 4.5 kV.

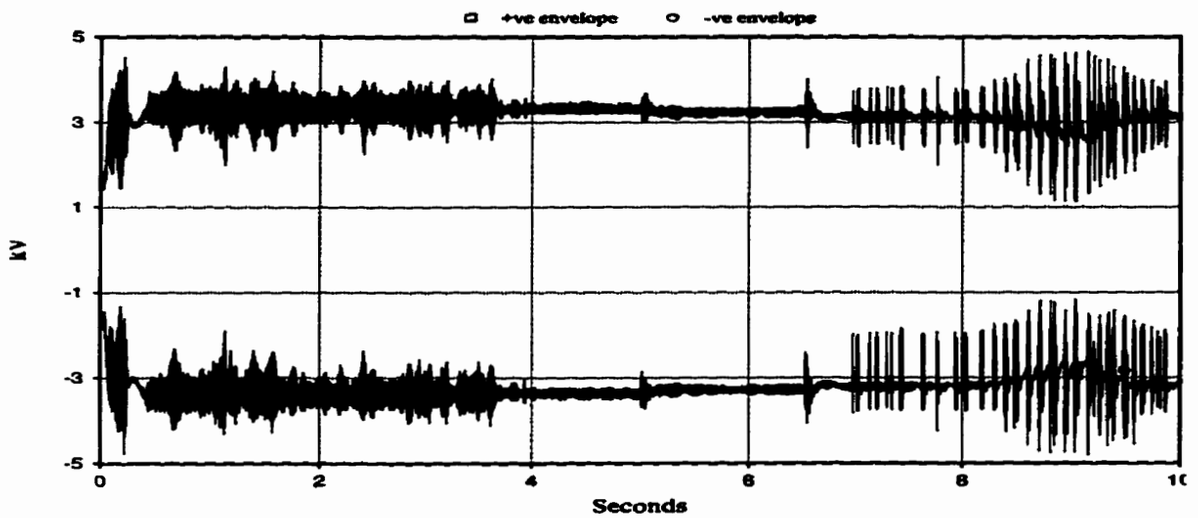

Fig. 4.12 - Voltage Envelopes for V_{C_1}

Fig. 4.13 shows the above mentioned voltage in the steady state.

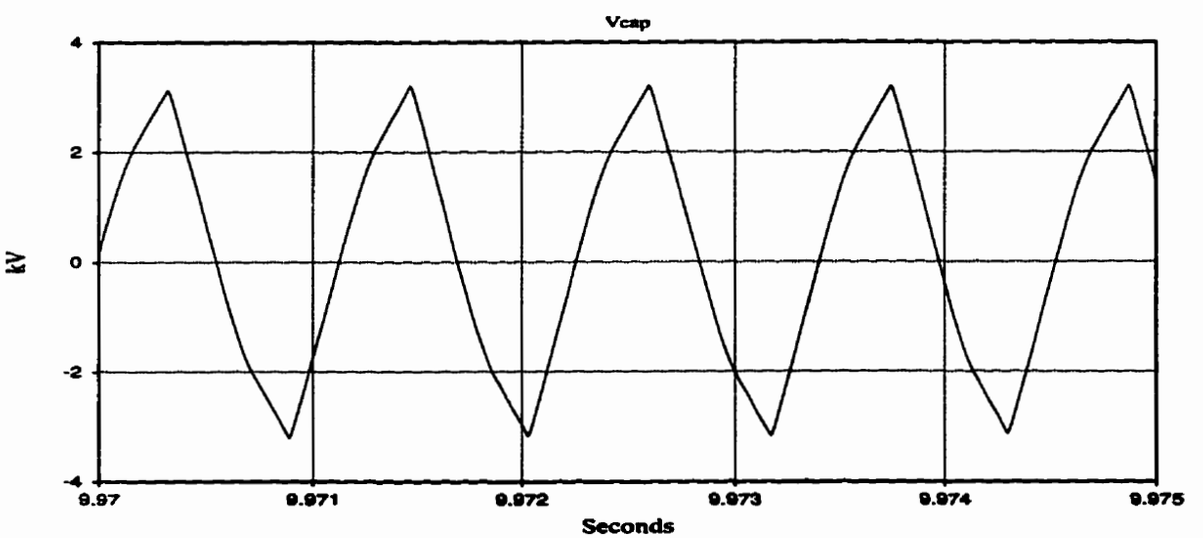

Fig. 4.13 - V_{C_1} in the Steady State

Fig. 4.14 shows the series tap voltage in the steady state. Because of the two-pulse action of the series GTO bridge, the frequency of this voltage is twice the frequency of the voltage across the tap's capacitor, V_{C_1}. Also, it is evident that this voltage has a DC value of about 0.5 kV, which when multiplied by the DC current of 2 kA passing through the tap, amounts to about 1 MW power, being tapped from the HVDC system, and fed to the local load and tap losses.

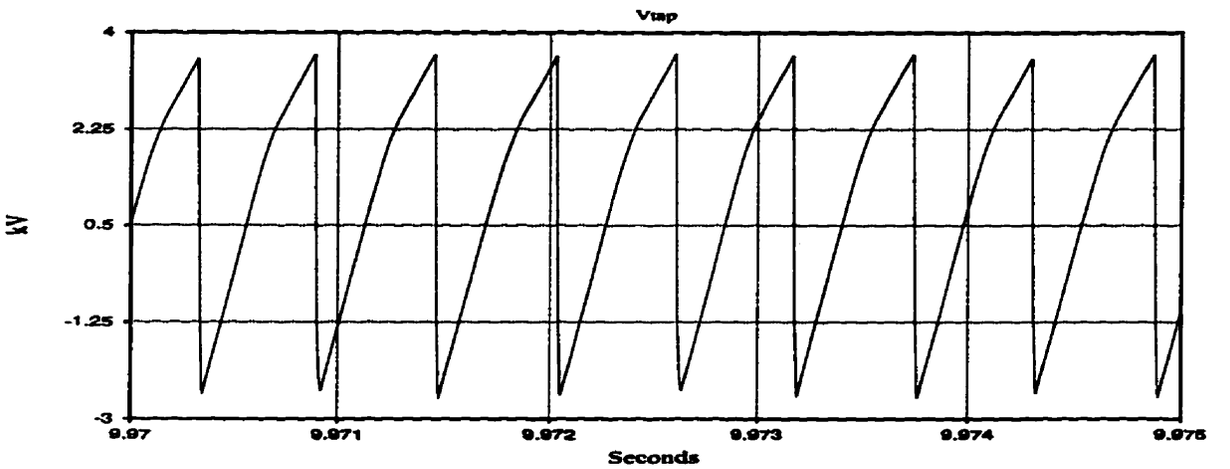

Fig. 4.14 - V_{Tap} in the Steady State

Fig. 4.15 shows the current passing through the tap capacitor, in the steady state, which is the combination of the DC line current and the primary current of the single-phase transformer.

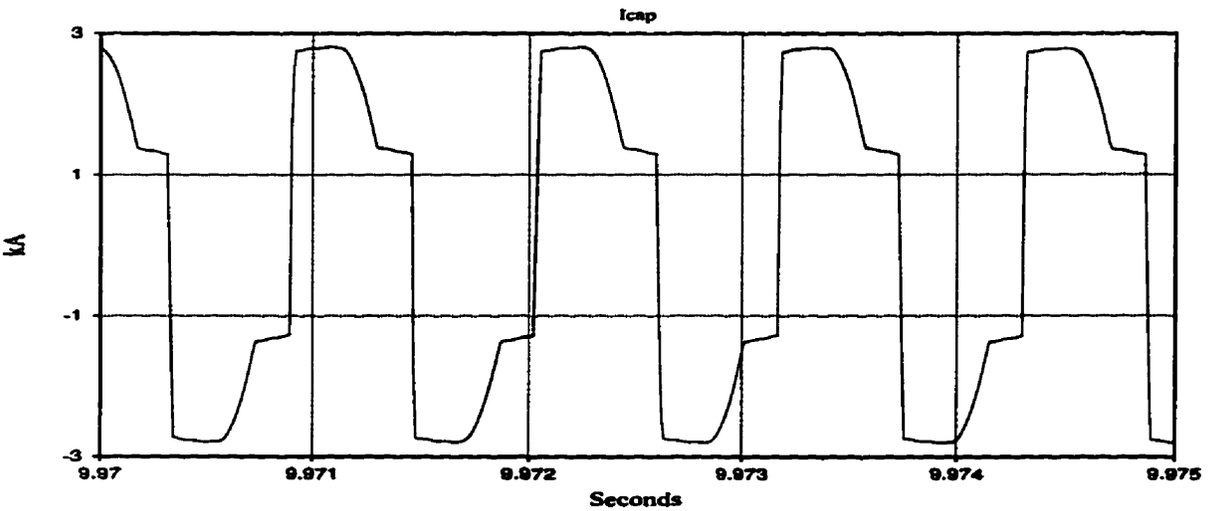

Fig. 4.15 - I_{C_1} in the Steady State

Fig. 4.16 shows the DC link voltage and the setting for the DC link voltage controller. In the course of the system simulation, it was found that maintaining a constant DC link voltage for the whole range of the load is quite hard, if not impossible, and the voltage setting of the controller needs to be adjusted for various values of the load, to maintain a stable operation. The adjustment was done in three steps, as was the application of the full load on the inverter. The decrease in the DC link voltage, which directly results in a decrease in the three-phase voltage output, was compensated by the tap-changer action in the three phase load transformer.

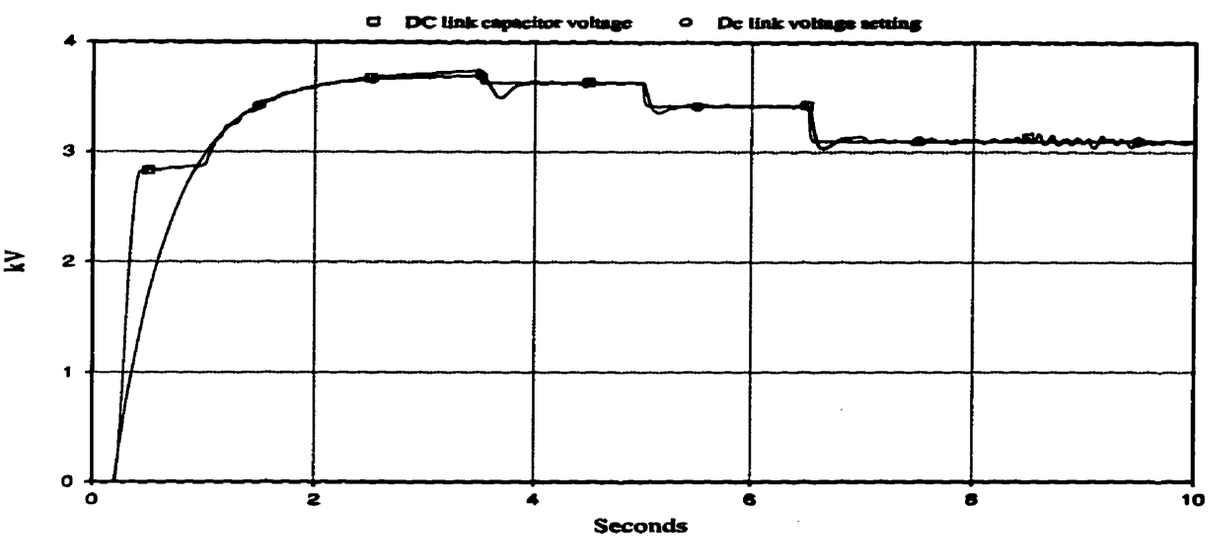

Fig. 4.16 - DC Link Voltage and Voltage Setting

This point, as well as the response of the system to variable DC current which will be shown later, indicate the necessity of considering alternative control methods which while providing the system with an acceptable performance, eliminate the need of a tap-changer in the three-phase transformer in order to maintain a constant load voltage. The SPWM method introduced in Section 3.4.3, combined with an uncontrolled bridge configuration for the single-phase rectifier will be employed in Chapter Five to eliminate this problem.

Fig. 4.17 shows the output of the DC link voltage controller, α_{order}, issued to the thyristors in the single-phase rectifier.

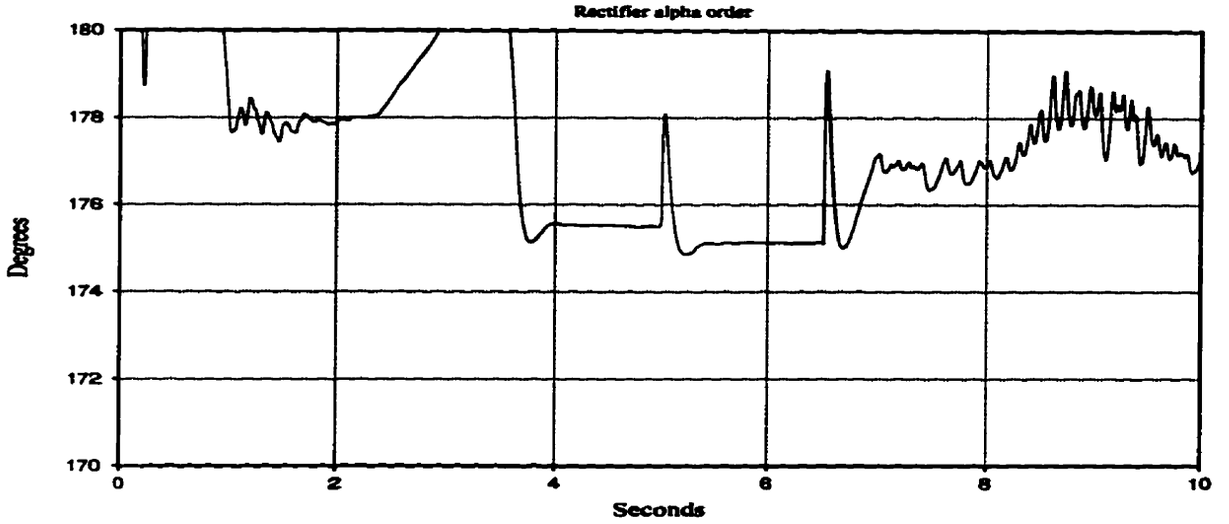

Fig. 4.17 - Rectifier Firing Angle

Fig. 4.18 shows the line-to-line voltage V_{ab} applied on the load.

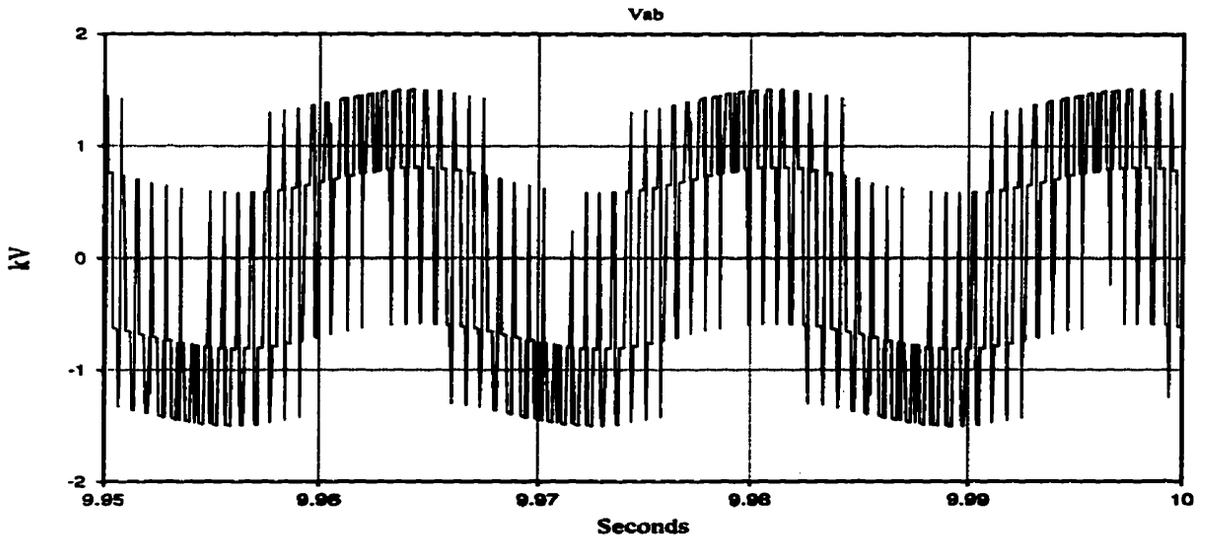

Fig. 4.18 - Load's Line-to-Line Voltage

Fig. 4.19 shows the Fourier harmonic spectrum of the same voltage. It is evident that the first significant harmonic is 23rd, as anticipated from the PPWM. The Total Harmonic Distortion (THD) of the voltage is about 75%, which is slightly smaller than the case where the three-phase transformer was not employed, but still too large for practical applications.

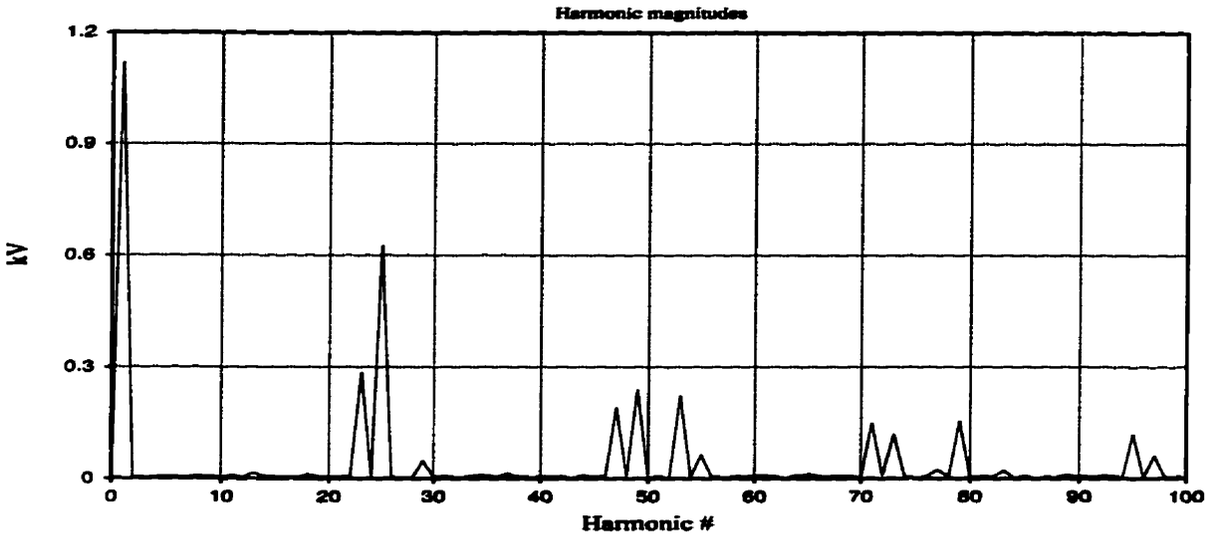

Fig. 4.19 - Load Voltage's Harmonic Spectrum

Fig. 4.20 shows the load currents I_a, I_b, and I_c.

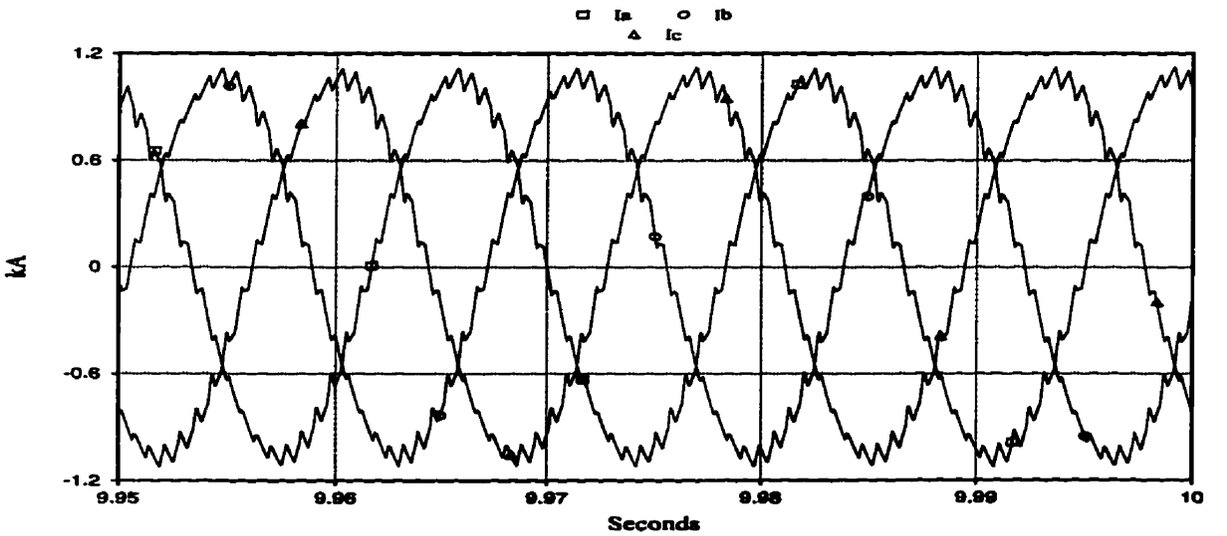

Fig. 4.20 - Load's Line Currents

Fig. 4.21 shows the harmonic spectrum of I_a. The currents, because of the filtering action of the inductive load and the three-phase transformer, are more sinusoidal, and the THD of the current, even in the absence of any filters, is about 4.5%. Again, the first significant harmonic is the 23rd.

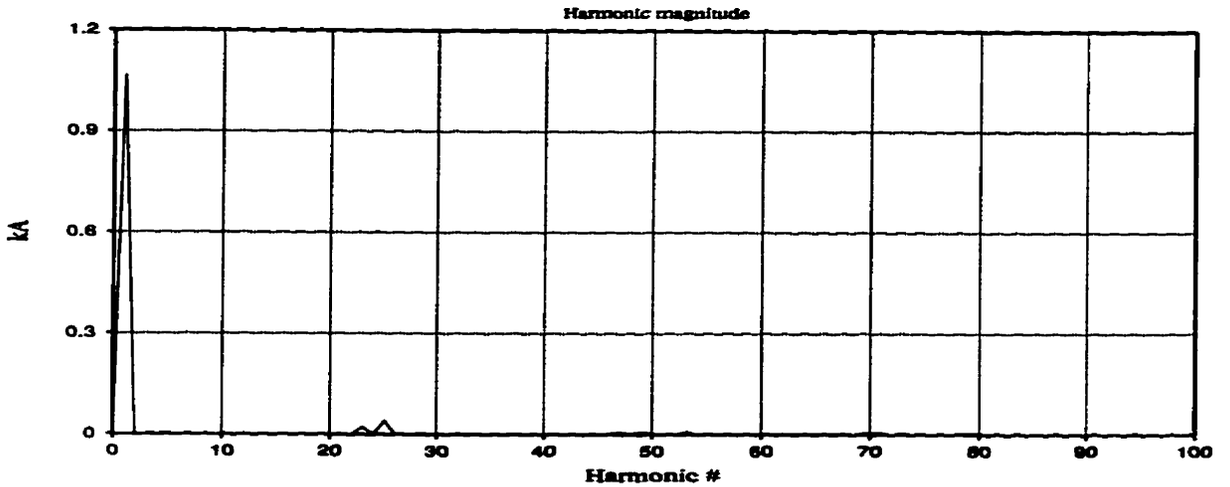

Fig. 4.21 - Load's Current Spectrum

And finally, Fig. 4.22 shows the active and reactive powers, tapped from the HVDC system, and fed to the local load. The flow of power is reasonably smooth for up to 80% of the peak load, and it starts to vary in a margin of about +/- 5%, as the load reaches its peak value.

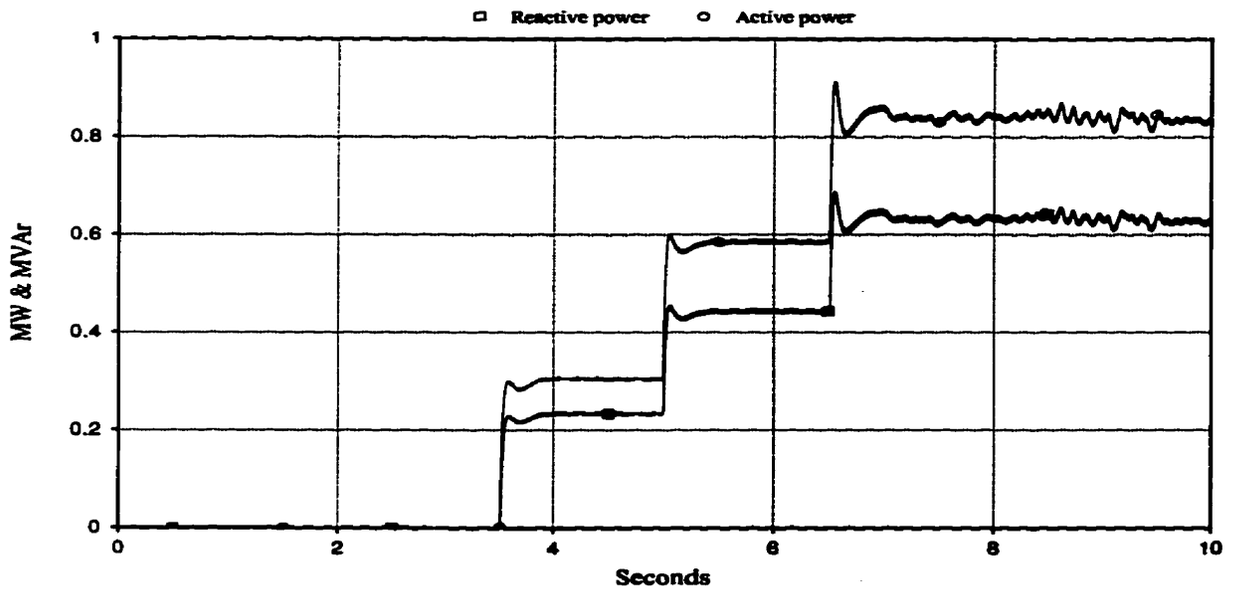

Fig. 4.22 - Load's Active and Reactive Powers

The oscillations become more severe, when the DC current in the HVDC system starts to vary, and the maximum oscillation occurs when the DC current is at its minimum of 0.5 p.u. This

can be attributed to the fact that the control system parameters are optimal for a certain range of the load. As mentioned earlier, this fact, among other things, is considered as the indication for the necessity of studying alternative control strategies in order to be able to select an optimum set of control regimes and converter bridge configurations.

4.3. Summary of the Chapter

It was shown, through the use of the digital simulation software package PSCAD/EMTDC, that the proposed scheme is able to operate as a small power tapping station to feed loads of up to 1.25 MVA from an HVDC transmission system. The waveshapes of the tap voltage, as well as the quality of the load voltage and current are within the expected margins. It was found, however, that the performance of the control systems studied in the first stage of the simulation needs improvement.

Chapter Five

System Operation with Alternative Control Regimes

In the previous Chapter, the operation of the proposed scheme was digitally simulated, and the results showed the technical feasibility of the tapping station, using the variable frequency regime for the series tap, both controlled and uncontrolled configurations for the single-phase rectifier, and PPWM technique for the three-phase inverter.

The performance of the control systems, however, proved to be not as satisfactory as expected. In this Chapter, the performance of the system, in conjunction with the alternative control regimes introduced in Chapter Three, will be studied. Also, the possibility of using ordinary thyristors instead of GTO thyristors in the series tap will be examined. Similar to Chapter Four, the air-core nature of the single-phase transformer has been modelled by a 0.3 p.u. leakage reactance and a 30% magnetizing current in the existing conventional transformer model in PSCAD/EMTDC, and the accurate representation of the air-core

transformer has been left for Chapter Six.

5.1. Control Technique for the Three-phase Inverter

To control the three-phase voltage-source inverter, the PPWM technique employed in the previous Chapter has been replaced by the SPWM throughout the present Chapter. The frequency of the triangular waveform is chosen to be equal to 15 times that of the load frequency. Fig. 5.1 shows the expected square-wave inverter output, and the result of a Fourier analysis on it.

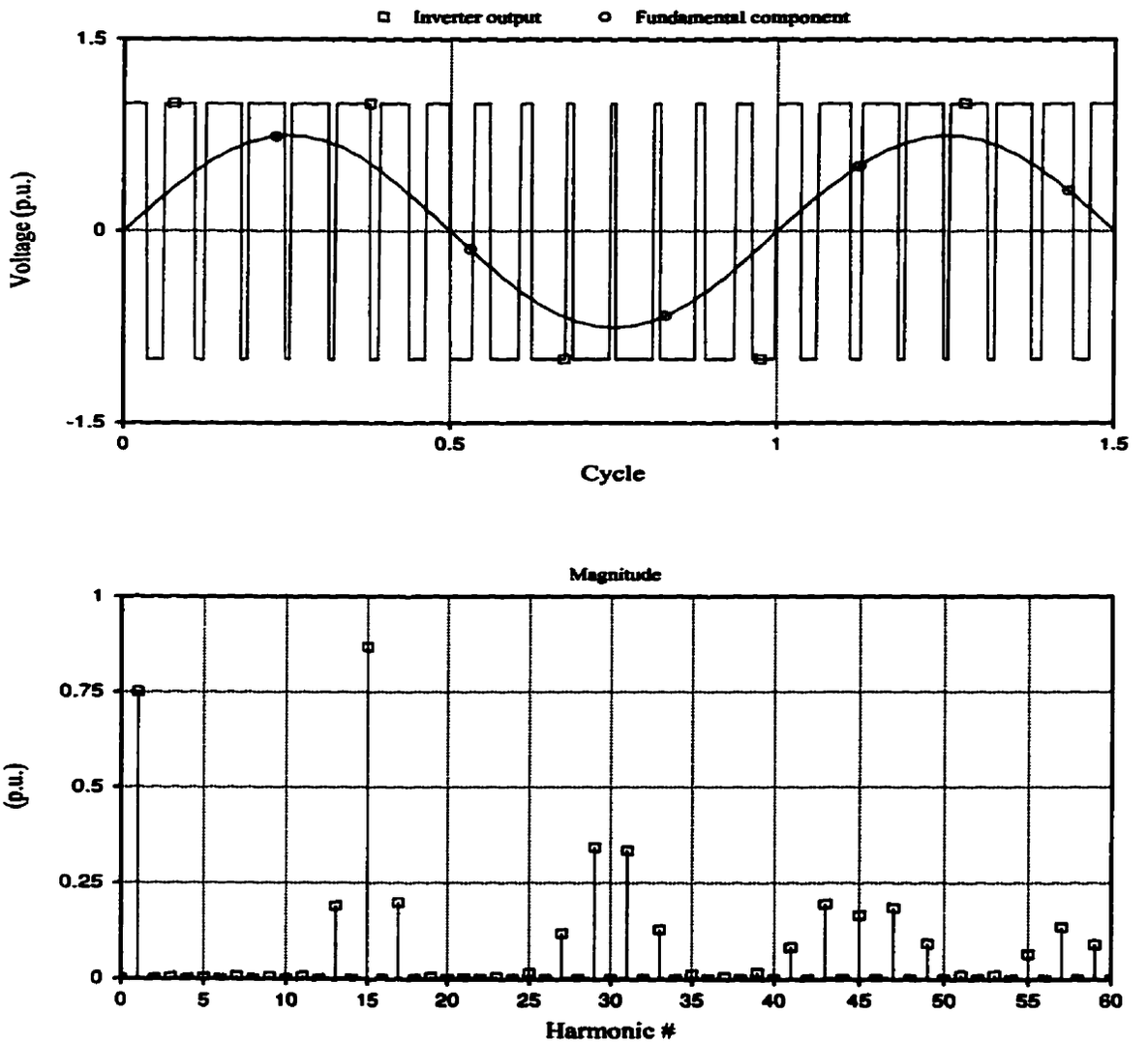

Fig. 5.1 - Inverter Output and its Harmonic Spectrum

As expected, the dominant harmonic is the 15th, with a 0.9 p.u. magnitude, and the fundamental component has a value of 0.75, equal to the selected modulation index, *m*. The dominant harmonic, as well as other tripplen harmonics present in the voltage harmonic spectrum, i.e. harmonic numbers 27, 33, 45, and so on, are expected to be eliminated by the three-phase transformer. For the other harmonics, 4 tuned filters, as well as one high-pass filter were designed and utilized in the simulation. Fig. 5.2 shows the configuration of these filters, and in Table 5.1 the numeric values of the filter components are presented.

a. Tuned Filter b. High-pass FIlter

Fig. 5.2 - Voltage Harmonic Filtering Configurations

Table 5.1 - Numeric Values of the Filtering Devices

Harmonic #	C (uF)	L (mH)	R (Ohms)
13	53.814	0.774	-
17	53.695	0.451	-
29	54.07	0.155	-
31	54.078	0.135	-
High-pass	54.105	0.0703	500

As mentioned in Section 3.4.2, since the SPWM technique, in conjunction with the variable modulation index, *m*, is capable of operating with variable DC link voltage, the uncontrolled

(diode) configuration has been selected for the single-phase rectifier throughout this Chapter.

5.2. Variable Frequency Voltage

The operation of the tapping scheme, initially, is simulated with the variable frequency regime for the series tap. The system is started at Time=0 with a maximum DC current of 2 kA. After the steady state is reached, the load is applied on the system in four steps, and at the peak load, the DC line current starts to decrease to 0.8 kA, and again, is increased to 2 kA. Fig. 5.3 shows the DC line current.

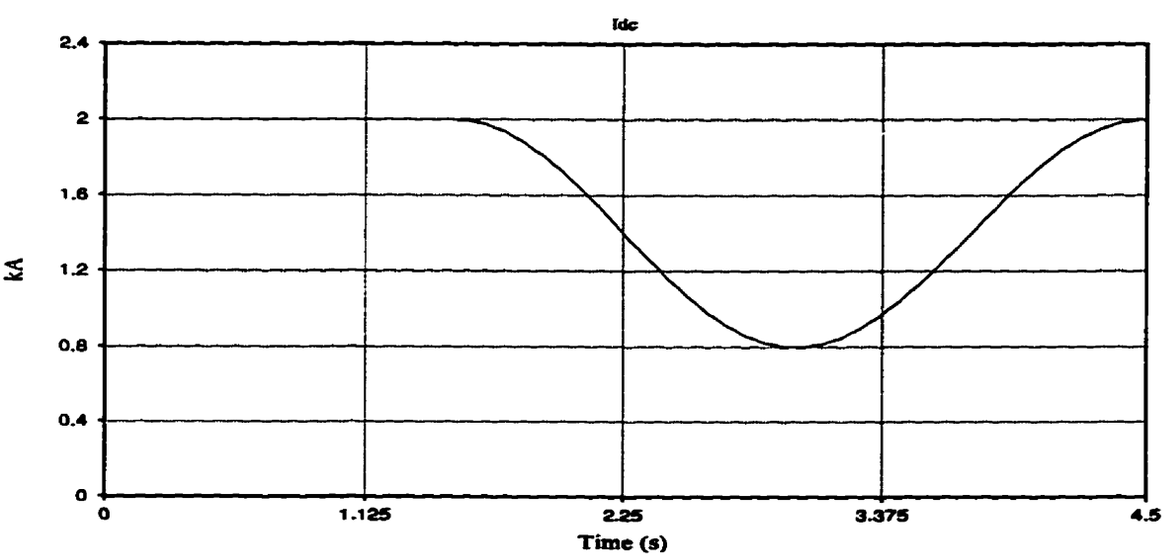

Fig. 5.3 - DC Line Current

The applied variation on the DC line current is somewhat faster than the variations in the normal working conditions of an HVDC system, and the practical variations are expected to be slower, thereby giving more time to the control systems to react. The result will be improved results compared to the ones presented here.

Fig. 5.4 shows the output of the firing frequency controller. In response to the variations in the DC line current, as well as in the local load, the frequency has changed to maintain a

smooth tapping operation.

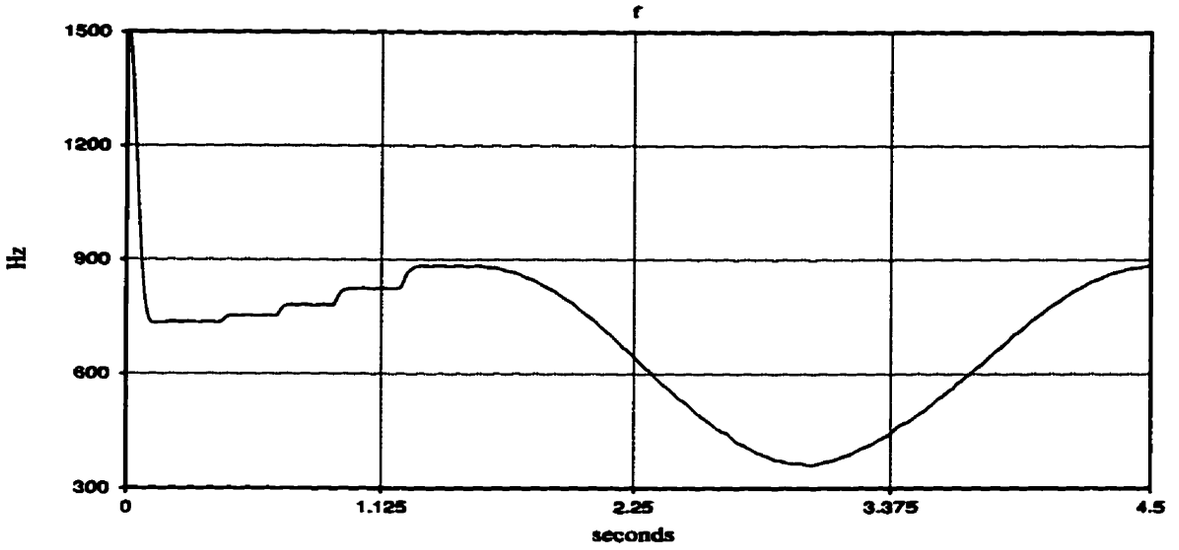

Fig. 5.4 - Firing Frequency

Fig. 5.5 shows the positive and negative envelopes of the capacitor C_1 voltage. The voltage has been kept within the set limit ±4 kV. The peak voltage is slightly smaller than the set limit at very low DC line currents, but the effect on the amount of power being tapped, if any, is negligible.

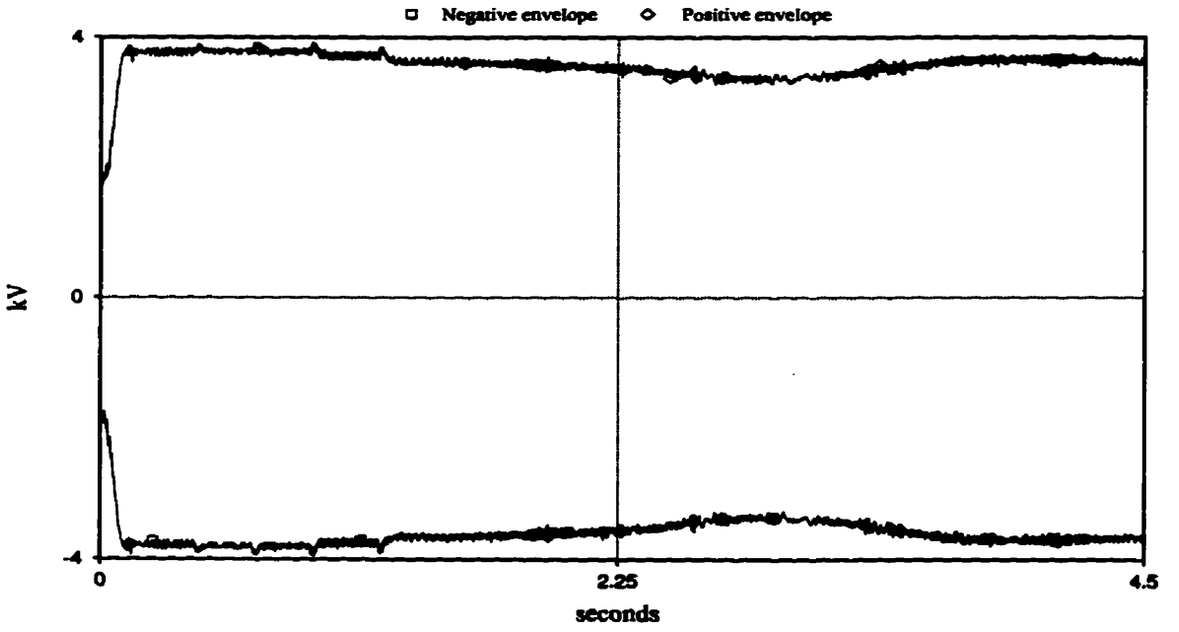

Fig. 5.5 - Vc1 Positive and Negative Envelopes

Fig. 5.6 shows the capacitor voltage, V_{C_1}, and the series tap voltage, V_{Tap}, in the steady state. Because of the two-pulse action of the series bridge, the frequency of V_{Tap} is twice the frequency of V_{C_1}.

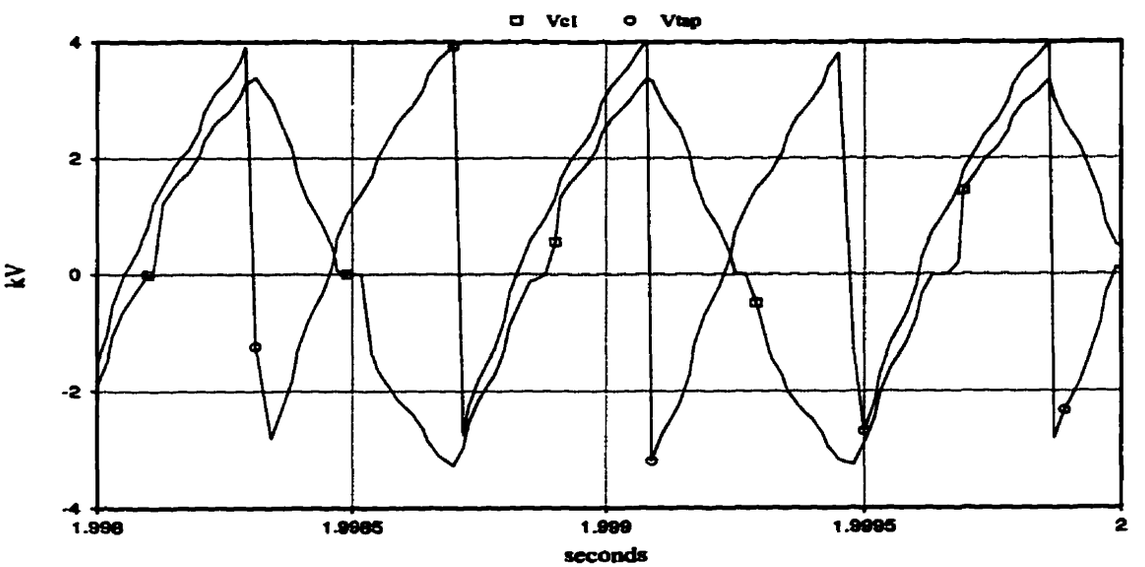

Fig. 5.6 - Vc1 and Vtap in the Steady State

Fig. 5.7 shows the DC link voltage V_{C_2}. The variations in the voltage, which have resulted from the variations in the DC line current, and in the local load, are compensated through the SPWM controller action.

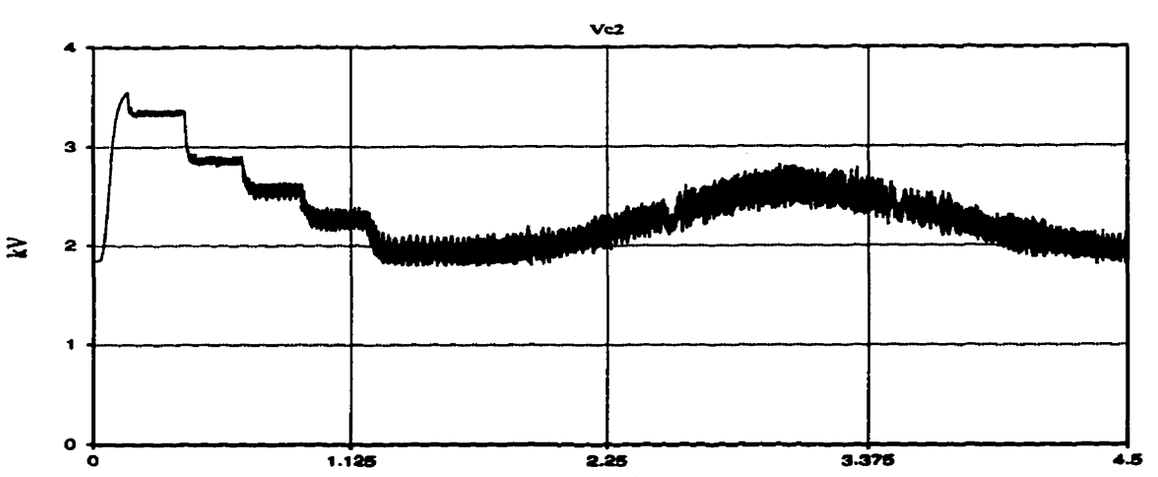

Fig. 5.7 - DC Link Capacitor Voltage

Fig. 5.8 shows the modulation index, *m*, which is being adjusted by the controller shown in Fig. 3.15, in order to maintain a constant fundamental component magnitude in the three-phase inverter output. The variations in *m* are the exact mirror of those in the DC link voltage.

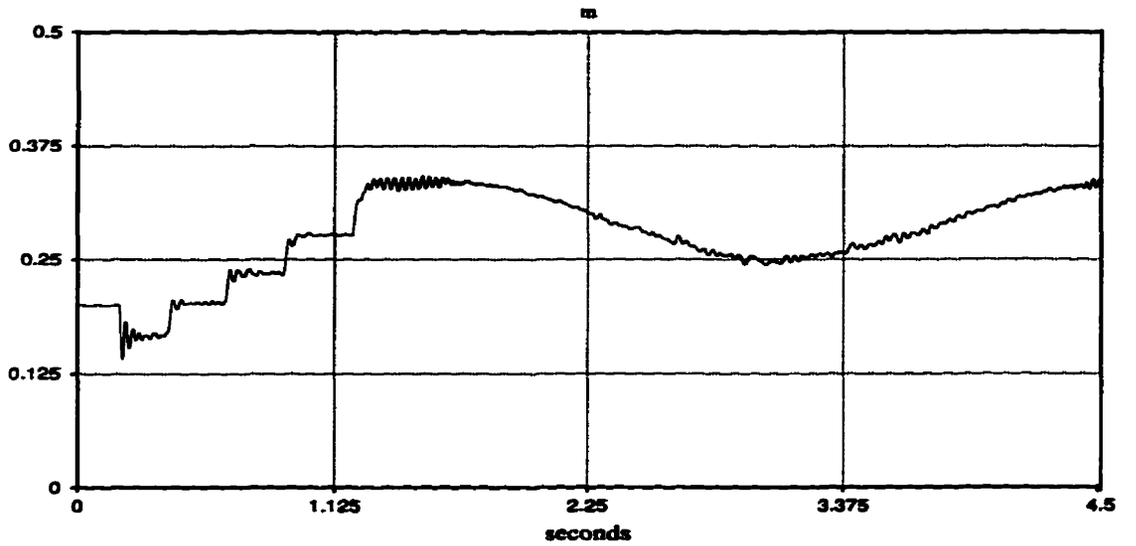

Fig. 5.8 - Modulation Index

Fig. 5.9 shows the line-to-line rms voltage, V_{rms}, applied to the load. The voltage remains reasonably constant at the set value of 0.7 kV throughout the system operation, thereby proving the efficiency of the SPWM technique employed.

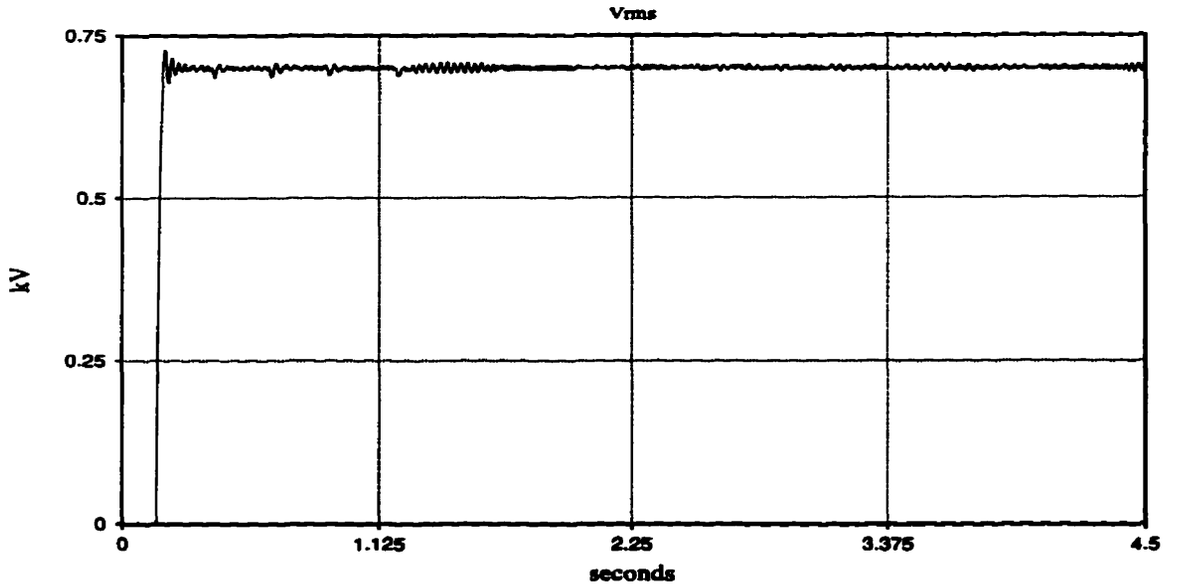

Fig. 5.9 - Load RMS VOltage

Fig. 5.10 shows the active and reactive powers, tapped from the HVDC system, and fed to the local load. The flow of power, because of the smooth load voltage, is reasonably smooth throughout the system operation.

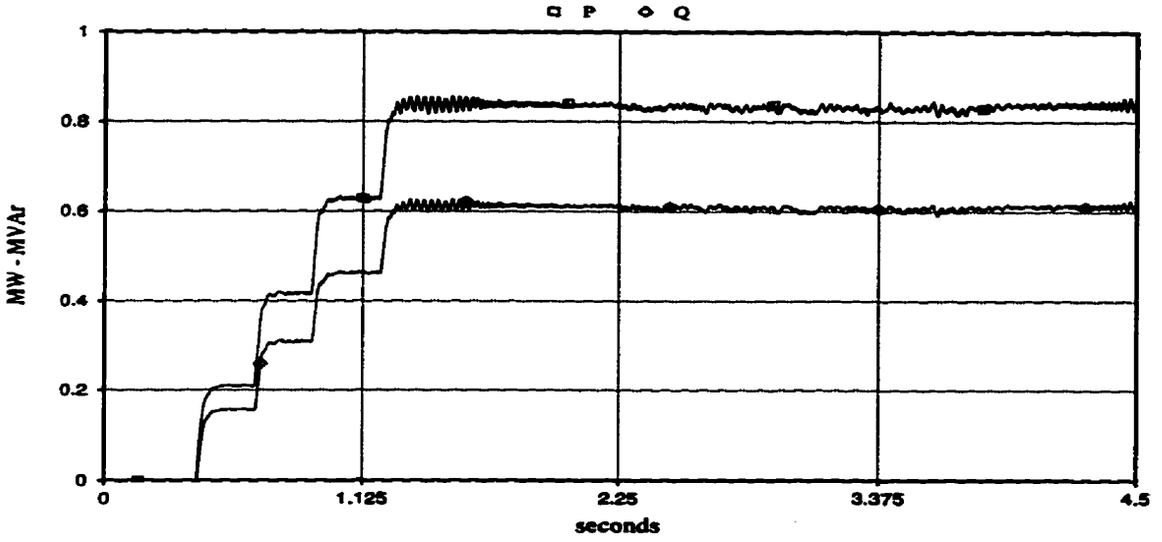

Fig. 5.10 - Load Active and Reactive Powers, P & Q

And finally, Fig. 5.11 shows the load voltage, V_{ab}, and current, I_a. The lower order harmonics have been successfully filtered out from the load voltage, but some higher order harmonics are still present in the harmonic spectrum. These harmonics can be further decreased by a better design for the high-pass filter.

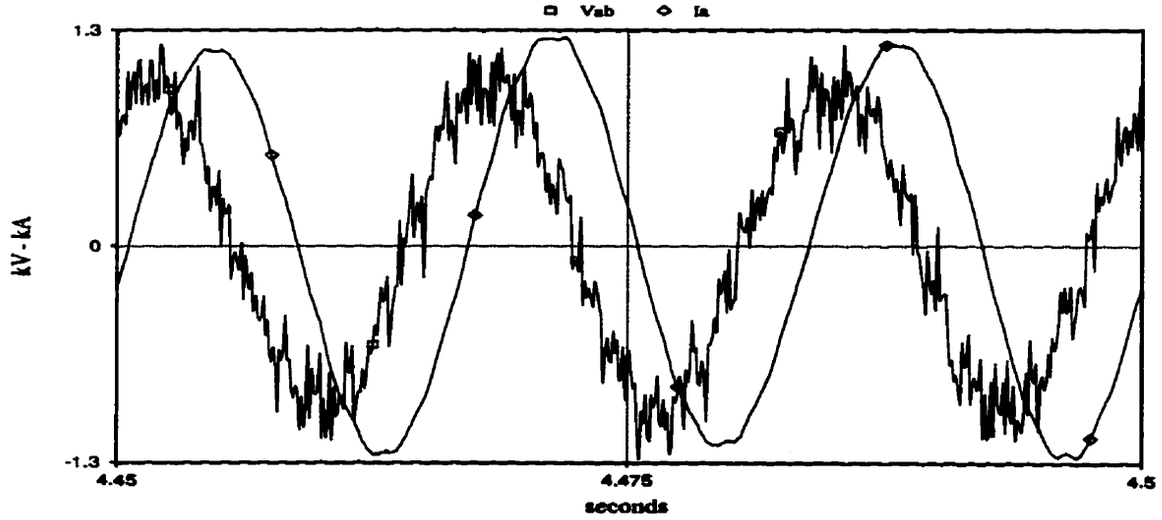

Fig. 5.11 - Load Voltage and Current, Vab & Ia

5.3. Constant Frequency Voltage

In the next stage, the system operation is simulated by employing a constant frequency control regime for the series tap. The simulation is performed in several steps to study different working conditions, and the results are presented here. The frequency is pre-set at 200 Hz and, except for the no-load conditions, a 1 MVA impedance load is applied on the tapping scheme. The selected capacitance for the series tap, i.e. C_1, is 180 μF.

5.3.1. No-load Conditions

In order to compare the actual voltage and current waveforms with the waveforms extracted theoretically in Section 3.4.1, the system is simulated at two different DC line current levels. Fig. 5.12 shows the system variables for I_{dc} = 0.6kA.

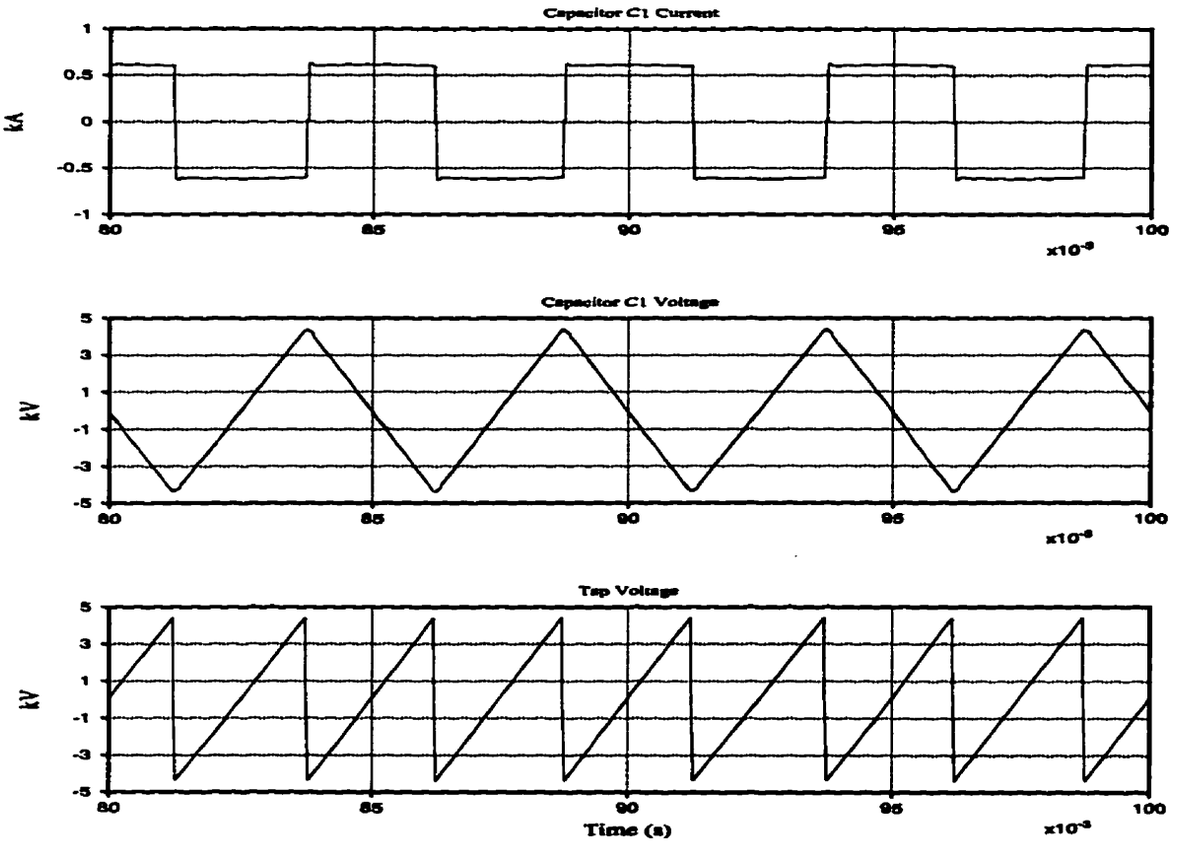

Fig. 5.12 - No-load Conditions for Idc=0.6 kA

Because of the low DC current, the by-pass time for the capacitor C_1 is zero, and the capacitor voltage is almost a complete triangular waveform. The tap voltage is the rectified version of the capacitor voltage.

Fig. 5.13 shows the system variables for $I_{dc} = 2kA$.

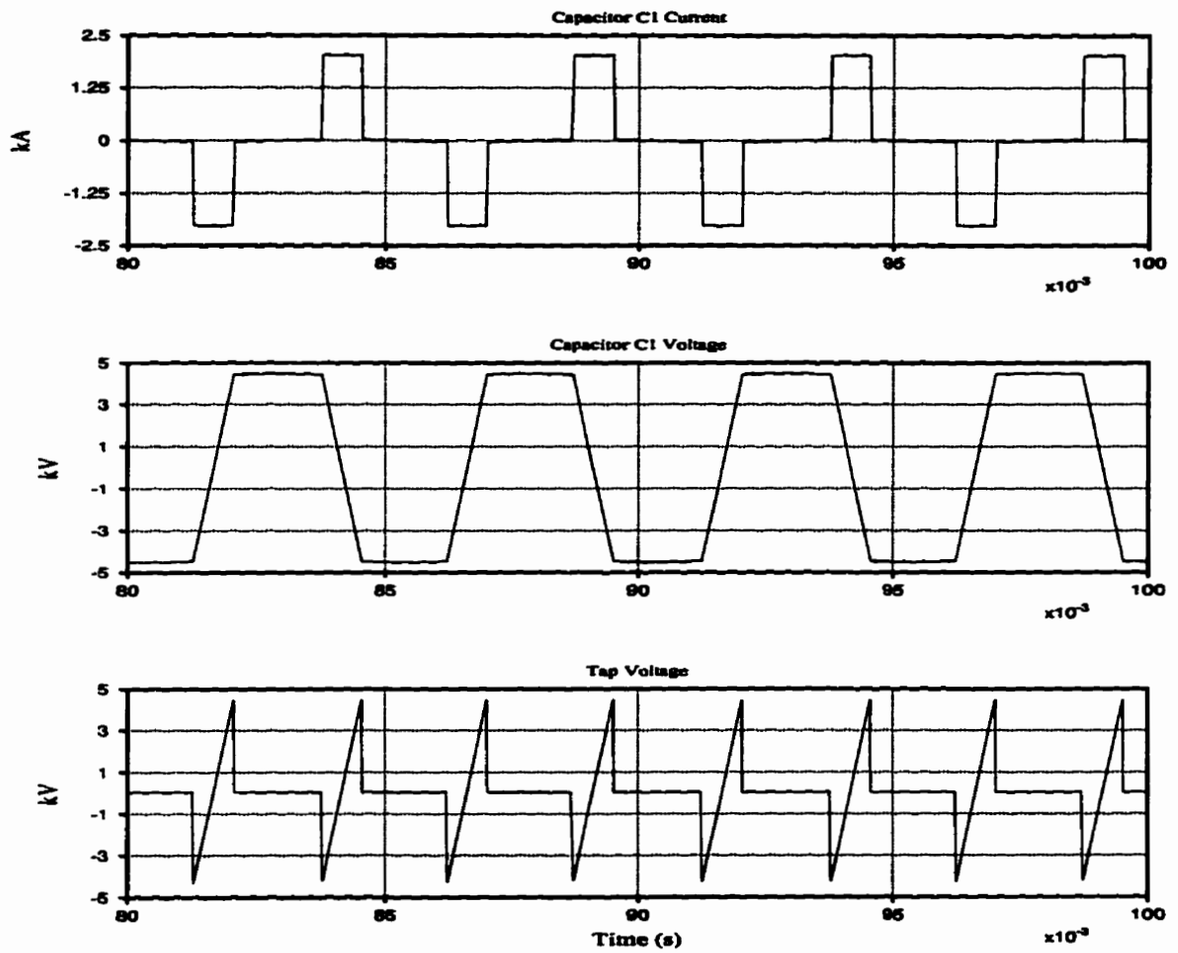

Fig. 5.13 - No-load Conditions for Idc=2 kA

In this case, because of the high DC current, the capacitor is being by-passed for a fraction of each half-cycle. During the by-pass period, the capacitor voltage remains constant because no load is applied on it. The fundamental frequency of the tap voltage, V_{Tap}, has remained the same, i.e. 200 Hz, but the harmonic spectrum has drastically moved towards

higher orders. This underlines the correlation between the harmonics imposed on the HVDC line and the DC current flowing trough it.

The simulation results are in agreement with theoretically expected ones.

5.3.2. System Operation with Constant DC Current

The system is simulated with two different constant values for the DC line current. The purpose of this stage of the simulation is to examine the ability of the control regime to perform at two reasonably distant extremes of DC line current. If the system is proved to be able to perform satisfactorily, it can be expected that the system will be able to work for variable DC currents within the two limits examined. In both cases, the load is applied on the tapping scheme in four steps.

1. DC Line Current of 0.6 kA:

Fig. 5.14 shows the current flowing trough the capacitor C_1. The capacitor is being by-passed for a very small fraction of each half-cycle, but the current in the capacitor experiences some jumps because of the primary current of the single-phase transformer.

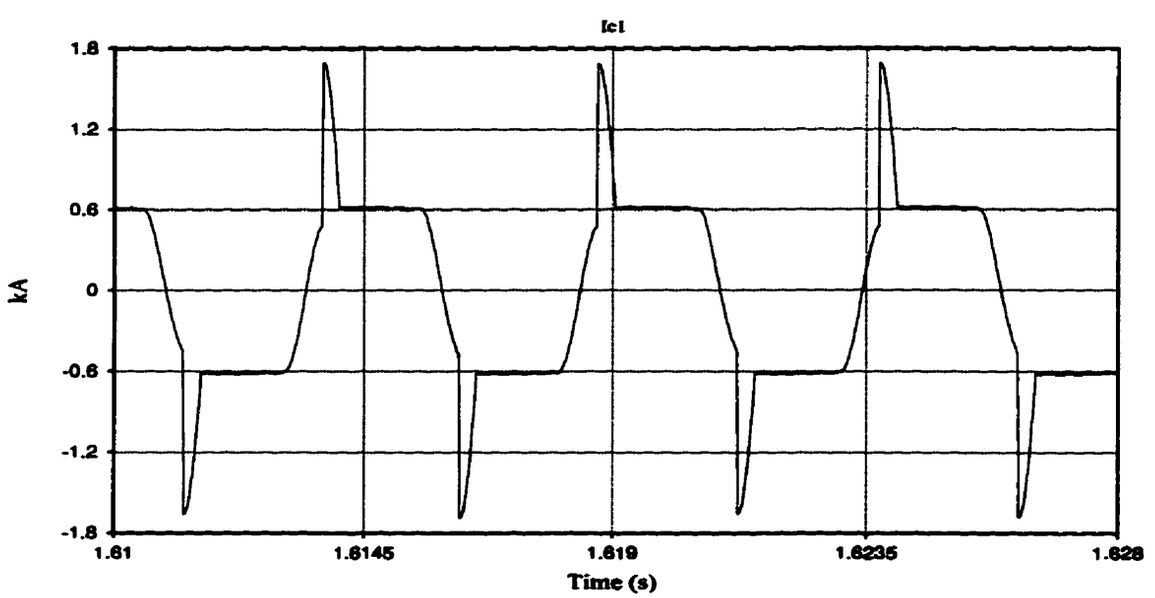

Fig. 5.14 - Current in Capacitor C1

Fig. 5.15 shows the voltage across the capacitor C_1. The voltage is very similar to the expected voltage, shown in Fig. 3.10.

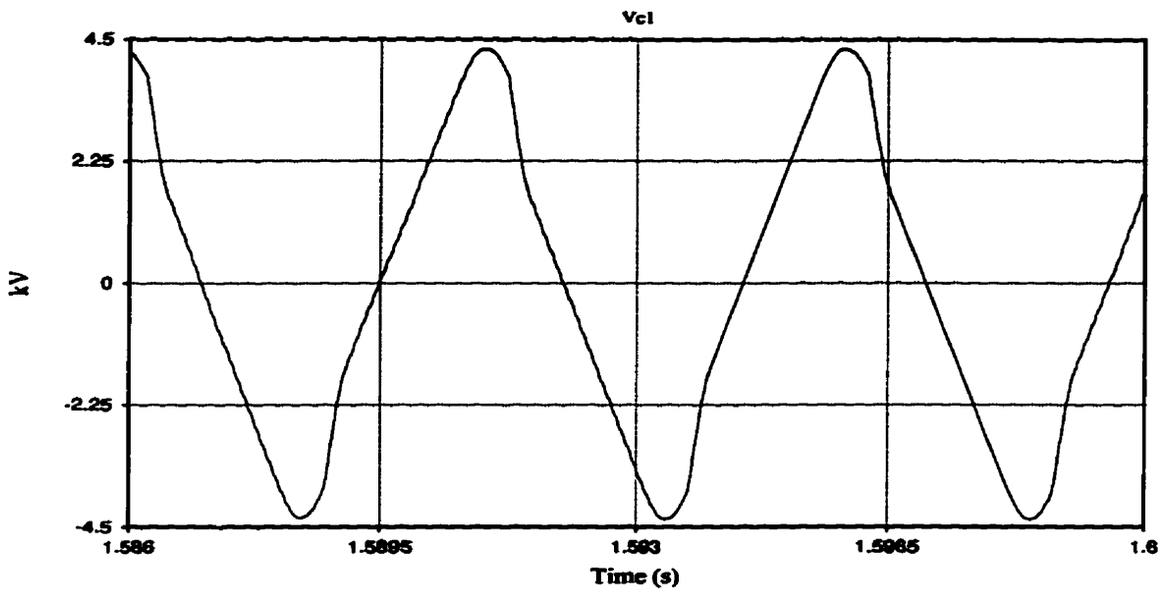

Fig. 5.15 - Voltage Across Capacitor C1

Fig. 5.16 shows the envelopes of the above voltage throughout the system operation. The peak voltage has been successfully kept within ±4.5 kV.

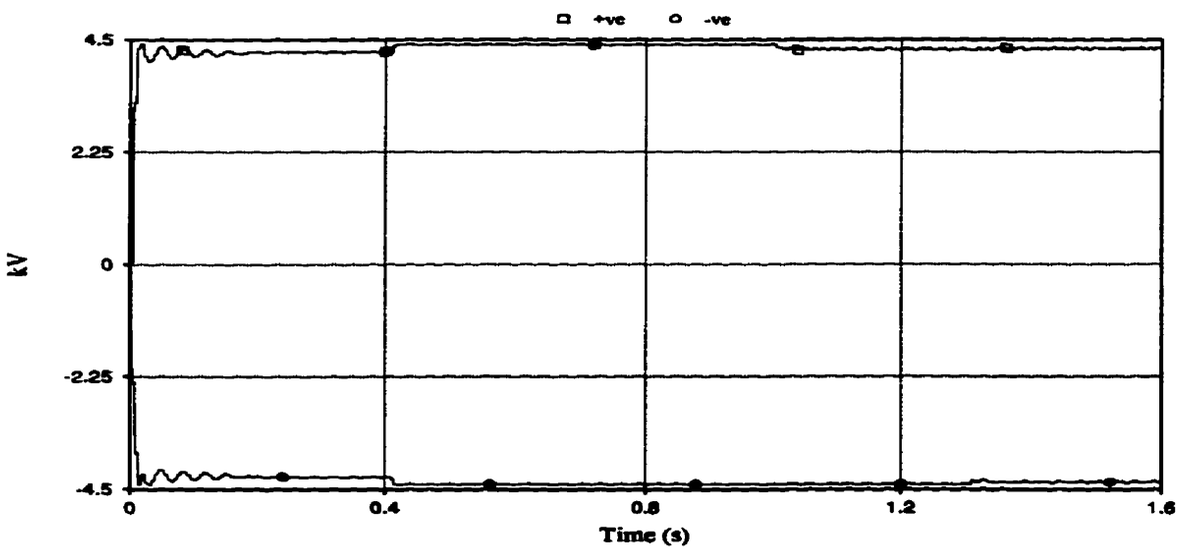

Fig. 5.16 - Voltage Envelopes for Capacitor C1

Fig. 5. 17 shows the tap voltage imposed on the HVDC line. A very short by-pass period is

reflected in the voltage waveform.

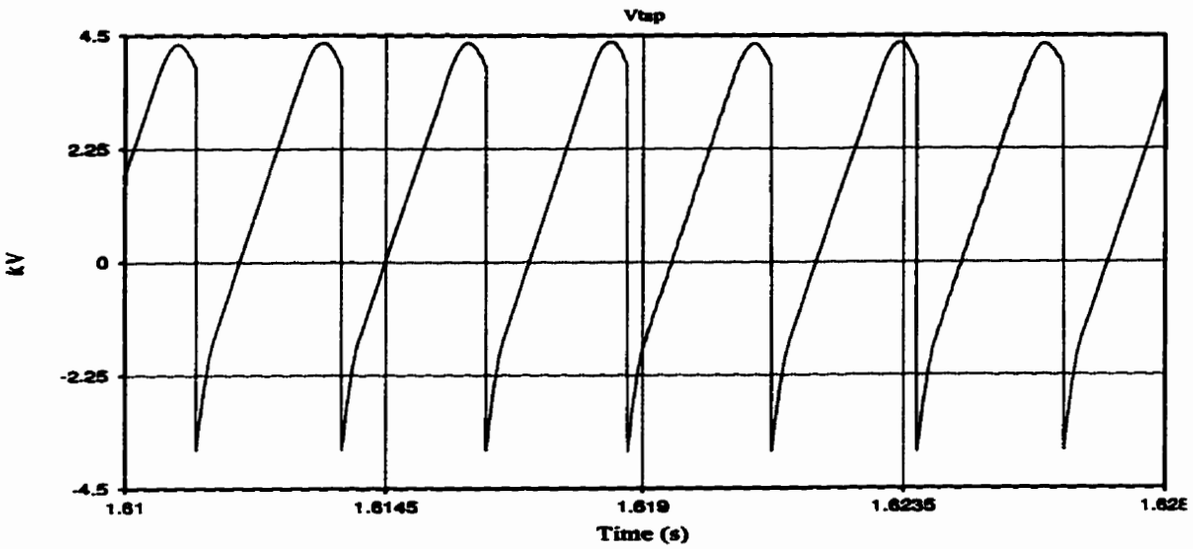

Fig. 5.17 - Tap Voltage, Vtap

Fig. 5.18 shows the harmonic spectrum of the tap voltage. The fundamental component has a frequency of 400 Hz.

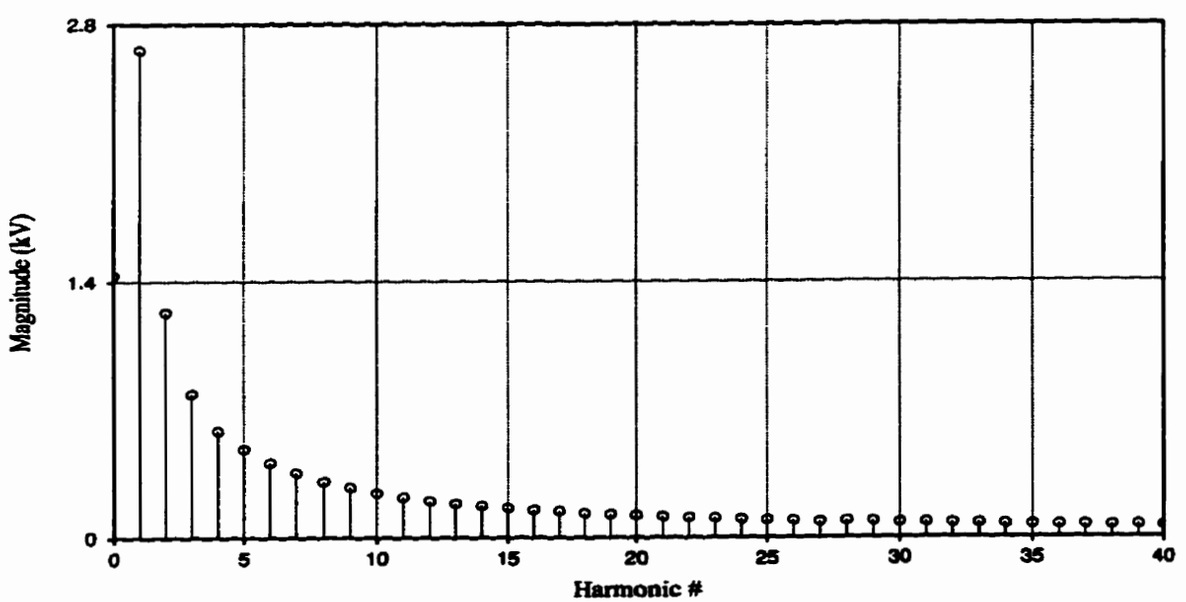

Fig. 5. 18 - The Harmonic Spectrum of the Tap Voltage

It is clear that a wide spectrum of non-characteristic voltage harmonics are being imposed on the HVDC line. Also, the tap voltage has a DC magnitude of about 1.4 kV, which when

multiplied by the DC current of 0.6 kA flowing through the series tap, results to a tapped power of about 0.84 MW, which is being supplied to the local load, as well as the tapping station's power losses. Detailed discussions about harmonics is left for Chapter Seven.

Fig. 5.19 shows the intermediate DC link voltage, V_{C_2}. Since the DC line current is constant throughout the system operation, this voltage drops slightly in response to various local load levels.

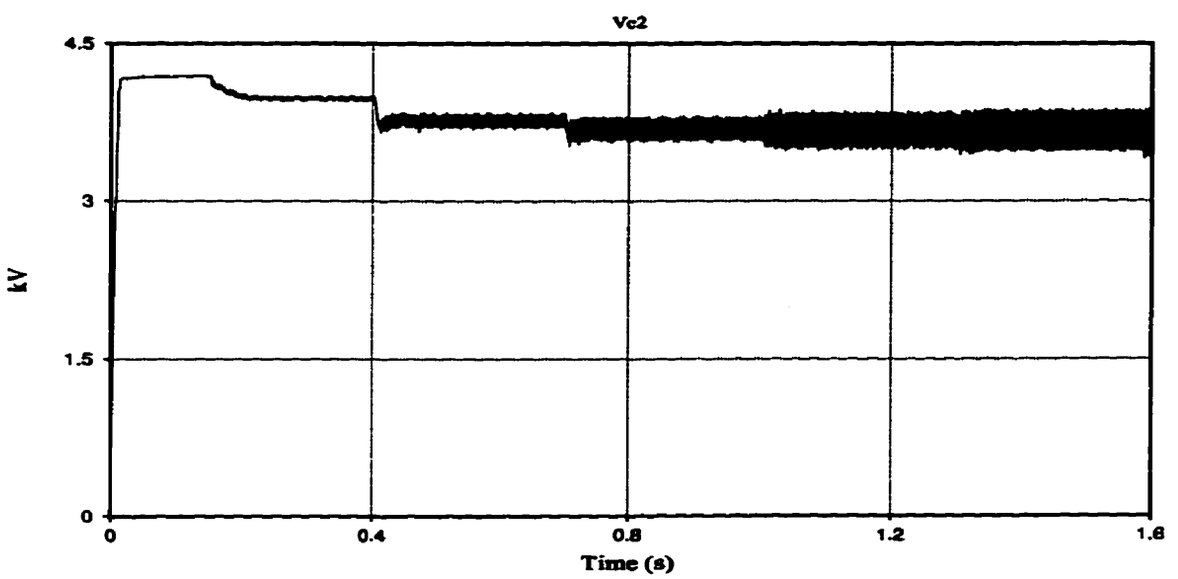

Fig. 5.19 - Intermediate DC Link Voltage

Fig. 5.20 shows the modulation index issued to the SPWM controller.

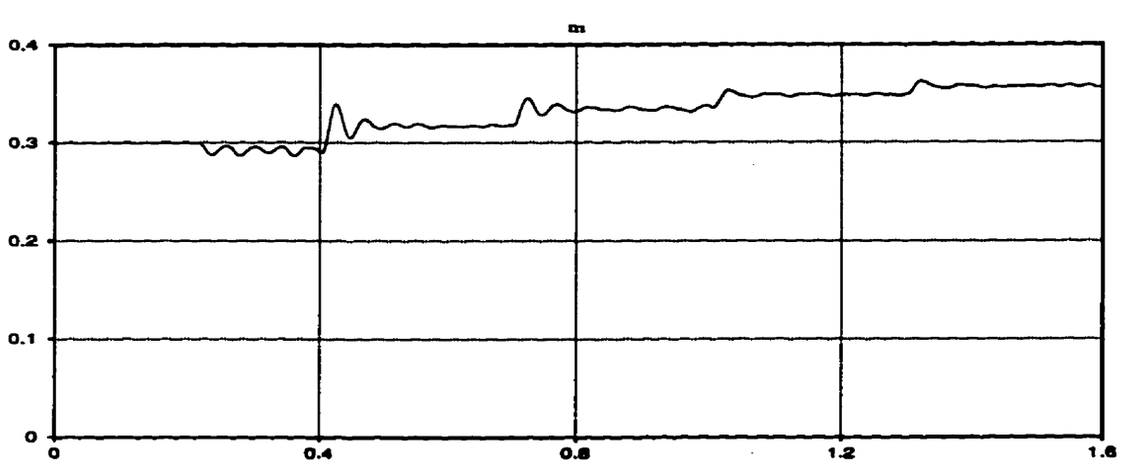

Fig. 5.20 - Modulation Index

Fig. 5.21 shows the rms load voltage, with a reference voltage setting of 0.7 kV.

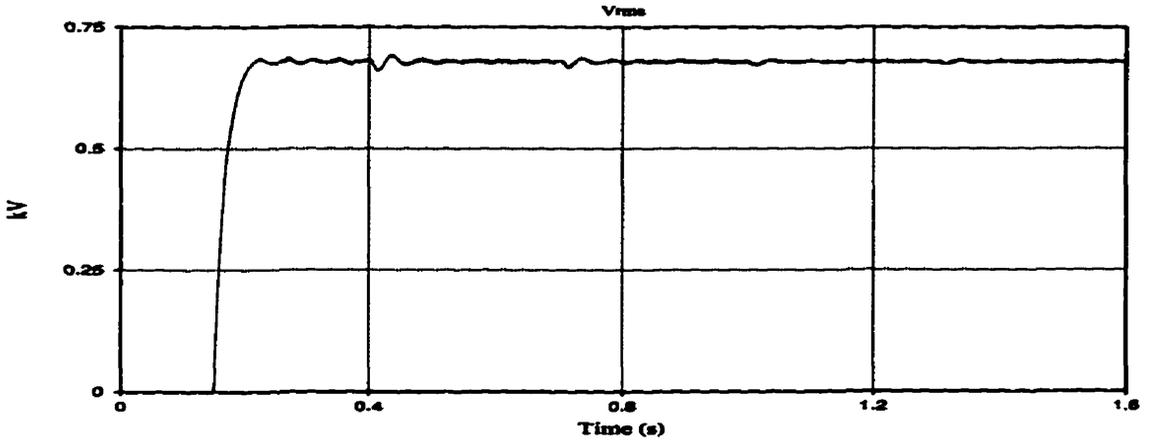

Fig. 5.21 - Load RMS Voltage

Fig. 5.22 shows the load active and reactive powers.

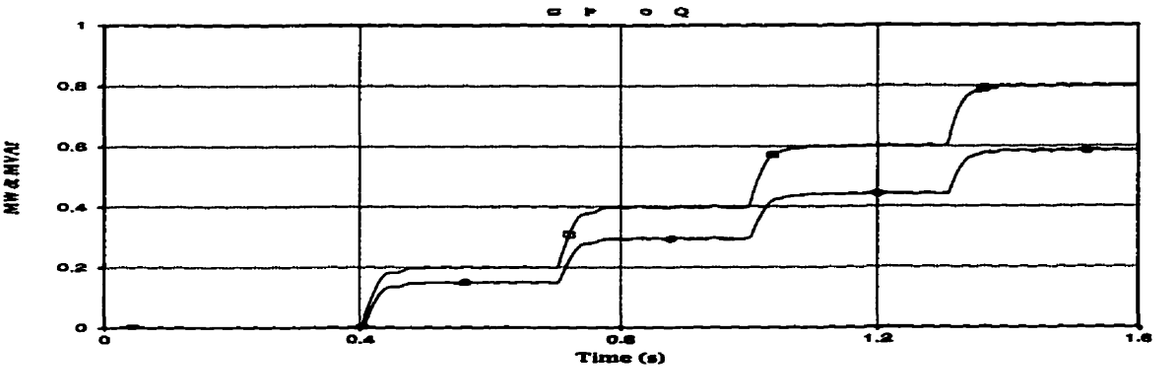

Fig. 5.22 - Load Active and Reactive Powers

And finally, Fig. 5.23 shows the load's line-to-line voltage, and line current.

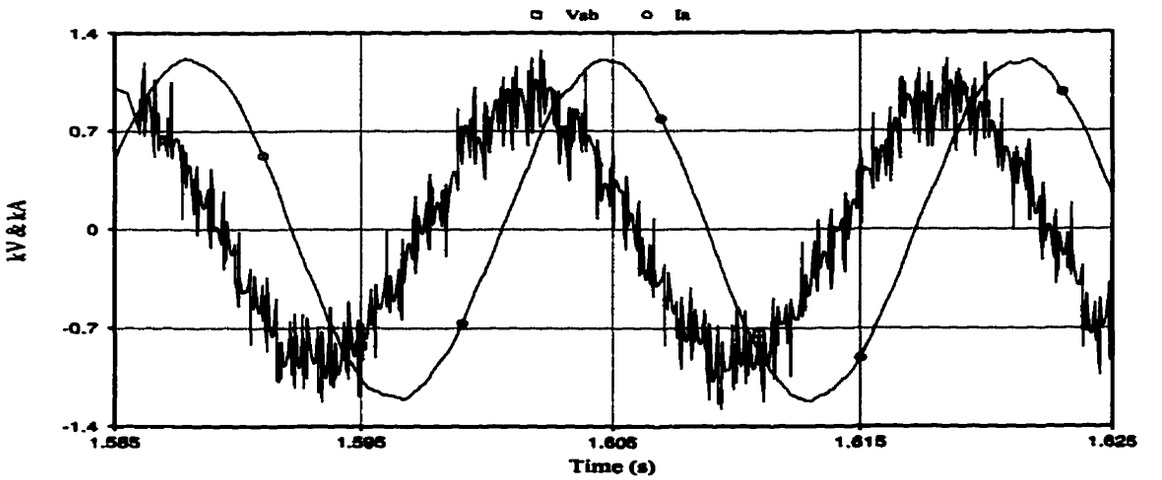

Fig. 5.23 - Load's Voltage and Current

2. DC Line Current of 2 kA:

A similar simulation is done on the system with a DC line current of 2 kA. Fig. 5.24 shows the current in the capacitor C_1.

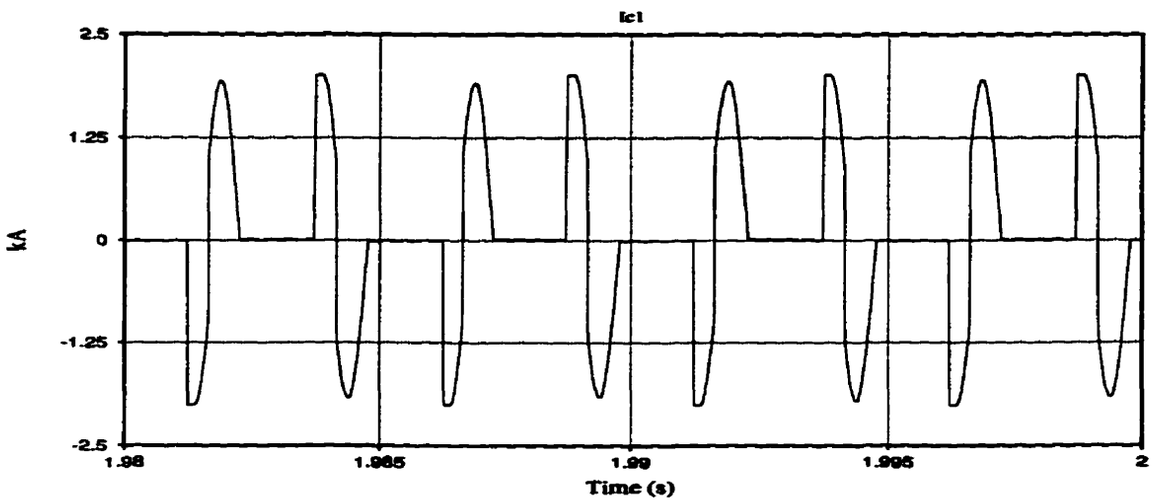

Fig. 5.24 - Capacitor C1 Current

The DC line current flows through the capacitor for a short time during each half-cycle, but the total capacitor current reverses its direction very quickly after the capacitor is by-passed. In the second half-cycle, the same process is repeated. In Fig. 5.24, 4 cycles of the system operation have been shown, and in each cycle, the two current reversals can be seen.

Fig. 5.25 shows the capacitor C_1 voltage.

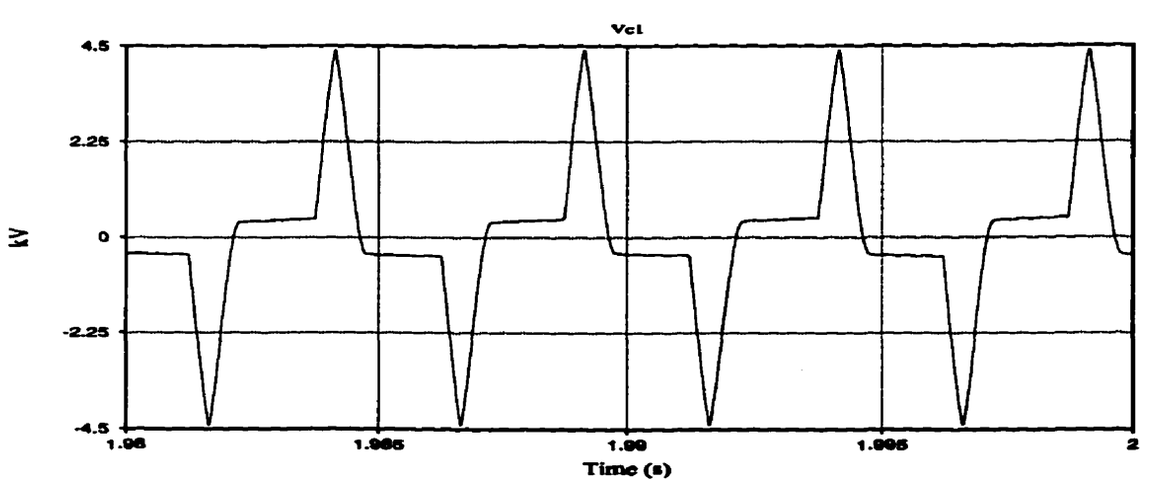

Fig. 5.25 - Capacitor C1 Voltage

Despite the peculiar shape of the capacitor current, the voltage is similar to what is expected, with the frequency of 200 Hz.

Fig. 5.26 shows the envelopes of the capacitor voltage. Again, the peak voltage is kept within the ±4.5 kV.

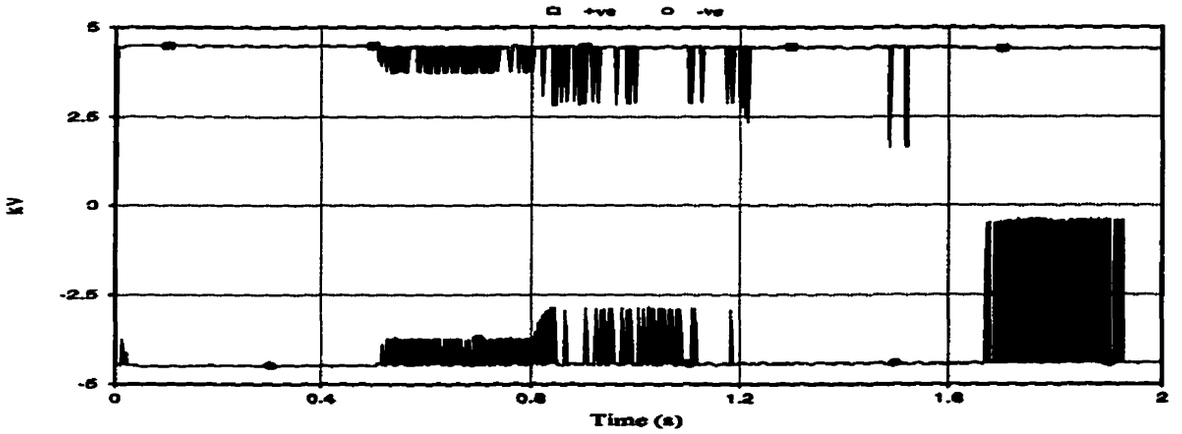

Fig. 5.26 - Capacitor Voltage Envelopes

Fig. 5.27 shows the tap voltage.

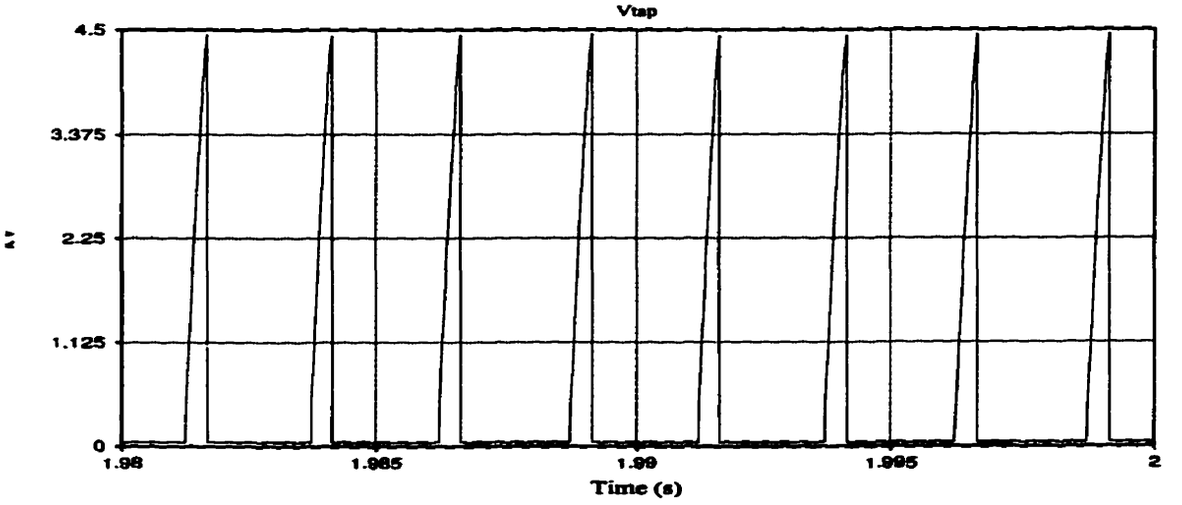

Fig. 5.27 - Tap Voltage

Fig. 5.28 shows the result of the Fourier analysis on the tap voltage. As mentioned in Section 5.3.1, the harmonics are expected to have moved towards higher orders, with a reduced magnitude for the fundamental component. Also, the DC component of the tap voltage is

about 0.45 kV, resulting in a tapped power of about 0.9 MW.

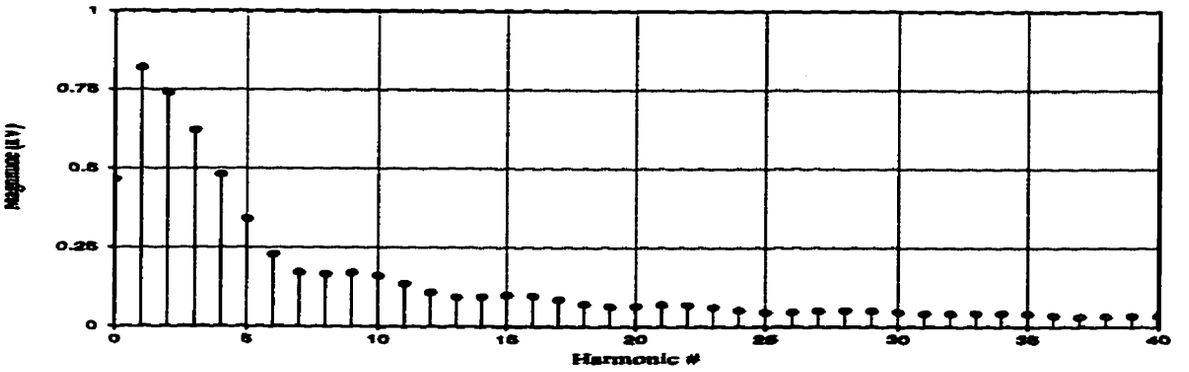

Fig. 5.28 - Harmonic Spectrum of the Tap Voltage

As mentioned earlier, the effects of these harmonics on the HVDC line's operation will be discussed in Chapter Seven.

Fig. 5.29 shows the DC link voltage.

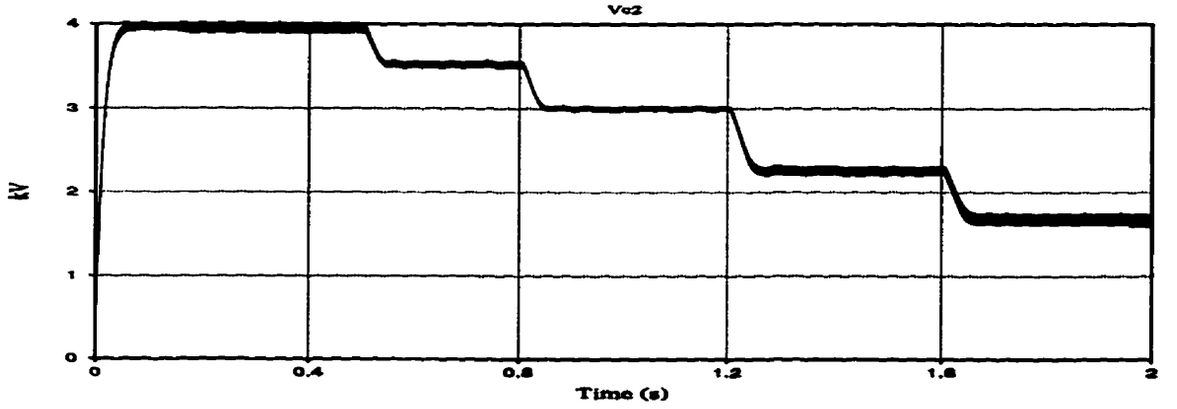

Fig. 5.29 - Intermediate DC Link Voltage

Fig. 5.30 shows the modulation index issued to the SPWM controller.

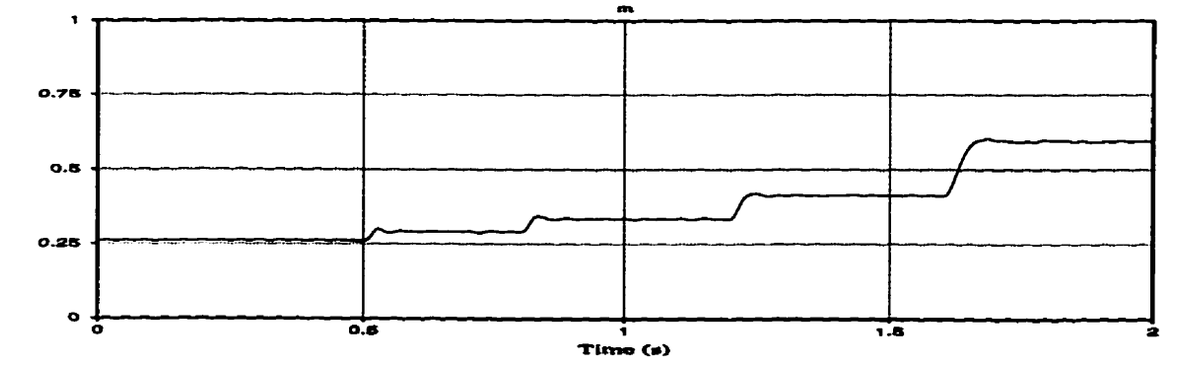

Fig. 5.30 - Modulation Index

Fig. 5.31 shows the load rms voltage with the set value of 0.7 kV.

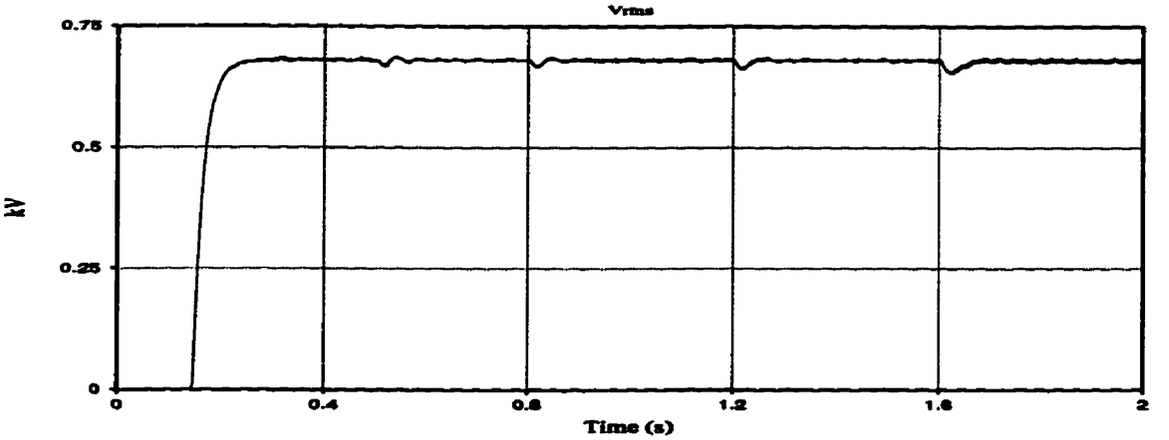

Fig. 5.31 - Load RMS Voltage

Fig. 5.32 shows the active and reactive powers of the load.

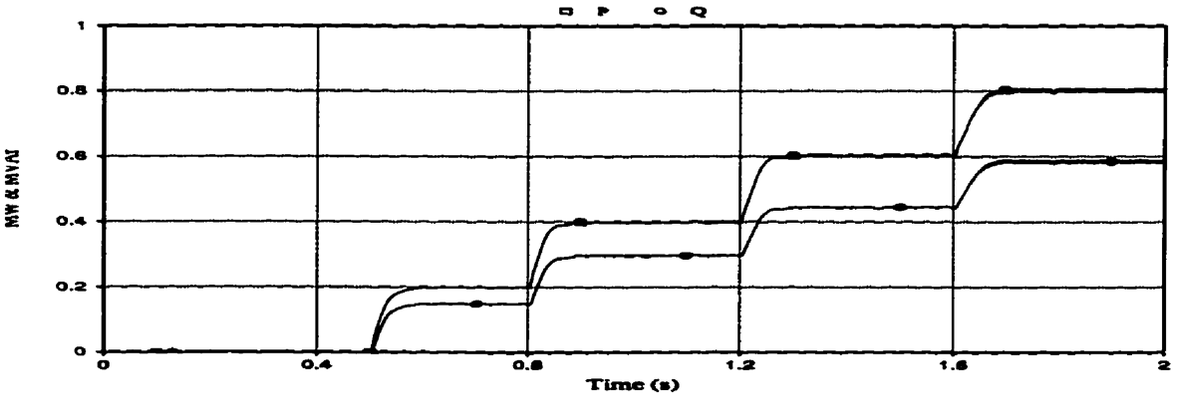

Fig. 5.32 - Load Active and reactive Powers

And finally, Fig. 5.33 shows the load's line-to-line voltage, V_{ab}, and current, I_a.

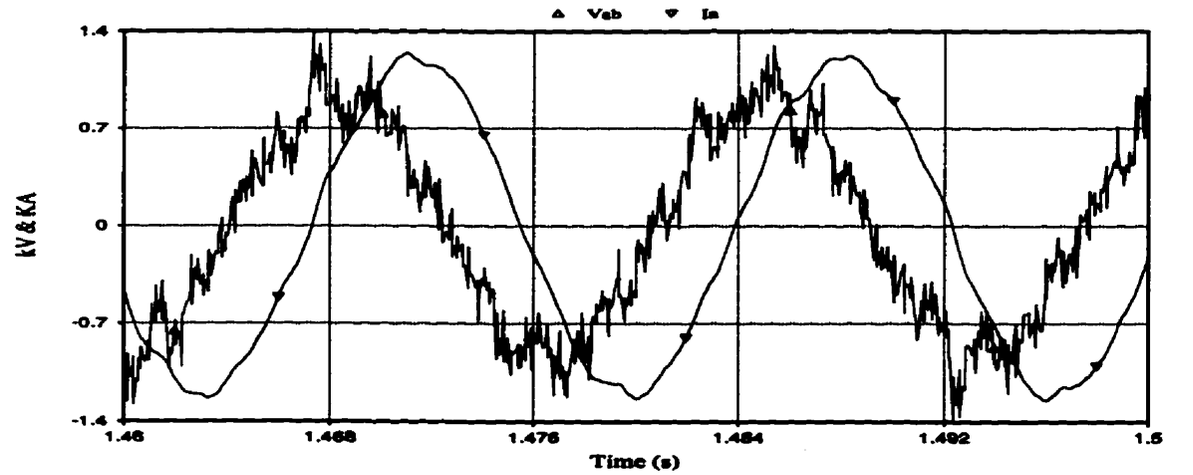

Fig. 5.33 - Load Voltage and Current

5.3.3. System Operation with Variable DC Current

After establishing the ability of the proposed scheme to work satisfactorily at two different DC current levels, the performance of the system, once more, is simulated for a case in which the DC current is decreased form 2.0 kA to 0.6 kA, and then increased back to 2.0 kA. The load is similar to the one in the previous two cases, and is applied on the tapping scheme, after the steady state is reached.

Fig. 5.34 shows the DC line current.

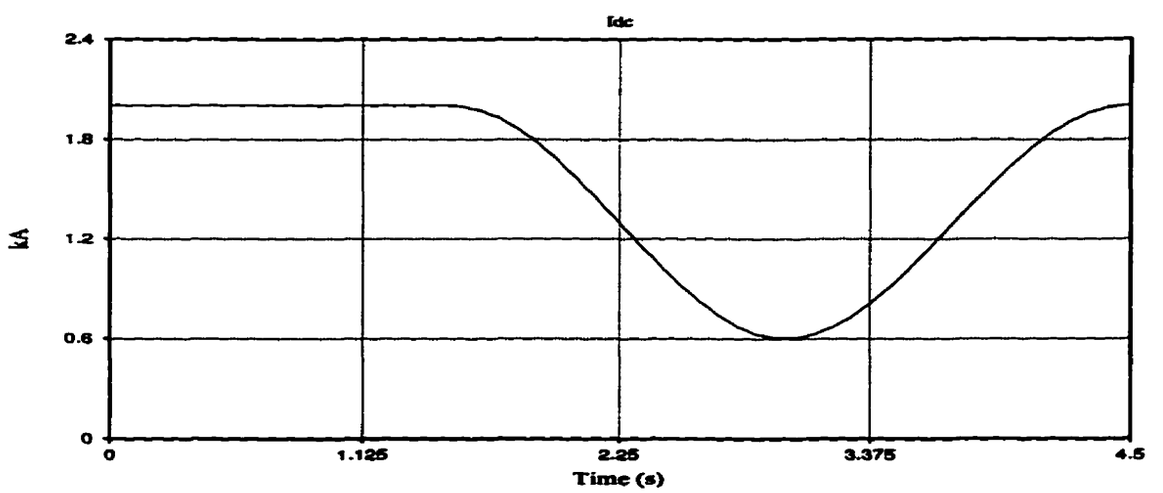

Fig. 5.34 - DC Line Current

Fig. 5.35 shows the positive and negative envelopes of the voltage across the capacitor C_1.

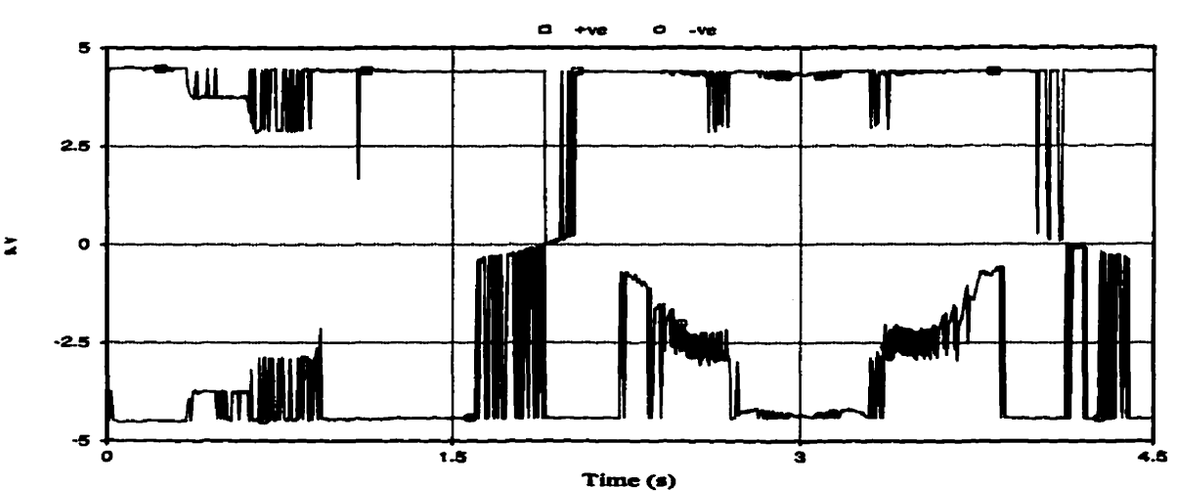

Fig. 5.35 - Voltage Vc1 Envelopes

Fig. 5.36 shows the DC link voltage.

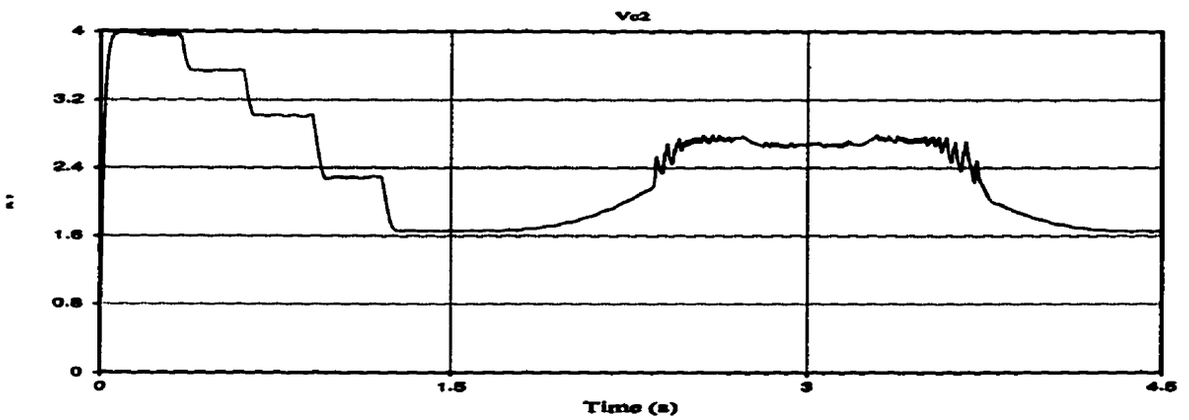

Fig. 5.36 - DC Link Voltage

Fig. 5.37 shows the modulation index issued to the SPWM controller. The changes in *m* mirror the ones in the DC link voltage.

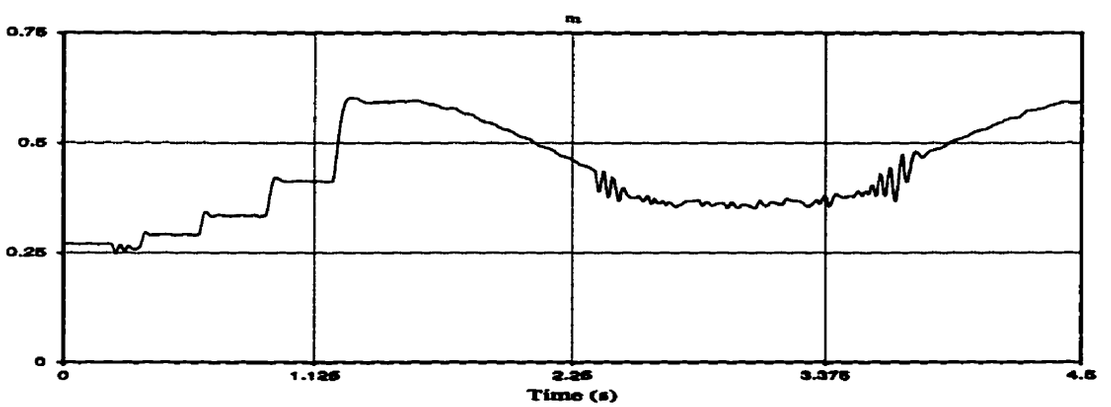

Fig. 5.37 - Modulation index

Fig. 5.38 shows the load rms voltage.

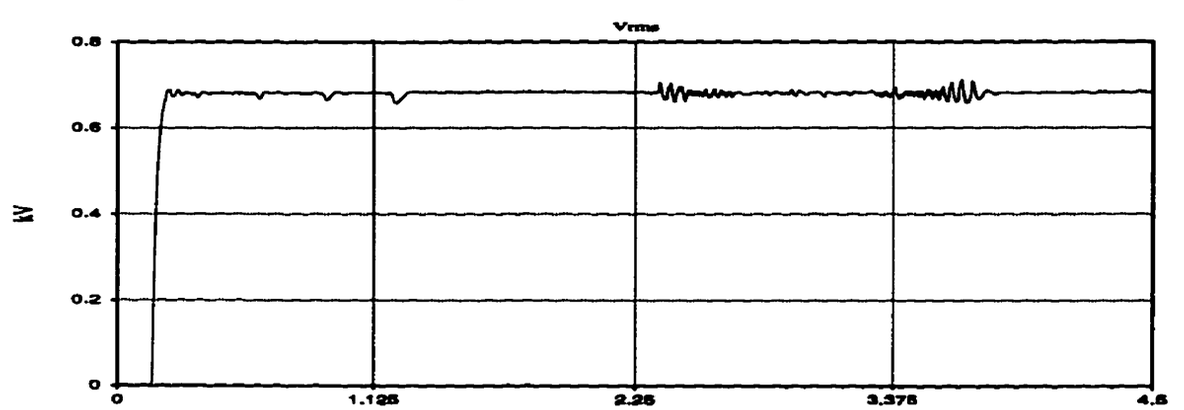

Fig. 5.38 - Load RMS Voltage

From the three figures presented in the previous page, it is evident that for the DC current range of 1.0 kA to 1.3 kA, some unwanted oscillations are present in the DC link voltage. These oscillations, in turn, make the output of the modulation index controller oscillatory, and result in similar oscillations in the load rms voltage.

The reason for the observed oscillations can be explained as follows. As was shown in Fig. 5.18 and Fig. 5.28, the harmonic spectrum of the voltage generated across the capacitor C_1, and consequently, the harmonic spectrum of the tap voltage, is a function of the DC current flowing through the HVDC line. At lower DC currents, the harmonics of lower order are the strongest, while at higher DC currents, the harmonic spectrum will shift towards the higher orders. It is possible that at the above mentioned range of the DC line current, the harmonics generated cause resonance between the intermediate DC link capacitor, C_2, and the single-phase transformer. Since the model used for the single-phase transformer is an approximation, this problem will be neglected at this point. The performance of the system in conjunction with an accurate model for the air-core transformer will be simulated in Chapter Six, and the presence of these oscillations, or lack of them, will be examined.

Finally, Fig. 5.39 shows the load's active and reactive powers. The oscillations are a natural consequence of an oscillatory load voltage.

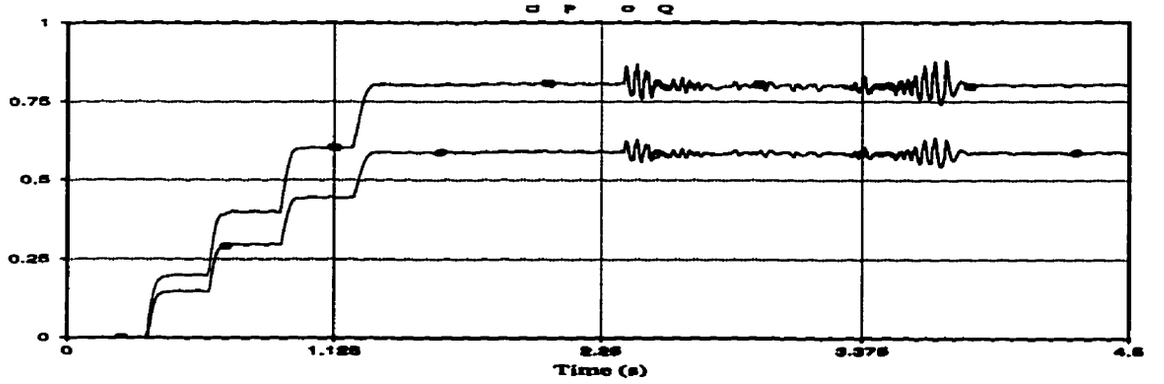

Fig. 5.39 - Load Active and Reactive Powers

5.4. Using Ordinary Thyristors or Series Connection of GTO Thyristors

The selection between ordinary thyristors and GTO thyristors to be employed in the series tap is an important issue which will affect the performance of the tapping scheme, the control methods used, the amount of power available for tapping, and finally, the fixed and operating costs associated with the tapping station.

The original proposal used GTO thyristors in the series tap, because in this way, there is no need for additional measures for performing commutation on the switches in the series tap. However, practical difficulties which used to be associated with the series connection of GTO thyristors meant that only one GTO thyristor can be employed in each leg of the series tap. Throughout the current study, consequently, the emphasis was on the use of single GTO switches. It was shown that with single switches capable of withstanding peak repetitive voltages of up to 4.5 kV, powers of up to 0.8 MW can be tapped from the HVDC system.

Recent developments in the solid state technology, however, have made the use of a number of GTO thyristors in series possible. For example, a Static Condenser (STATCON) rated at ±100 MVA and installed by the Tennessee Valley Authority (TVA) as a controllable reactive power source in Sullivan Substation near Johnson City, Tennessee, USA, uses 5 GTO thyristors in series [25]. This means that by using a number of GTO thyristors in series, the power rating of the tapping station can be multiplied by the same number.

A look at Fig. 5.6. reveals that with the variable frequency voltage control, the voltage across the capacitor C_1, which is very close to a triangular waveform, always provides a positive voltage across the non-conducting switches. This means that if instead of GTO thyristors, ordinary thyristors are to be used in the series tap, this positive voltage will turn the non-

conducting switches on, when the firing signal is issued to them, and the negative voltage experienced by the conducting switches at the same instant will turn them off, thereby performing natural commutation in the series tap. Although as it was mentioned in the above, using GTO thyristors in series has become possible recently, the use of ordinary thyristors means that no limitation will exist on the way of using a number of switches in series tap, which in turn, will make the tap's rating even higher. It also leads to a decrease in the switching losses in the series tap, which seems to be considerably less for a thyristor bridge, compared to a GTO bridge with the same power rating [5].

The possibility of using ordinary thyristors instead of GTO thyristors in the series tap was examined by simulating the system's performance in presence of a thyristor bridge as the series tap. The number of thyristors in series is 3, and the load has been increased to 3 MVA accordingly. The performance of the system was found to be exactly similar to the one reported earlier in this Chapter. Fig. 5.40 shows the envelopes of the voltage across capacitor C_1 kept within a range of ±13.5 kV.

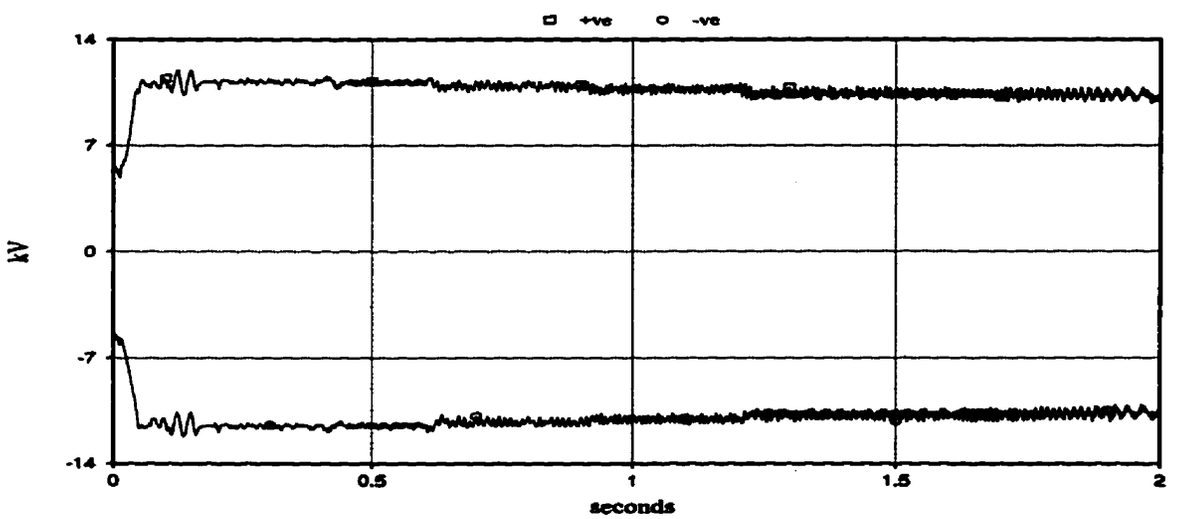

Fig. 5.40 - Positive and Negative Envelopes of Vc1

Fig. 5.41 shows the active and reactive powers tapped from the HVDC system, and fed into

the local load.

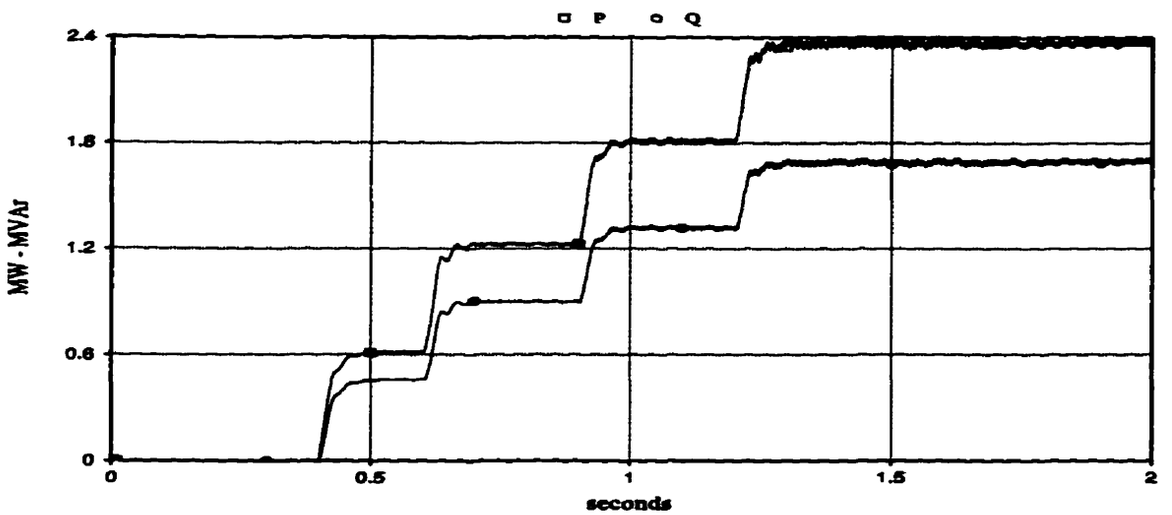

Fig. 5.41 - Load Active and Reactive Powers

Other variables of the system, because of their similarity to previously presented results, are not presented here to avoid redundancy.

It is concluded that in a tapping scheme which uses variable frequency voltage, GTO thyristors can be replaced by ordinary thyristors, without any compromise with regard to the performance standards of the station. However, with the constant frequency method, this is not necessarily possible, because the waveshape of the voltage V_{C_1} is not necessarily a triangular one. Looking at Fig. 5.25, it is evident that at high DC line currents, V_{C_1} has drastically departed from a triangular waveshape to a new form, prediction of which for all situations seems impossible, and from Fig. 5.35 it is evident that the positive or negative envelope of this voltage can be equal to zero for considerably long durations, compared to the time between each switching in the series tap. For this reason, the use of ordinary thyristors in conjunction with the constant frequency method is not expedient, because of the fact that the voltage across the non-conducting switches can not be guaranteed to be

large enough at all switching instances.

5.5. Summary of the Chapter

In this Chapter, the performance of the system with SPWM control technique for the three-phase inverter was studied. The system is capable of tapping necessary power from the HVDC system with both variable and constant frequency voltages. It was also shown that if the variable frequency regime is to be used, ordinary thyristors can replace GTO thyristors in the series tap. Finally, the series connection of switches will increase the power rating of the tapping station.

Chapter Six

Air Core Transformer: Analysis and Simulation

As it was mentioned in Chapter Three, a significant advantage of the proposed scheme is the possibility of using a single-phase air-core transformer to achieve de-coupling between the high potential HVDC line and the ground potential local load to be supplied. Such a transformer, compared to the conventional iron core transformers, will be less expensive, the losses are expected to be lower, and the weight of the transformer will be lighter, which makes the tapping station easier to build.

Different aspects of the proposed scheme's operation in conjunction with a conventional single-phase, iron core transformer, which has high leakage reactance and high magnetizing current, were studied and the results were presented in Chapter Four and Chapter Five. This Chapter is devoted to the theoretical analysis and modelling of the air-core transformer and its performance in conjunction with the proposed scheme.

6.1. The Air Core Transformer

The transformer which is going to be used in the proposed tapping scheme, must have the following specifications for the normal operating conditions:

- It has to be able to de-couple DC voltages of up to 500 kV from the ground potential,
- It has to withstand peak AC voltages of up to 5 kV applied to its windings; and,
- It has to carry peak AC currents of up to 2 kA.

Considering the above requirements, the configuration shown in Fig. 6.1 has been proposed for the transformer. This specific configuration allows the transformer to isolate the HVDC line, connected to the upper winding, from the ground potential, and to withstand AC voltages applied to its windings by using ordinary insulation materials, and air-core inductor winding techniques.

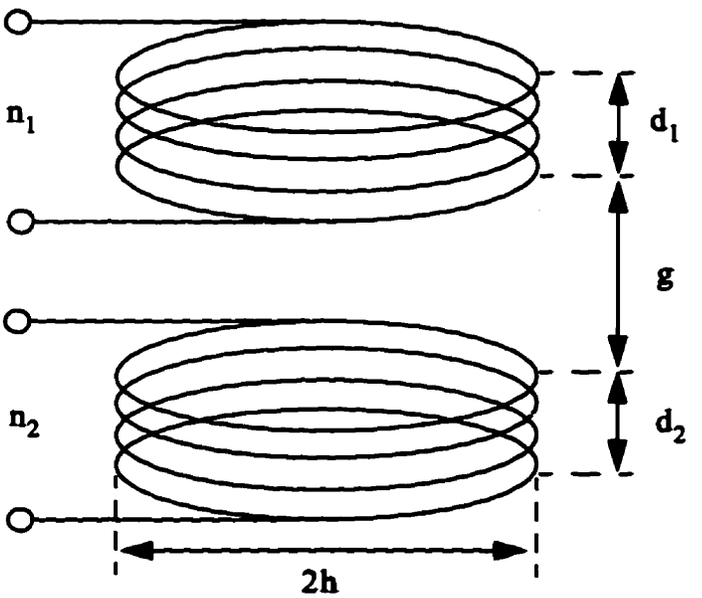

Fig. 6.1 - The Air Core Transformer

6.2. Theoretical Analysis

In order to be able to study the performance of the transformer for various diameter and air-gap sizes, it is necessary to develop mathematical relationships for the self inductance of

each coil, as well as the mutual inductance between the two coils, as functions of the coils' dimensions. To achieve this, several methods, including computational methods using finite element theory, or similar theories, can be used. In the current study, classical electromagnetic theory was used to develop necessary relationships [26]. These relationships serve to give a general idea about the required dimensions of the transformer suitable for a small tapping station. Detailed study/design of the transformer, probably, would have to be based on the specifications of each tapping station independently.

Inductance of a conductor, L, is defined as the ratio of the conductor's total flux linkages to the current, I, which the flux links, or:

$$L = \frac{N \cdot \varphi}{I} , \qquad (6.1)$$

in which N is the number of turns of conductors and φ is the flux crossing the conductor's surface. Therefore, to calculate the inductance of coils similar to the ones shown in Fig. 6.1, the flux which is created by a single current-carrying circular conductor at a similar circular surface placed at a vertical distance g from it, as shown in Fig.6.2, must be found.

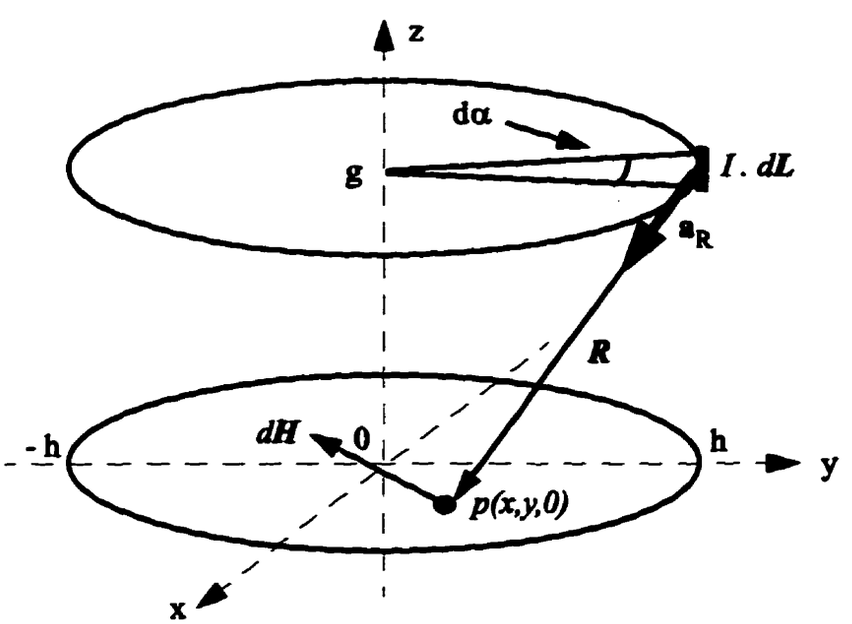

Fig. 6.2 - Two Co-axial Circular Conductors

In order to calculate the total flux, due to the current I in the upper conductor, and crossing the area on the $z=0$ plane which is inside the circle $r=h$, the following relationship, known as Biot-Savart Law, is used to find the magnetic field intensity at a general point $p(x,y,0)$:

$$dH = \frac{I \cdot dL \times a_R}{4\pi R^2}, \tag{6.2}$$

in which dH is the magnetic field intensity created by the differential current element $I.dL$. Having the differential magnetic field intensity at the point p, and considering the fact that the magnetic medium in this particular case is air, the differential magnetic flux density is equal to:

$$dB = \mu_0 \cdot dH, \tag{6.3}$$

in which $\mu_0 = 4\pi \times 10^{-7}$ is the permeability of the air.

A linear integral of $\oint \mu_0 \cdot \mathrm{dH}$ over the upper circle, gives the total magnetic flux density for the point p, i.e. B(x,y,0). Finally, a surface integral of $\oint \mathbf{B} \cdot \mathrm{ds}$ over the surface $z=0$ and $r=h$, gives the total flux crossing the lower circle, due to the current in the upper circle. In other words, if the coordinates in the x-y plane are represented by their polar equivalents, i.e. (r, θ), and if the angle on the upper circle is denoted by α, then the total flux divided by current as a function of the conductor's radius, h, and the distance between the two circular planes, g, is found by equation (6.4).

$$\frac{\varphi(h,g)}{I} = \frac{h\mu_0}{4\pi} \int_0^h \int_0^{2\pi} \int_0^{2\pi} \frac{\left(rh - r^2 \cos\alpha\cos\theta - r^2 \sin\alpha\sin\theta\right)(d\alpha)\,(d\theta)\,(dr)}{\left[(h\cos\alpha - r\cos\theta)^2 + (h\sin\alpha - r\sin\theta)^2 + g^2\right]^{1.5}} \tag{6.4}$$

Note that in order to develop equation (6.4), the following equalities have been employed:

$$R^2 = (h\cos\alpha - r\cos\theta)^2 + (h\sin\alpha - r\sin\theta)^2 + g^2, \quad (6.5)$$

$$dL = hd\alpha a_\alpha , \quad (6.6)$$

and

$$ds = rd\theta a_z . \quad (6.7)$$

Also, because of the symmetry of the configuration, only vertical components of dH exist, and other components are cancelled out, thus simplifying the process of finding equation (6.4).

Because of obvious difficulties in finding an analytical solution for the triple integral in equation (6.4), a commercial mathematical software package, Mathematica, was used to numerically find values of $\varphi(h, g)/I$ for different values of h and g. Fig. 6.3 shows the curves for $1 < h < 20$, and $g = 0,1,2,$or 3. Both h and g are in meters.

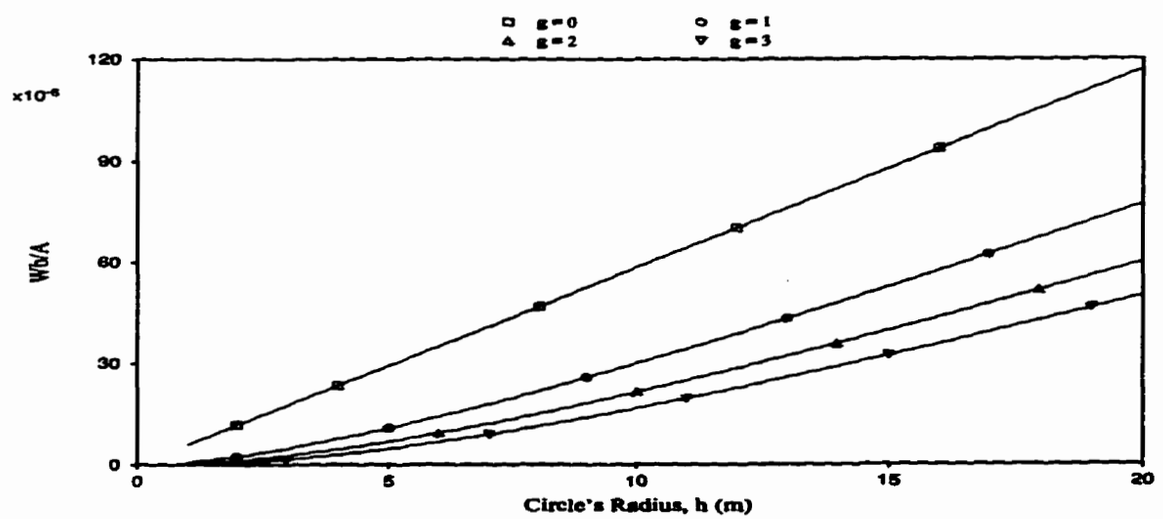

Fig. 6.3 - Flux per Current

For g=0, the relationship is linear and can be represented by:

$$\frac{\varphi(h, 0)}{I} = \frac{3\pi\mu_0}{2}h . \quad (6.8)$$

The self-inductance of a single circular conductor, therefore, is simply found from equation (6.8). Also, the mutual inductance between two single circular conductors with radius of h

and separated by g, is equal to $\varphi(h, g)/I$ which can be found by numerical integration.

If coil number one is assumed to have n_1 concentrated turns, i.e. all turns can be considered with the same radius h, and at the same vertical position, its self-inductance is equal to:

$$L_{11} = n_1^2 \frac{\varphi(h, 0)}{I} = \frac{3\pi\mu_0 n_1^2}{2} h \cdot \tag{6.9}$$

Similarly, the self-inductance of the coil number two with concentrated turns is equal to:

$$L_{22} = \frac{3\pi\mu_0 n_2^2}{2} h \cdot \tag{6.10}$$

The mutual inductance between coils number one and two, with the above conditions, is equal to:

$$M_{12} = n_1 n_2 \frac{\varphi(h, g)}{I} \cdot \tag{6.11}$$

For transformers, or in general, any two coupled coils, the coupling coefficient is defined as [18]:

$$k_{12} = \frac{M_{12}}{[L_{11} L_{22}]^{1/2}} \cdot \tag{6.12}$$

Using equations (6.9) to (6.11), the coupling coefficient is found to be equal to:

$$k_{12} = \frac{\varphi(h, g)/I}{\varphi(h, 0)/I} \cdot \tag{6.13}$$

Fig. 6.4 shows the coupling coefficient of the transformer for g=1,2,3,4 m and 1 < h < 20 m.

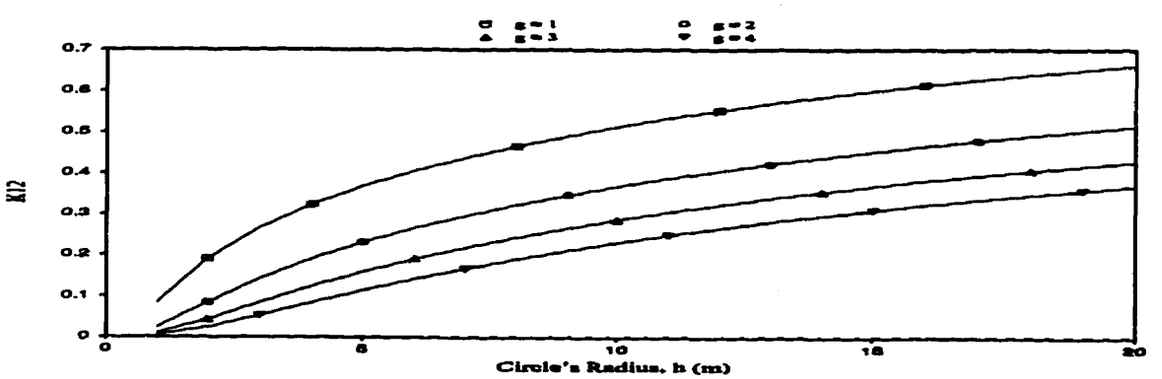

Fig. 6.4 - Coupling Coefficient

With concentrated turns in each coil, the coupling coefficient is independent from the number of turns in each coil. Also, the coupling between the two coils improves as the radius of the transformer increases, and/or as the two coils get closer to each other.

6.3. Distributed Coil Model

The relationships developed in the previous Section for the self-inductances and the mutual inductance of the two coaxial coils, were found based on the assumption of concentrated turns in each coil. The configuration proposed for the air-core transformer, however, employes two cylindrical one-layer coils, each consisting of a number of equi-radius turns, n, which are placed vertically on the top of each other. This distributed configuration directly affects the amount of flux linkage at any given position, and thus the inductances associated with the coils will be different than the ones given by equations (6.9) to (6.11). To take into consideration the effect of distributed coil turns, a short computer program was used. The results of the program, to be shown in the following, were verified experimentally.

In order to take into consideration the effect of the distribution in the coils, the $\varphi(h, g)/I$ curve must be found for a constant radius, h, and with the air-gap, g, as the variable. Fig. (6.5) shows these curves for $5 < h < 20$ m, and $2 < g < 6$ m.

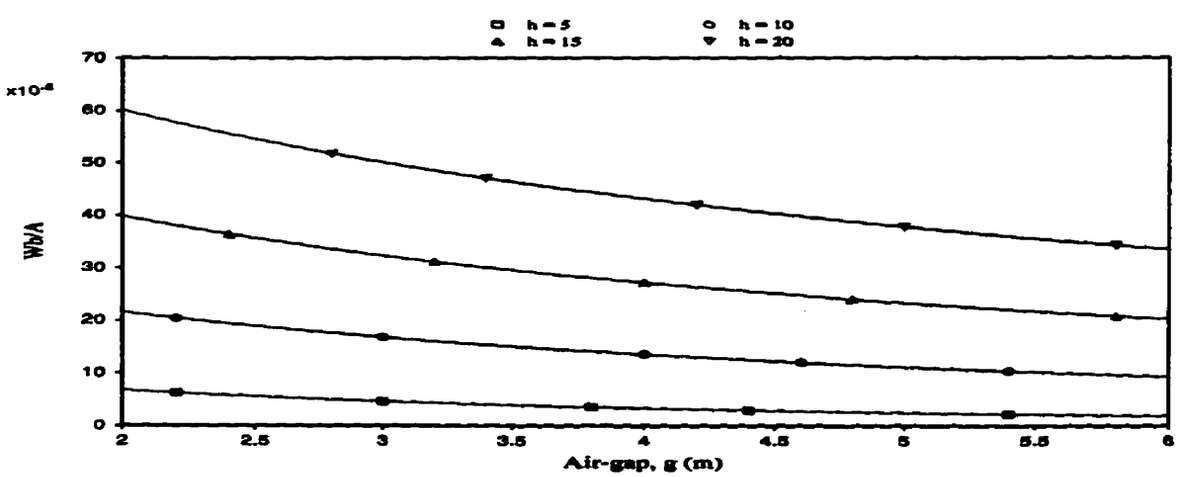

Fig. 6.5 - Flux per Current

The computer program, then, is used to calculate the contribution of each turn to the total flux linking the same coil, as well as its contribution to the total flux which is linking the other coil, based on that turn's vertical position. Each turn is considered to be an independent single circular conductor. This assumption seems reasonably accurate, considering the large radius of the coil compared to the conductor's diameter. The program inputs include the number of turns in each coil, the height and radius of each coil, and the air-gap distance. Using the specific $\varphi(h, g)/I$ curve numerically found for that specific radius, h, the self-inductances and the mutual inductance are found. The degree of accuracy of these quantities, obviously, depends on the number of points calculated for the flux/current curve. Fig. 6.6 shows the flowchart of the algorithm used for calculating the self-inductances. A similar algorithm, in which the contribution of each turn of a coil to the total flux linking the other coil is considered, is used for calculating the mutual inductance. The flowchart for calculating the mutual inductance is not presented because of its similarity to Fig. 6.6.

6.4. Experimental Analysis

In order to examine the accuracy of the theoretically found relationships, as well as the computer program which deals with the distribution in the coils, a prototype transformer with the same configuration as the proposed air-core transformer was built and studied. Table 6.1 shows the specifications of the prototype transformer.

Table 6.1 - Prototype Transformer Specifications

g = 20 mm	Coil #1	Coil #2
N	20	20
Height, d (mm)	39	39
Radius, h (mm)	175	175

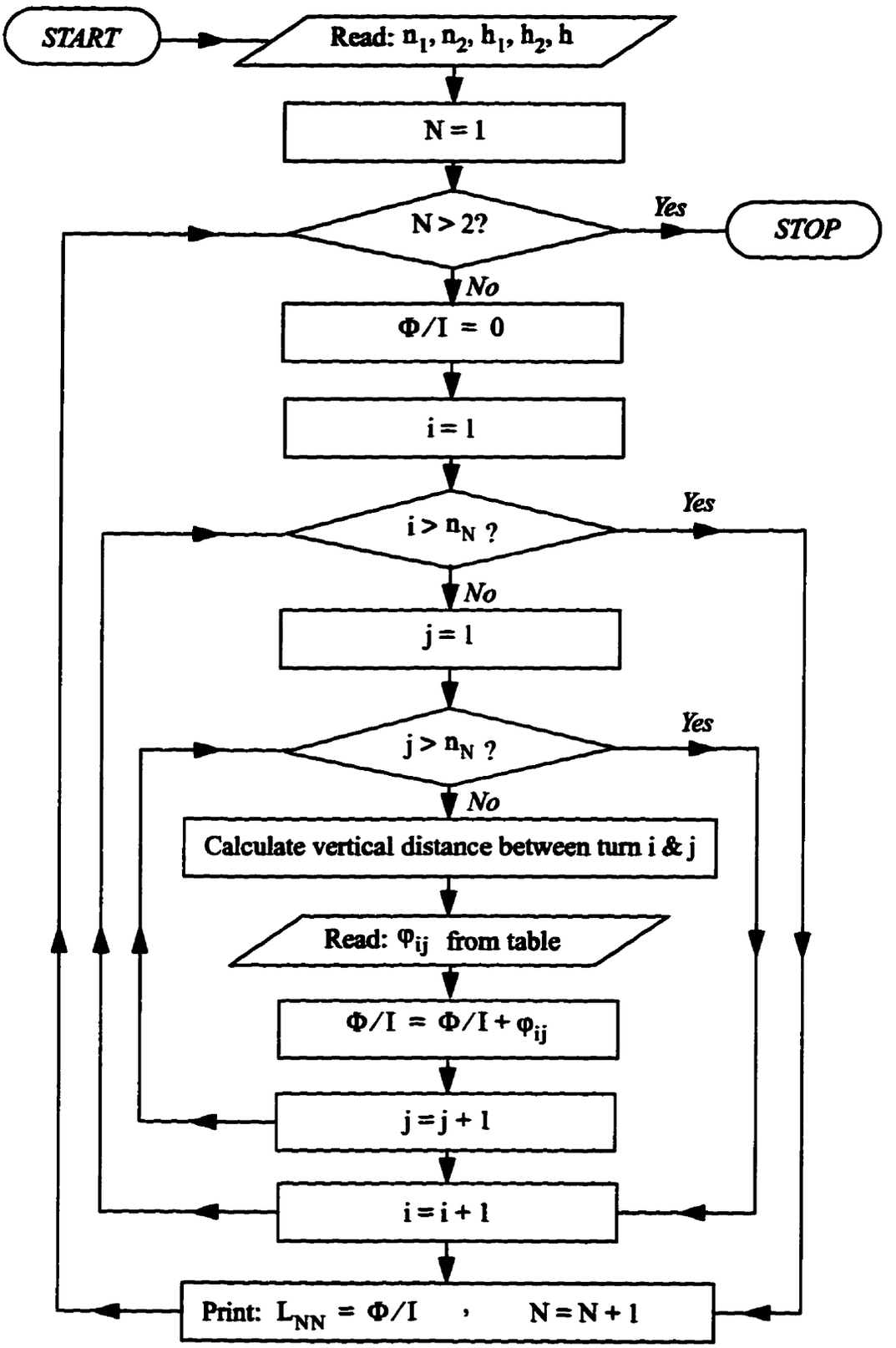

Fig. 6.6 - Flowchart for Calculating the Self-inductances

Using equation (6.4), the $\varphi(h, g)/I$ curve for $0 < g < 105$ mm and h=175 mm was found, and is shown in Fig. 6.7.

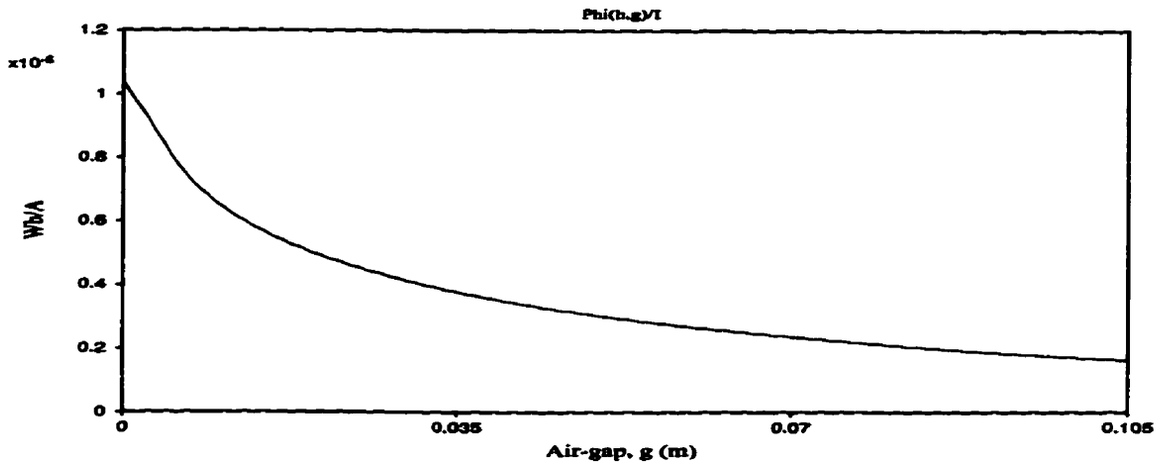

Fig. 6.7 - Flux per Current for h=0.175 m

6.4.1. Laboratory Work

The self-inductance of each coil was directly measured by a digital inductancemeter, and was found to be equal to 0.255 mH for coil #1 and 0.258 mH for coil #2. To measure the mutual inductance between the two coils, the following configuration was used:

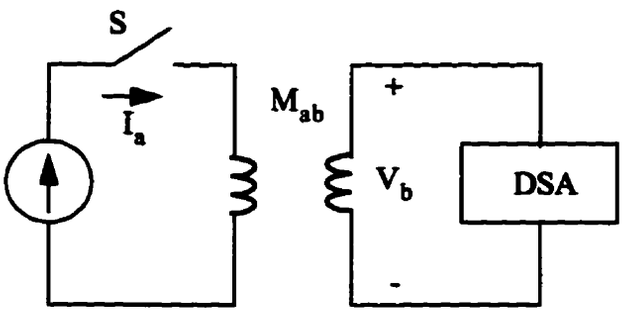

Fig. 6.8 - Measuring the Mutual Inductance

A DC current is injected into coil *a*. After the current reaches the steady-state level of I_a, the switch S is opened. The voltage induced in the coil b, then, is equal to:

$$V_b = M_{ab}\frac{di_a}{dt} \quad . \tag{6.14}$$

The digital signal analyzer, DSA, integrates the voltage across the coil *b*, and therefore:

$$M_{ab} = \frac{\int_0^\infty V_b dt}{\int_0^\infty di_a} = \frac{\int_0^\infty V_b dt}{-I_a} . \qquad (6.15)$$

Table 6.2 shows the results of the measurement for the mutual inductance. The average measured mutual inductance is equal to 0.107 mH.

Table 6.2 - Measured Mutual Inductance

I_a (A)	1.97	2.10	2.21	2.30	2.39	2.49
$\int V_b dt$	211.0	237.0	226.5	249.0	249.0	272.0
M_{ab} (μH)	107.0	113.0	103.0	108.0	104.0	109.0

It is noteworthy that several other methods, including using an AC voltage source, for finding the mutual inductance can be used. In this specific case, however, because of the very low impedance of the prototype transformer, it is very difficult to find an AC voltage source capable of supplying relatively high currents at very low levels of AC voltage (at a voltage of 0.5 V and a frequency of 60 Hz, the current will be about 2 A).

The self-inductances and the mutual inductance between the two coils, were also calculated theoretically. Table 6.3 shows the results.

Table 6.3 - Measured and Calculated Quantities

	Measured (μH)	Calculated (μH)	Error
L_{11}	255	257.93	1.1%
L_{22}	258	257.93	0.03%
M_{12}	107	112.06	4.5%
k_{12}	0.417	0.434	3.9%

The low level of error verifies the validity and the accuracy of the theoretical relationships.

6.4.2. Digital Simulation

In order to examine the degree of agreement between the prototype transformer's performance, and the transformer model in the digital simulation software package PSCAD/ EMTDC, an open-circuit (O.C.) test was performed on the transformer, and the same conditions were digitally simulated. Table 6.4 shows the results of the O.C. test, as well as the circuit quantities derived from them.

Table 6.4 - Open-circuit Test results

Measured Quantities	Calculated Quantities
V_a = 2.43 V (rms)	Z_a = 243.7 mΩ
I_a = 9.97 A (rms)	R_a = 224.3 mΩ
P_a = 2.23 W	L_{11} = 252.8 μH

Fig. 6.9 shows the voltages observed in the lab, and the corresponding EMTDC simulation results.

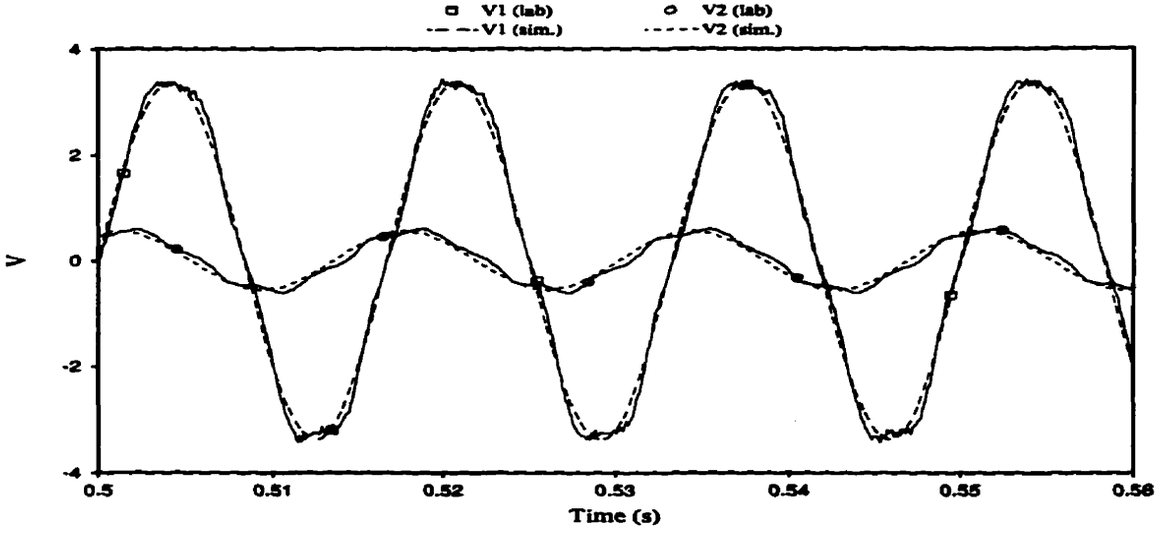

Fig. 6.9 - Comparison Between Lab and Simulation results

The digital model accurately simulates the behavior of the transformer, and therefore, it can be used to simulate the performance of larger transformers, to be employed in the tapping scheme. It is noteworthy that the primary voltage used in the laboratory, because of the specific power supply used, is distorted due to harmonics, and the harmonics are reflected in the secondary voltage. The fundamental components of the simulated and measured voltages, however, are in good agreement.

6.5. Larger Transformers

Having established the validity and the accuracy of the theoretical relationships, and because of the linear property of air, it is concluded that any air-core transformer with the proposed configuration, and with any size, can be analyzed and its inductances can be found very accurately. The PSCAD/EMTDC software package, then, can be used to predict the behavior of the whole tapping scheme.

Table 6.5 shows the results of calculations for a number of large size air-core transformers.

Table 6.5 - Calculation Results for Larger Transformers

Radius (m)	$L_{11} = L_{22}$ (mH)	M_{12} (mH)	k_{12} (%)
1.8	5.70074	0.17383	3.0
3.0	10.90006	0.81207	7.5
5.0	20.51667	2.92318	14.2
10.0	46.26232	11.93017	25.8
15.0	73.94557	24.09618	32.6
20.0	102.90337	38.26720	37.2

As the length of the insulator strings in Manitoba's Nelson River HVDC scheme transmission lines is about 3.6 m, the air-gap, g, is assumed to be equal to this value. Also, all

transformers have been assumed to have 30 turns in each coil, and each coil is assumed to have a height of 0.5 m.

It is noteworthy that the author's correspondence with a Canadian manufacturer of air-core reactors for high voltage applications, revealed that present manufacturing equipment limits the radius of the reactors to 1.8 m, for which the coupling coefficient will be around 3%. Calculations for $h=1.8\ m$ and $g=3.6\ m$ have resulted in the same value. It is, however, believed that manufacturing equipment might be adjusted for larger diameters, if there is enough demand for such coils.

6.6. System Performance

In order to study the performance of the proposed tapping scheme with an air-core transformer, one such transformer was incorporated into the system, and the system operation was digitally simulated. The air-core transformer has the specifications shown in Table 6.6.

Table 6.6 - Transformer Specifications

	N	Height	Radius	L (mH)
Coil #1	60	1.2 (m)	5 (m)	65.677
Coil #2	60	1.2 (m)	5 (m)	65.677

With an air-gap of 3.6 m, the mutual inductance of the transformer, M_{12}, is equal to 9.56 mH, and therefore, the coupling coefficient, k_{12}, is 14.6%.

The scheme is run with the constant frequency control regime for the series tap, and the frequency of the switching is set at 200 Hz.

6.6.1. Uncompensated Case

At the first step, the system is run in a no-load situation to observe different system variables.

The only difference between the present system and the ones studied in previous Chapters is the replacement of the single-phase transformer with the accurate model developed for the air-core transformer. No measures have been employed for compensating the high magnetizing current in the transformer and/or low coupling between the two coils. At this stage, the DC line current is set at a constant value of 2 kA.

Fig. 6.10 shows the current flowing through the capacitor C_1 , and the tap voltage.

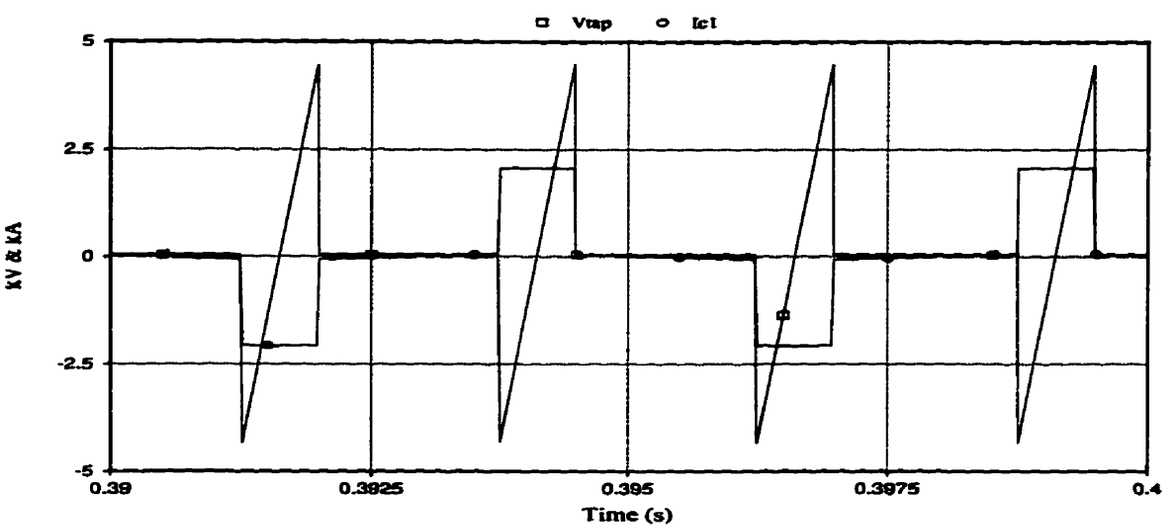

Fig. 6.10 - Ic1 and Vtap

Fig. 6.11 shows the positive and negative envelopes of the voltage across the capacitor C_1 .

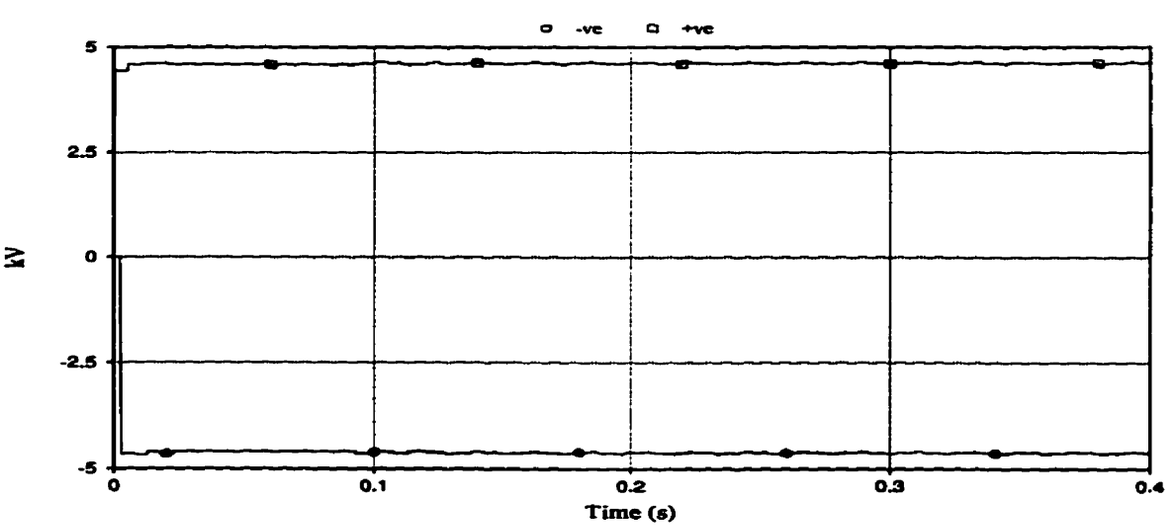

Fig. 6.11 - Positive and Negative Voltage Envelopes

Fig. 6.12 shows the voltage across the transformer's primary, which is the same as the voltage across C_1 , and the resulting secondary voltage.

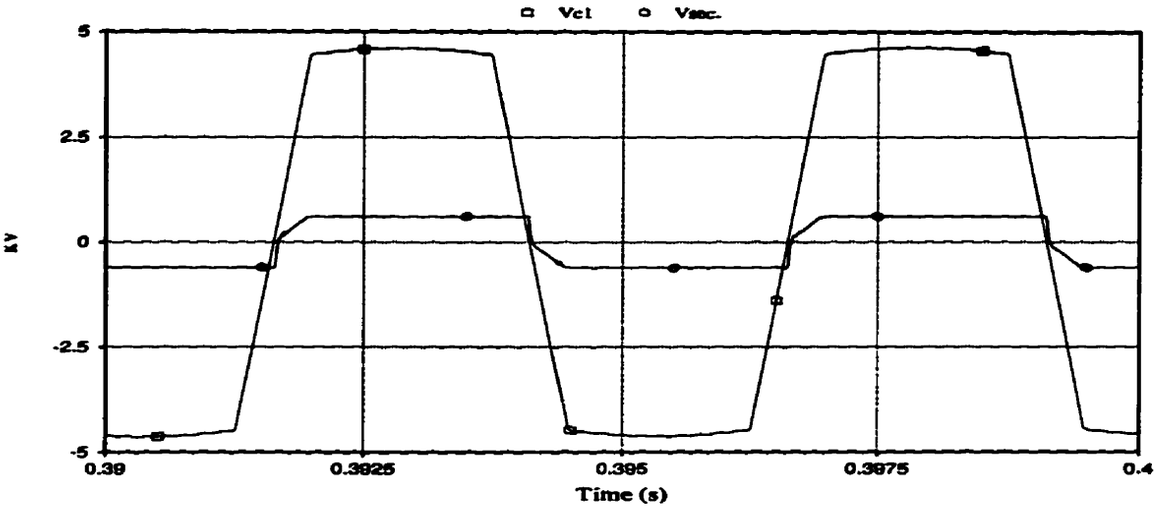

Fig. 6.12 - Transformer Voltages

The effect of low coupling between the two coils is obvious from the low secondary voltage. Fig.6.13 shows the currents in the transformer windings. Despite the no-load conditions, a relatively high magnetizing current is flowing through the primary winding.

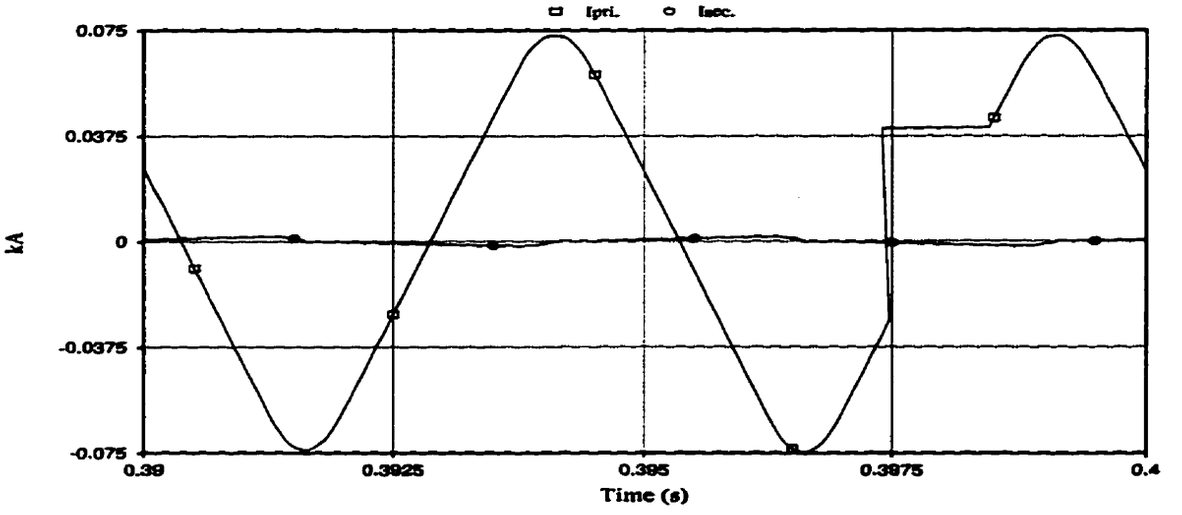

Fig. 6.13 - Transformer Currents

And finally, Fig. 6.14 shows the DC link voltage, and the rms value of the load voltage with a modulation index, *m*, of 0.3. The load voltage, obviously, is very small (113 V rms) and

will not be sufficient to feed even a small fraction of the local load.

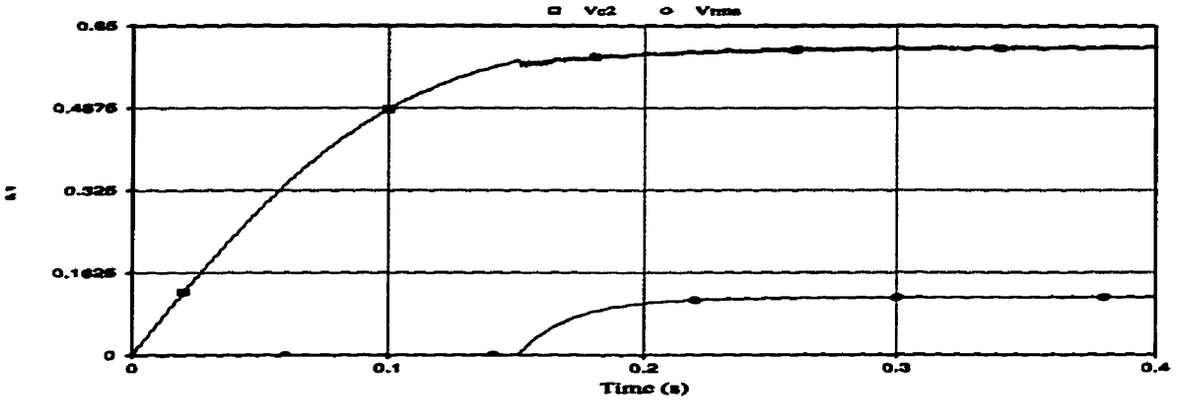

Fig. 6.14 - DC Link and Load RMS Voltages

For the above reason, and to compensate the high magnetizing current, it is necessary to connect a capacitor in series with each coil.

6.6.2. Compensated Case

To compensate for the high magnetizing current in the air-core transformer, a 15 μF capacitor is connected in series with each one of the coils. This will cause the series capacitor and the self-inductance of each coil to resonate at a frequency of 160 Hz, which is below the applied frequency of 200 Hz. The system is brought to steady state at a DC line current of 2 kA, and then, the local impedance load is applied on the tapping station in three stages. At the full load, i.e. a load of 0.75 MVA with a lagging power factor of 0.8, the DC line current is decreased to 0.6 kA, and then increased back to 2 kA.

Fig. 6.15 shows the DC line current.

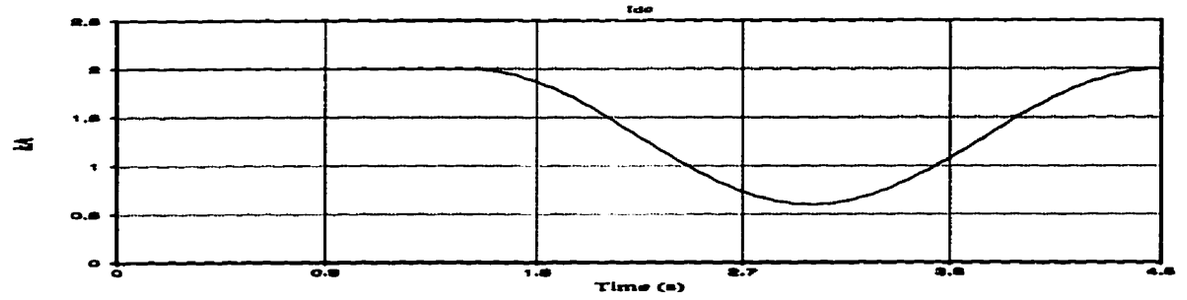

Fig. 6.15 - DC Line Current

Fig. 6.16 shows the current flowing through the capacitor C_1 , and the tap voltage in the steady state. The tap voltage has a DC value of about 0.32 kV.

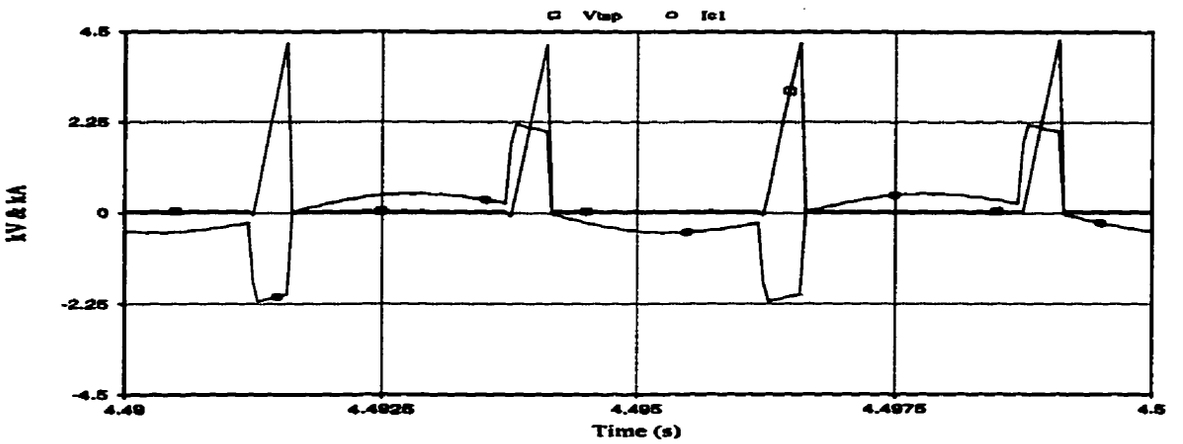

Fig. 6.16 - Capacitor Current and Tap Voltage

Fig. 6.17 shows the DC link voltage.

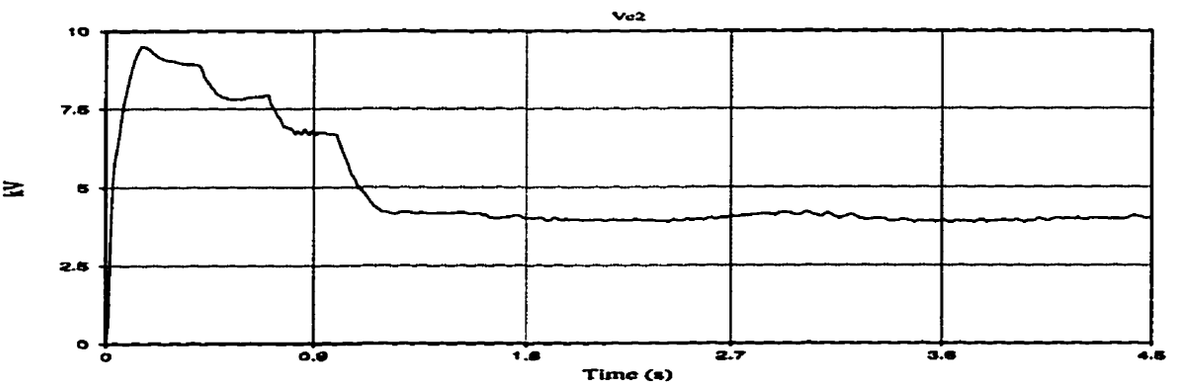

Fig. 6.17 - DC Link Voltage

Fig. 6.18 shows the modulation index, *m*, issued to the SPWM controller.

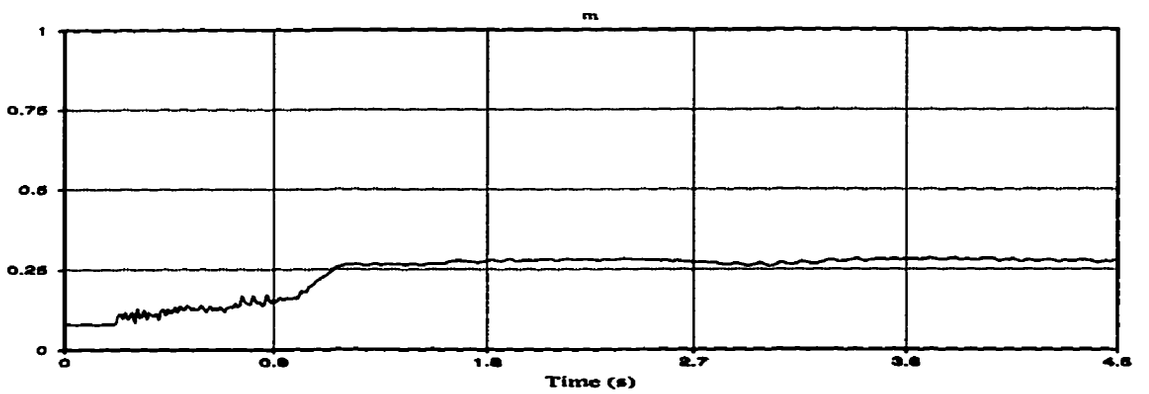

Fig. 6.18 - Modulation Index

Fig. 6.19 shows the load rms voltage, kept at 0.68 kV.

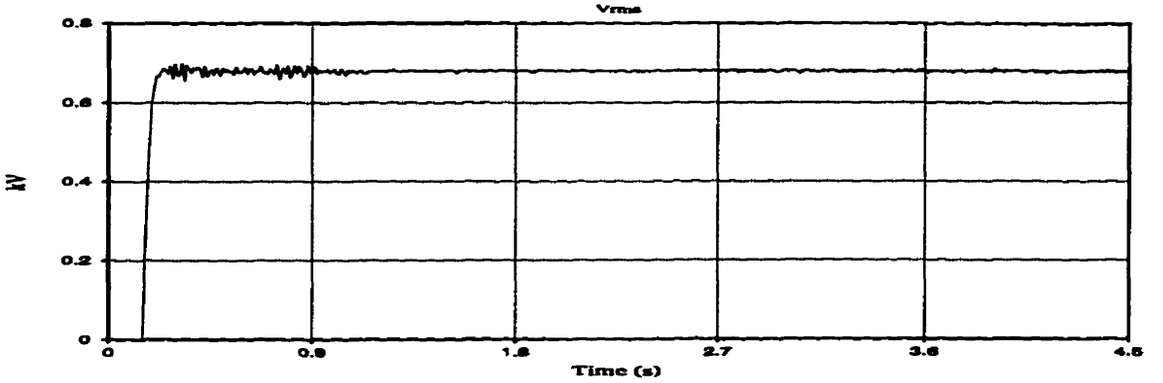

Fig. 6.19 - Load RMS Voltage

Fig. 6.20 shows the three-phase voltages applied on the load in the steady state.

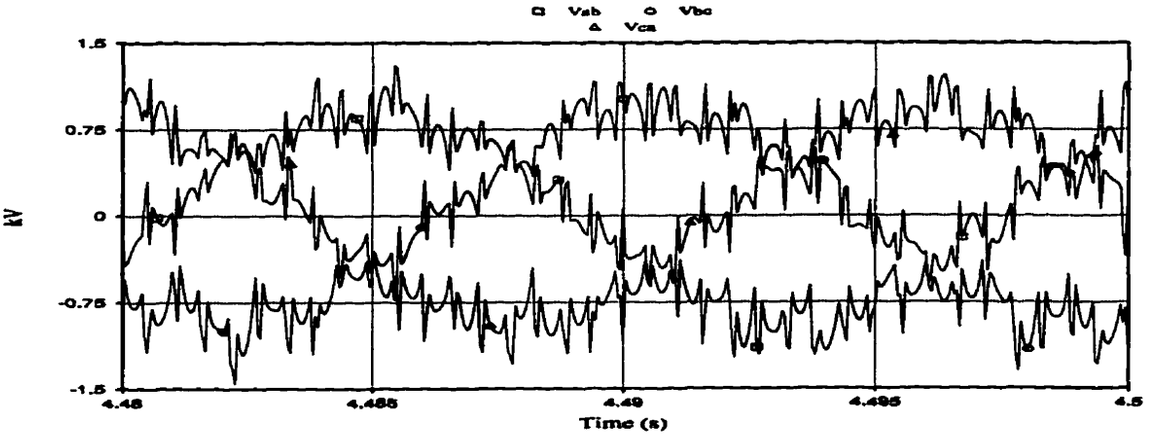

Fig. 6.20 - Load Voltage

Fig. 6.21 shows the three-phase line currents in the steady state.

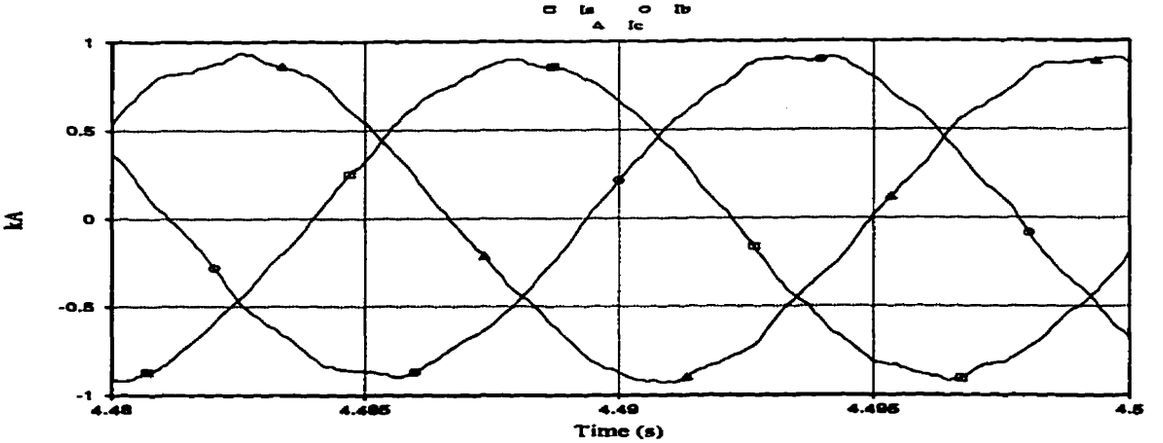

Fig. 6.21 - Load Current

And finally, Fig. 6.22 shows the real and reactive power fed to the local load from the HVDC system.

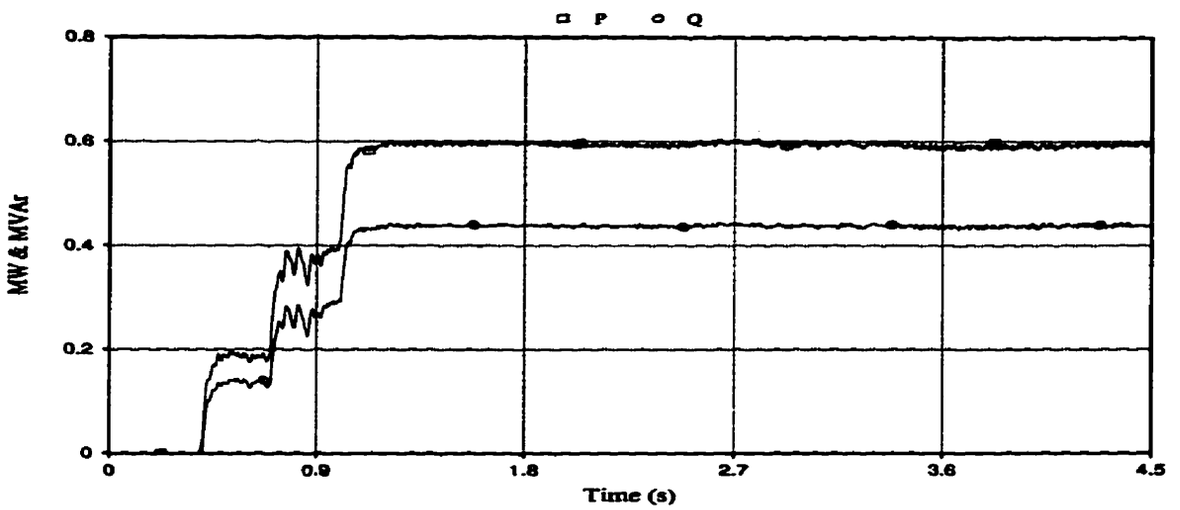

Fig. 6.22 - Load Active and Reactive Powers

It is noteworthy that the 600 kW tapped power is the maximum level which can be tapped through the air-core transformer, and the system is unable to deliver power levels higher than this. Nevertheless, this power level still seems acceptable for most of the isolated loads, as discussed in Chapter Two.

Also, unlike the case studied in Section 5.3.3, and illustrated through Fig. 5.36 to Fig. 5.39, there is no oscillations in the DC link voltage, the load rms voltage, and consequently, the load power. This strengthens the merit of the assumption made in Section 5.3.3, which attributes the oscillations to the inaccurate model of the air-core transformer used there.

The simulation results so far presented in the current Section, are in agreement with what is expected from the tapping station. However, looking at some other variables of the system, the results are not exactly within the anticipated limits. This variables are presented and discussed in the following.

Fig. 6.23 shows the voltage across the capacitor C_1 in the steady state.

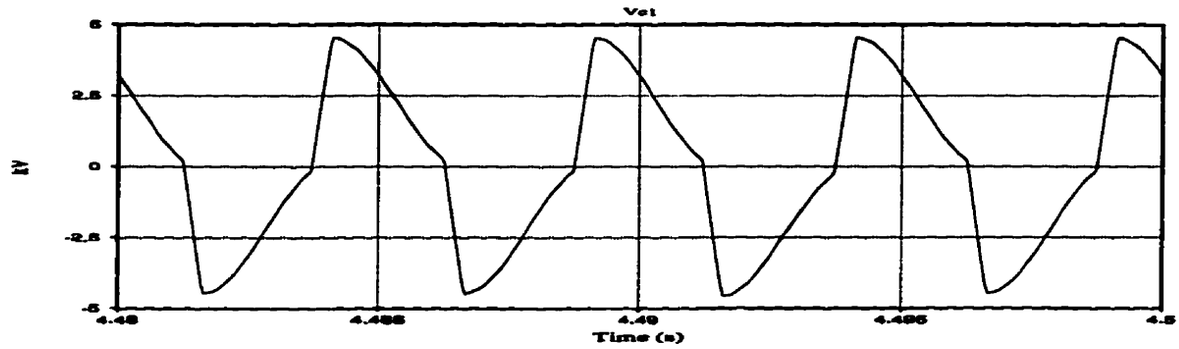

Fig. 6.23 - Capacitor C1 Voltage

At full load, the voltage is within the ±4.5 kV. But as Fig. 6.24 shows, the voltage positive and negative peaks are nearly double this value at no-load, or lower load levels.

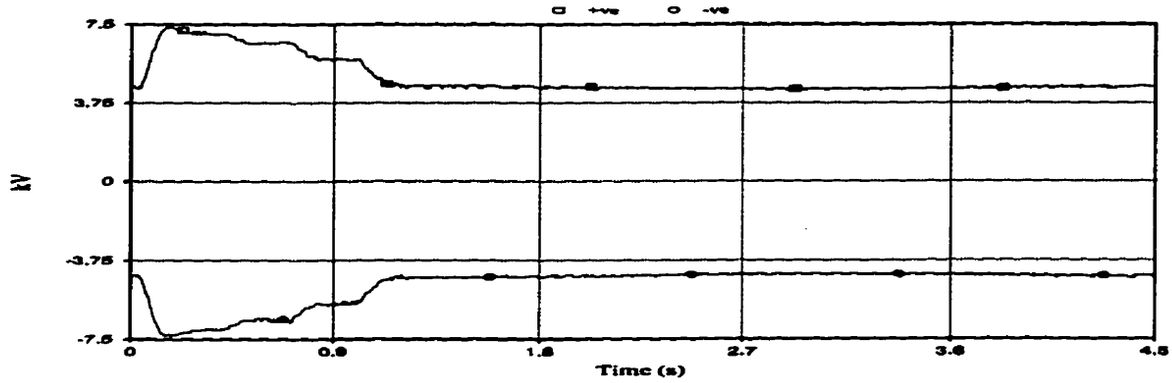

Fig. 6.24 - Vc1 Voltage Envelopes

The levels are even higher for the voltage applied on the transformer's primary winding, as shown in Fig. 6.25.

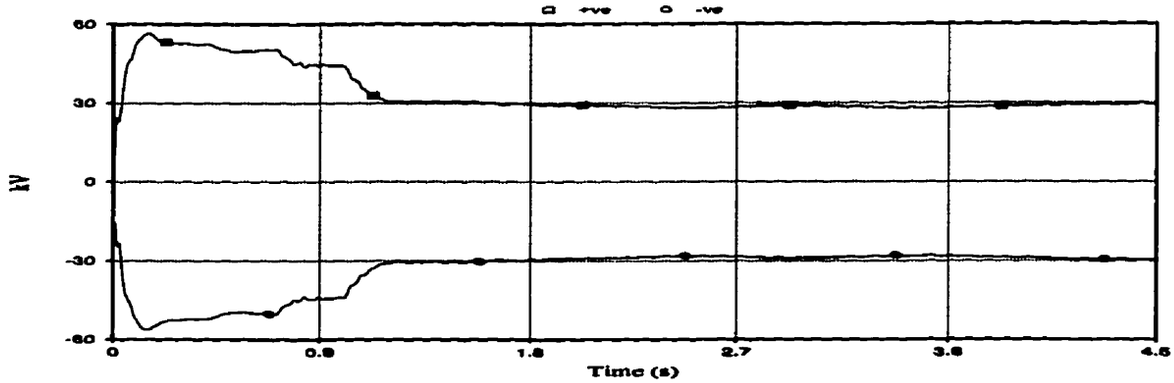

Fig. 6.25 - Primary's Voltage Envelopes

At no-load conditions, the voltage is as high as nearly 55 kV, and at full load, the level is around 30 kV. The high voltage is caused by the series capacitor which is employed to compensate the high magnetizing current. The mechanism through which the voltage across the primary winding is increased can be illustrated through the following simple circuit. If the AC voltage across the capacitor C_1 is represented by a voltage source, V_s, and if the whole tapping station is represented by an *R-L* equivalent, the phasor diagram of the voltages is as follows:

$$V_1 = V_s = RI + jX_L I$$

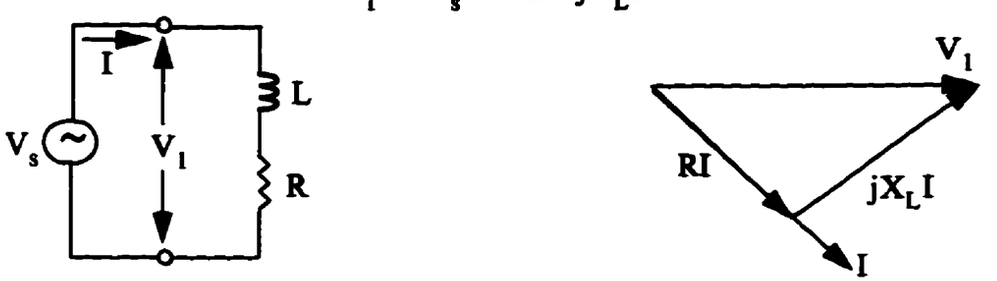

Fig. 6.26 - Uncompensated Equivalent Circuit

The voltage applied on the primary winding is simply the source voltage.

However, if a capacitor is placed in series with the primary winding, the voltage applied on the primary is no longer the source voltage. The phasor diagram of this situation is as follows:

$$V_1 = V_s - (-jX_C I) = RI + jX_L I$$

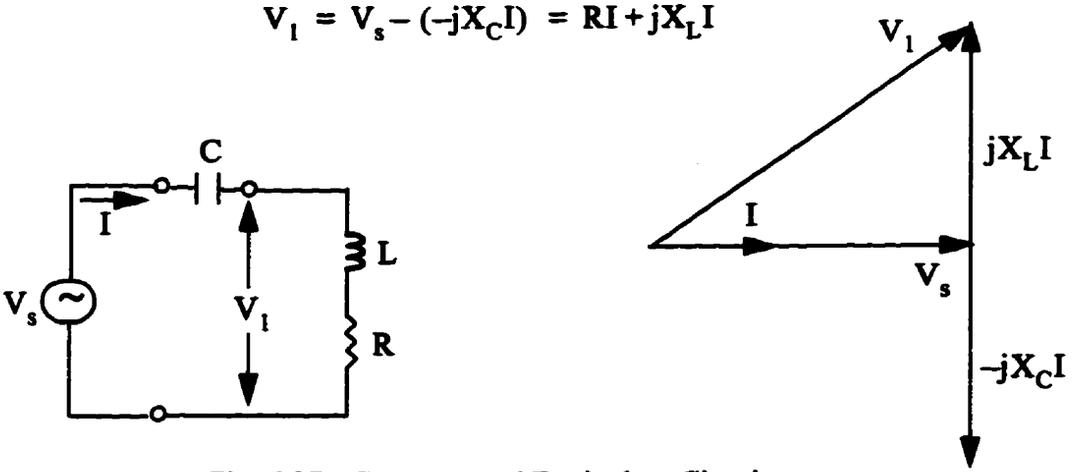

Fig. 6.27 - Compensated Equivalent Circuit

In drawing Fig. 6.27, it has been assumed that the capacitor C and the inductor L are resonating at the frequency in question, so the current is in phase with the voltage source. It is evident that the voltage across the primary winding of the transformer is larger than the source voltage, and it gets larger for higher capacitive reactances placed in series with the transformer.

Fig. 6.28 shows the envelopes of the voltage across the secondary winding of the transformer.

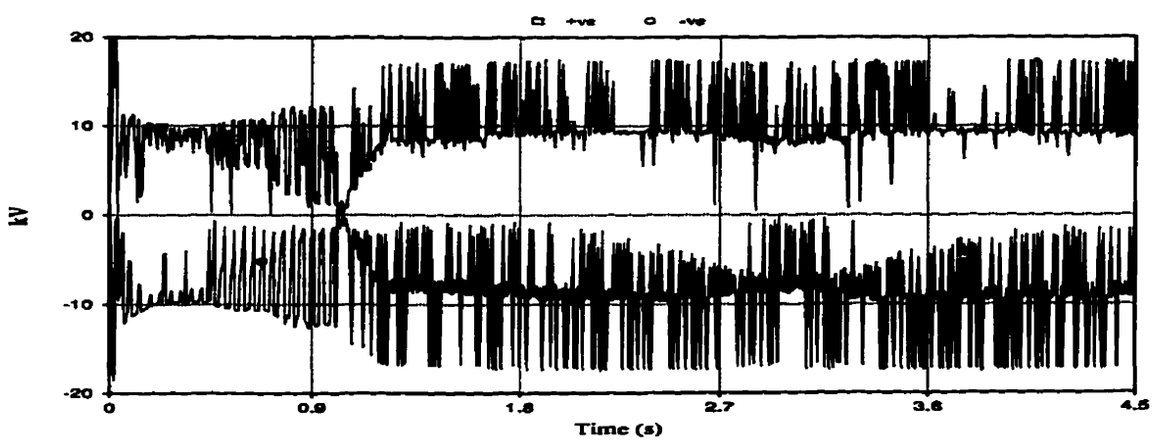

Fig. 6.28 - Secondary's Voltage Envelopes

Because of the low coupling of the transformer, the secondary voltage is lower than the primary voltage.

Fig. 6.29 shows the envelopes of the AC voltage applied on the single-phase rectifier.

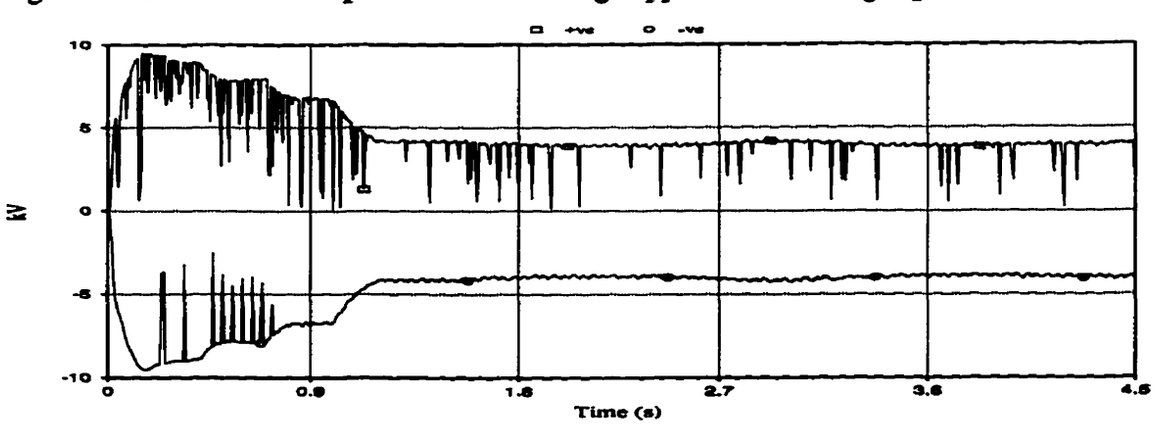

Fig. 6.29 - Envelopes of the Rectifier's AC Voltage

Regarding the high voltage across the capacitor C_1 , it can be remedied by the series connection of two GTO thyristors in the series tap, which is presently possible as discussed in Section 5.4. This will increase the allowable peak repetitive voltage to 9 kV, which is sufficiently high for the case under study.

Regarding the high voltage across the primary winding of the transformer, which has a peak of nearly 55 kV at the worst conditions, it may or may not be acceptable, but the definite answer is dependent on the design characteristics of the air-core transformer. However, considering the fact that the coil under study has 60 turns, and a height of 1.2 meters, a peak voltage of 55 kV does not seem an impossible level to handle.

6.7. Biomedical Effects of the Air-core Transformer

Having established the feasibility of using air-core transformer in the tapping station, and the possibility of tapping up to 600 kW through a transformer with a radius of 5 meters, it is worthwhile to study the biomedical effects which the transformer may have on the living objects around it.

Almost concurrent with the development of electric networks, there has existed a concern for possible health effects from the electric and magnetic fields which pervade the space around these networks. During the past few decades, numerous studies have been undertaken to examine the effects of these fields on human beings. Nevertheless, a universally accepted standard for defining the safe levels of these fields has yet to be established. Regardless of this, it is worthwhile to examine the magnetic field around the air-core transformer. A reasonable guideline will be the magnetic field generated by ordinary home appliances, and/ or the earth's natural magnetic field.

To calculate the magnetic field outside the two coils, a computer program is used. The program, briefly, uses the following relationship, known as Ampere's law [26]:

$$\oint \mathbf{H} \cdot d\mathbf{L} = I, \tag{6.16}$$

to find the magnetic field intensity due to the current in the two coils at any given point outside the transformer. Based on Ampere's law, the line integral of the magnetic field intensity around any closed path is equal to the net value of the current crossing the area inside the closed path. Because of the AC current passing through the transformer, the magnetic field, too, has an alternating nature, but the maximum field magnitude can be found by considering the peak currents in the coils. Also, the two currents, because of the large leakage reactance of the coils, are well out of phase, but for simplicity, a worst case scenario of having both currents in phase has been considered. The program, using equation (6.16), finds the horizontal and vertical components of the magnetic field intensity at the point under consideration for each turn of the coils. The summation of all horizontal and vertical components leads to the total magnetic field intensity at the point of interest, which when multiplied by the air's permeability, i.e. μ_0, will result in total magnetic flux density at that point.

Fig. 6.30 shows the transformer currents at the peak load, i.e. 600 kW. The peak primary current is 560 A, and the peak secondary current is 350 A.

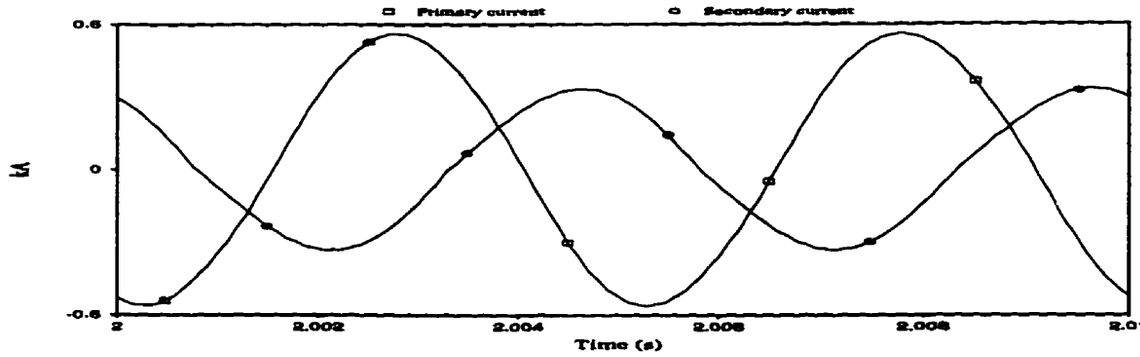

Fig. 6.30 - Transformer Currents

Fig. 6.31 shows the magnetic flux density around the transformer.

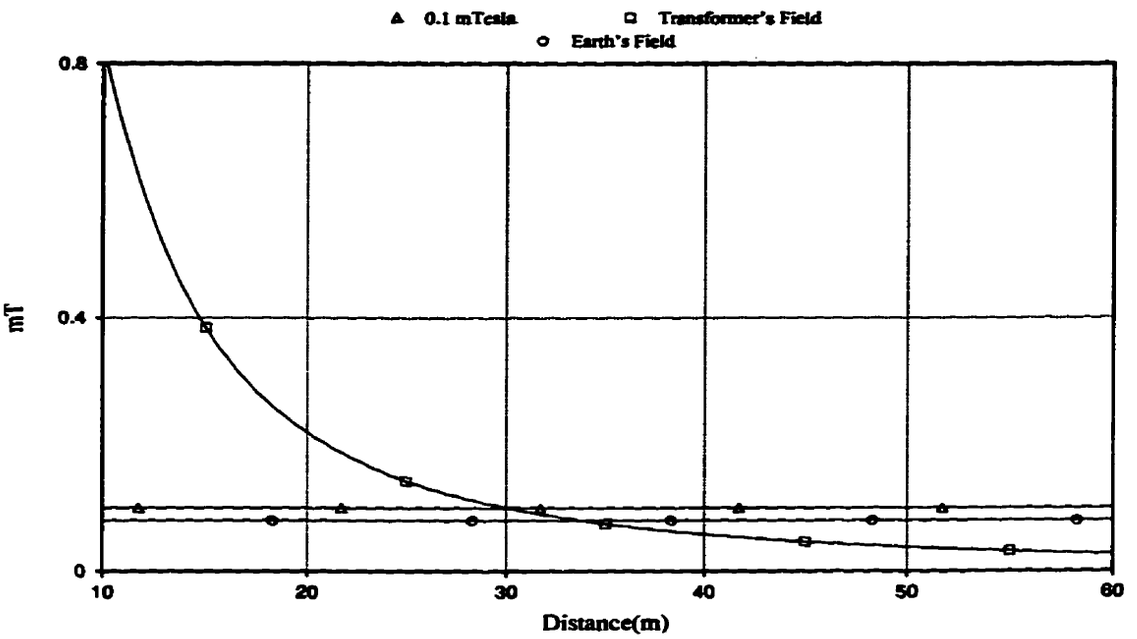

Fig. 6.31 - Magnetic Flux Density around the Transformer

For comparison, the earth's magnetic flux density, around 0.08 mT, and the maximum magnetic flux density associated with many home appliances, around 0.1 mT [27], are also shown. The transformer's field is equal to the 0.1 mT limit at a distance of 30.1 m, and it's equal to the earth's field at a distance of 33.8 m. Assigning a protected area with a radius of up to 30-40 meters around the transformer presents no practical difficulties, as such an area is already covered by the HVDC line's right of way. Consequently, it is believed that an air-core transformer, with dimensions and power levels considered in this study, poses no health risks to the communities around it.

6.8. Summary of the Chapter

In this Chapter, using classical electromagnetic theory, relationships for calculating the inductances of the air-core transformer, proposed to be employed in the tapping scheme, were developed.

A prototype transformer was built, and the laboratory results proved the validity and the accuracy of theoretical relationships. Also, the performance of the prototype transformer was compared to the results of the digital simulation performed by the PSCAD/EMTDC software package. Experimental and simulation results are in good agreement.

Next, the performance of the tapping scheme with a large air-core transformer, with a radius of 5 m, was studied and it was shown that a load of up to 600 kW can be successfully tapped from the HVDC system.

And finally, the possible biomedical effects of the transformer was studied. It was shown that the magnetic flux density created by the transformer beyond the system's right of way, is less than that of ordinary home appliances, and hence poses no health risks to human beings.

Chapter Seven

Design and System Considerations

In Chapter Four, Chapter Five, and Chapter Six, the technical feasibility of the proposed tapping scheme was studied and proven. The criteria for proving the technical feasibility of the scheme included the characteristics of the solid-state devices available on the market, the range of the power demanded by most of the isolated communities, and the reliable flow of power to the local load for various levels of DC power being transmitted through the HVDC system. Besides these factors, however, several other design and system considerations must be addressed. Some of the features associated with a tapping station, e.g. switching losses, protection of solid-state devices, the use of fiber optic channels for transmitting the control and firing signals to the high potential segments, are common to the majority of HVDC systems, and have been addressed and examined extensively in the literature and in practical HVDC and/or power electronic installations. In this Chapter, the

emphasis is placed on the features which are more or less specific to a series tap.

7.1. Start-up and Bypassing the Tapping Station

Besides the electric and solid state devices, introduced in this study so far, which seem as necessary parts of the tapping station, some other elements, including three breakers, need to be present in the scheme. Fig. 7.1 shows the necessary configuration of the series tap in conjunction with the HVDC system [5].

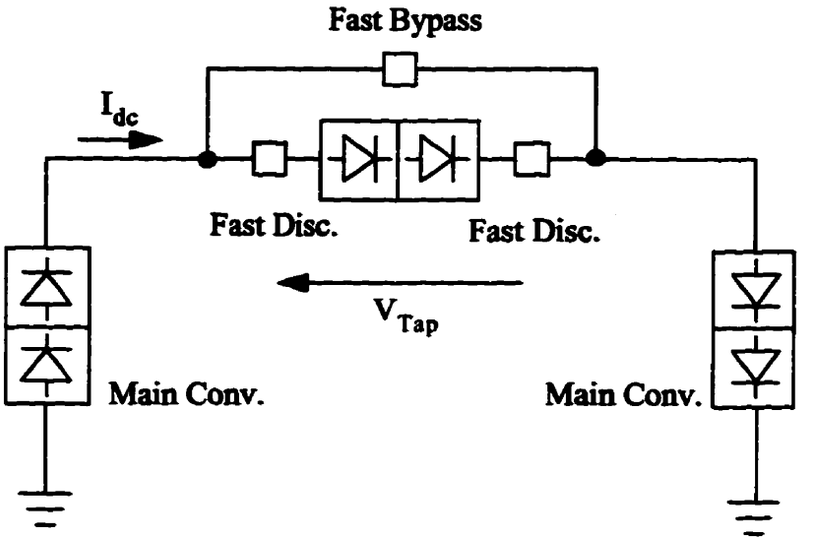

Fig. 7.1 - Series Tap Configuration

To start the tapping scheme up, while the DC current is flowing through the Fast Bypass breaker, firing signals are issued to all the four GTO thyristors in the series tap, and the Fast Disconnect breakers are closed. Then the fast Bypass breaker is opened, thereby, forcing the DC current to flow through the series tap, without any disruption in the flow of the DC current/power. When the DC current is completely diverted through the tap, because of its lower impedance compared to that of the opened Bypass breaker, the current in the Bypass breaker comes to a natural zero, without the need to any additional extinguishing measures. Then the control regime of the tap can turn two of the GTO thyristors off, and start the

process of generating the sawtooth voltage across the capacitor C_1.

To bypass the tapping station, be it because of local or system faults, or for maintenance purposes, again, firing signals are issued to all 4 GTO thyristors in the tap. The Fast Bypass breaker is closed, and the disconnect breakers are opened, while GTO thyristors are signaled to turn off. The current will commutate through the Fast Bypass breaker.

While the Fast Bypass breaker needs to withstand peak voltages of the order of a few kV, i.e. that of V_{Tap}, the Fast Disconnect breakers must be able to isolate the HVDC line potential from the ground potential, to ensure the safety of the maintenance crew. All the three breakers, however, need to be rated for the system's maximum DC current.

7.2. Switch Protection

In conventional HVDC systems, each thyristor (switch) is equipped with a number of protective devices. Fig. 7.2 shows two thyristors, in series, with their control and protection peripheral devices.

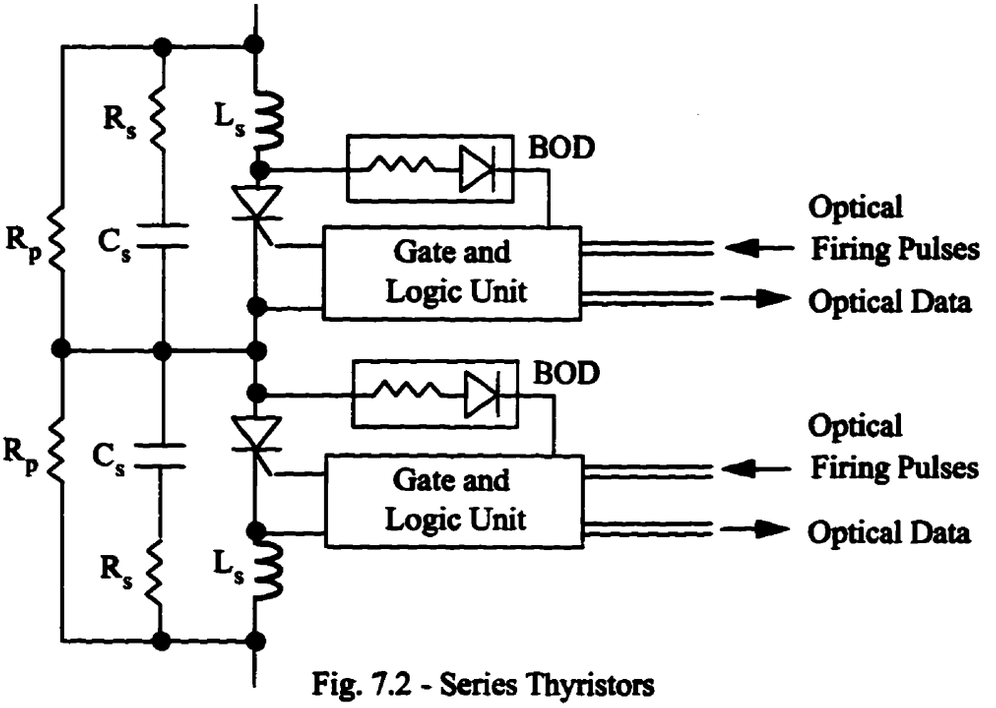

Fig. 7.2 - Series Thyristors

GTO thyristors, too, can be protected by means similar to those of ordinary thyristors, as shown in Fig. 7.2.

7.2.1. dI/dt Protection

The rate at which the current can build up in a turning-on switch, or diminish in a turning-off one, must be constrained to prevent the switch from over-heating damage. This rate (which can usually be higher for a switch which is turning off) depends on the design specifications of the switch in use, and is supplied with the device by the manufacturer [23]. Typical maximum permitted *dI/dt* values are between 300 to 600 $A/(\mu s)$ for available GTO thyristors[15]. Inductor L_s, which is placed in series with each switch, ensures that the current does not change more rapidly than allowed by the switch's *dI/dt* capability. Typical values of L_s are around a fewμH [23].

For the specific configuration used in the proposed tapping scheme, one might want to place one single inductor in series with the capacitor C_1, instead of one inductor for each switch, to provide *dI/dt* protection. This will obviously lead to some savings in the fixed cost of the station. However, since in some cases, including start-up and bypassing, the capacitor C_1 may be bypassed through firing all four switches, and the current will not go through the capacitor, each switch must have its own series inductor for *dI/dt* protection.

7.2.2. dV/dt Protection

Similar to the *dI/dt* limitation, the rate at which the forward and reverse voltage applied on a thyristor changes, must be constrained. A fast-changing forward voltage, because of the junction capacitance in the switch, *C*, may inject a current equal to $C\frac{dV}{dt}$ to the switch's

gate, which may turn the switch on at the wrong time. To prevent this from happening, and in order to limit the rate at which the voltage can change, a R-C branch, called the snubber, is placed in parallel with each switch. Resistor R_s and capacitor C_s are the snubber elements. The values of these elements depends on the specifications of the switch they are to protect, as well as system variables like the switching frequency. Typical values range from 5 to 50 Ω for the resistance, and from 0.1 to 2 μF for the capacitance[23]. Typical maximum permitted *dV/dt* values are between 500 to 1400 $V/(\mu s)$ for available GTO thyristors[15].

7.2.3. Even Voltage Distribution

When a number of switches are placed in series, it is important to ensure that the voltage which is to be blocked by the switches is distributed evenly across all the switches to prevent over-voltage damage on some of them. Resistor R_p, which is placed in parallel with each switch, ensures an even distribution of voltage [23].

7.2.4. Break-over Diode (BOD)

In some rare instances, the firing signals issued to the switch are unable to turn it on, thereby causing commutation failure in other switches which are supposed to be turned off. Also, the control system, in some situations, may fail to issue a firing signal at all. The break-over diode (BOD), which is placed in the gate's circuit, will force the switch to turn on, if the voltage across it exceeds a set limit.

7.3. System Protection Considerations

Protection concerns associated with the tapping station and the main system can be divided to two main categories.

7.3.1. Problems Presented to the Tapping Station from the Main System

The problems which can be presented by the main HVDC system are as follows:

1. DC Over-Voltage: Regardless of the possibility, or lack of it thereof, of a DC overvoltage, this situation can not harm the series tap per se, but could cause flashover in the air-core transformer, or stress the bushings of the conventional transformer, whichever is used in the scheme. The risk is similar with or without the tapping station and can be prevented by the surge arresters at the two ends of the DC line. If the flow of the DC current is interrupted because of this protective action, the tapping station needs to be restarted after the fault is cleared and the DC current flow is re-established.

2. DC Over-Current: This situation can harm the switches in the series tap, but it also can harm the switches in the main converters. This situation will be prevented by the over-current protective measures assigned to the main converters. However, the series tap must be rated for the same transient overcurrents as the main converters to handle fault currents or commutation failures. If the fault or disturbance is prolonged, the station's by-pass switch can decrease the time of the overcurrent. Again, the tapping station has to be re-started after the DC current has returned to the normal range of operation.

3. DC Under-current and Under-voltage: These issues have been addressed in the Section 7.5. Briefly, it was found, through digital simulation, that currents of as low as 0.3 p.u. are acceptable for the tapping station, and a DC under-voltage will have no effect on the tapping station's performance, as long as the DC current is present.

7.3.2. Problems Presented to the Main System from the Tapping Station

The problems which can be presented by the tapping station are as follows:

1. Turn-on Failure: Theoretically speaking, if a GTO thyristor fails to turn on, while the GTO thyristor providing the alternative route for the current has been successfully turned off, the flow of DC current, and consequently, the flow of DC power will be interrupted. In practical cases, however, this situation will be prevented by the BOD protection.

2. Over-voltage in the series capacitor C_1 : This situation does not present any serious problem to the main system, but may cause serious damage to the non-conducting switches. The BOD protection, however, will ensure that this can not happen by firing the non-conducting switches.

3. Local AC Faults: In case of a local AC fault (at the ground potential), the single-phase rectifier can be disconnected from the intermediate DC link, and the DC link capacitor can supply the local load for a short time, depending on the size of the capacitor. The rectifier can be re-activated after the fault is cleared. Since the DC link capacitor may have some charge remaining in it (again, depending on the size of the capacitor, and the duration of the fault) the transients imposed on the series tap might be lower than normal start-up conditions.

7.4. Faults on the Single-phase Transformer

The most serious disturbances which can be imposed on the main system by the tapping station, seem to be short-circuit and open-circuit faults on the windings of the single-phase transformer. To study the impact of such faults, the tapping station is simulated in conjunction with a modified version of the CIGRE Benchmark Model [28], [29]. This model, briefly, is a 1000 MW, 500 kV, 12 pulse, monopolar HVDC system. The only modification in the system is the replacement of lumped elements representing the transmission line, with

the distributed model of a 900 km overhead line in PSCAD/EMTDC. The height of transmission towers is 40 m, and the sag at the midpoint of adjacent towers has been assumed to be equal to 10 m.The tapping station has been placed at the midpoint of the transmission line, i.e. 450 km from each end. Fig. 7. 3 shows the study system used for simulation.

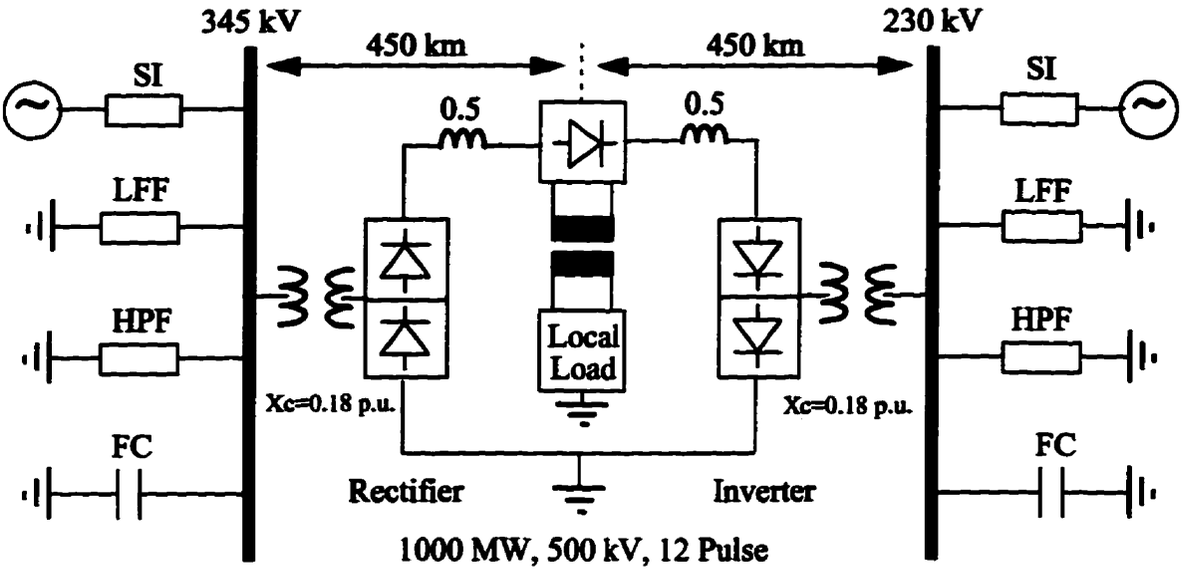

SI: System Impedance FC: Fixed capacitor

LFF: Low Frequency Filter HPF: High Pass Filter

Fig. 7.3 - The Study System

7.4.1. Loading and Cut-off Fault

First the impact of loading the tap on the HVDC system is studied. After the tap is brought to the steady-state operation at full load (around 600 kW), the secondary of the single-phase transformer is opened to observe its impact on the operation of the main system. The following is the chain of events at this stage of simulation (all times are in seconds):

- Time = 0.0: The main system is started,

- Time = 0.6: The tap's single-phase rectifier is activated,

- Time = 0.9: 33% of the load is applied on the tap,

- Time = 1.3: The load is increased to 66%,

- Time = 1.6: The load is increased to 100%,

- Time = 2.0: Rectifier's breaker is opened, the DC link voltage starts to collapse,

- Time = 2.1: Rectifier's breaker is closed, the DC link voltage starts to recover,

- Time = 2.25: The system is not able to recover fully, 33% load-shedding is performed,

- Time = 2.5: The system has stabilized with 66% load,

- Time = 2.7: The load is again increased to 100%,

- Time = 3.2: The system is working stably.

Fig. 7.4 shows the DC link voltage, the modulation index, and the local load's rms voltage.

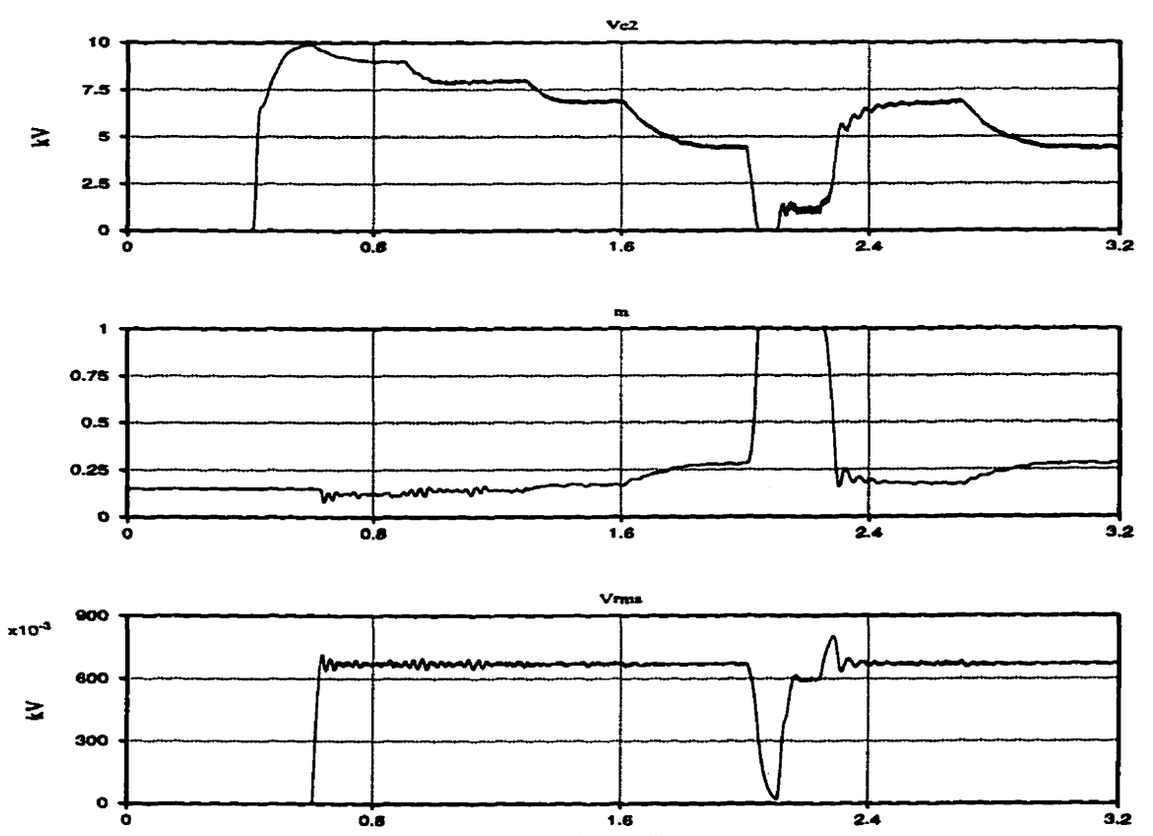

Fig. 7.4 - Tap's Variables

Fig. 7.5 shows the local load's active and reactive powers.

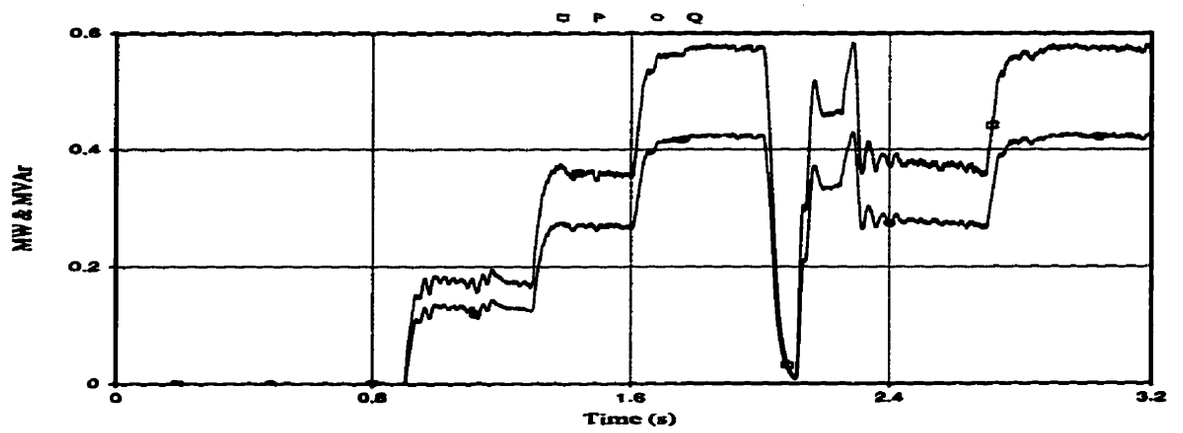

Fig. 7.5 - Load's Active and Reactive Powers

The small capacitance chosen for the intermediate DC link (1.0 mF) is not able to supply the local load in the event of a cut-off, so a larger capacitance may be needed, if the supply of power is to last longer during the faults. Also, the jump in the local load's rms voltage after the load-shedding is performed may cause some over-voltage protective measures to react and disconnect the tap from the local load altogether, so a smaller percentage of load-shedding might be able to help the system recover without too much jump in the load voltage.

Fig. 7.6 shows the envelopes of the voltage across the capacitor C_1. The peak voltage does not greatly surpass that of the no-load conditions.

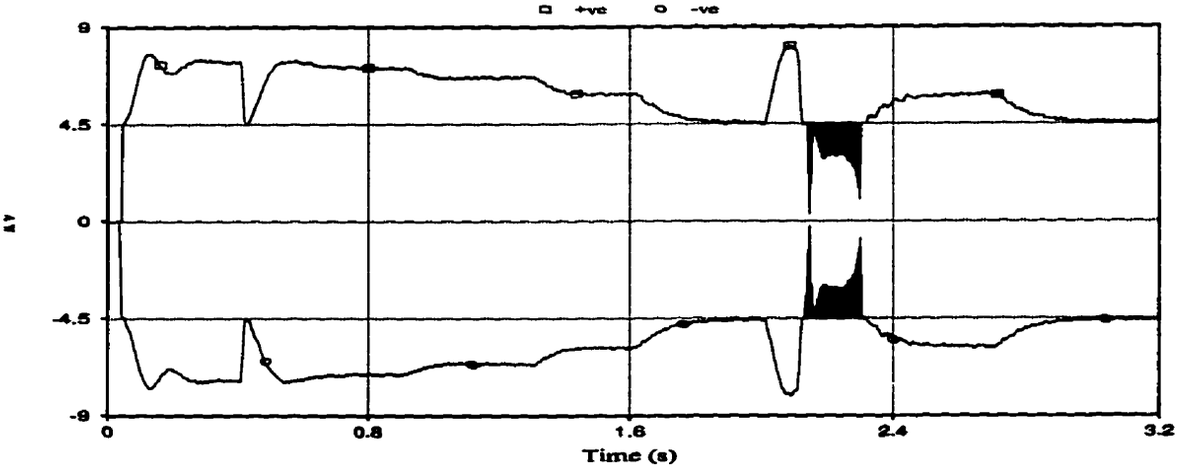

Fig. 7.6 - Envelopes of Vc1

Fig. 7.7 shows the variables of the main system.

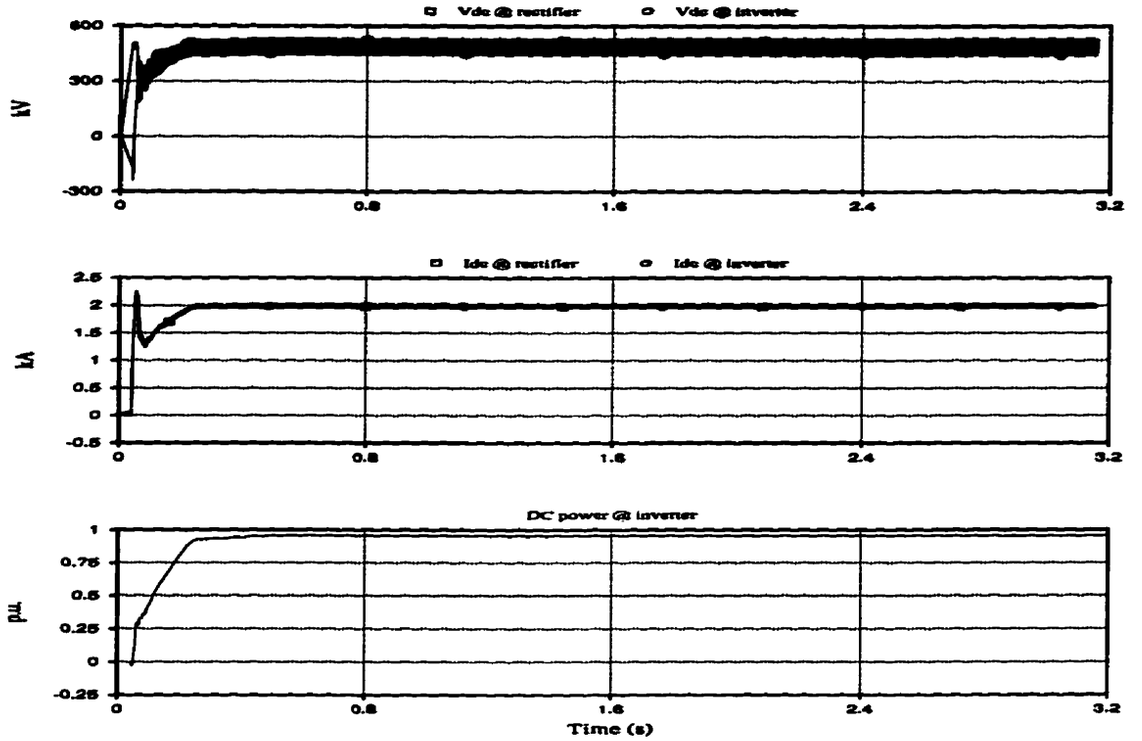

Fig. 7.7 - Main System's Variables

Due to lack of DC filters in the study system, DC voltages are rich in characteristic harmonics.

Fig. 7.8 shows the firing angles issued to the rectifier and the inverter by the control system.

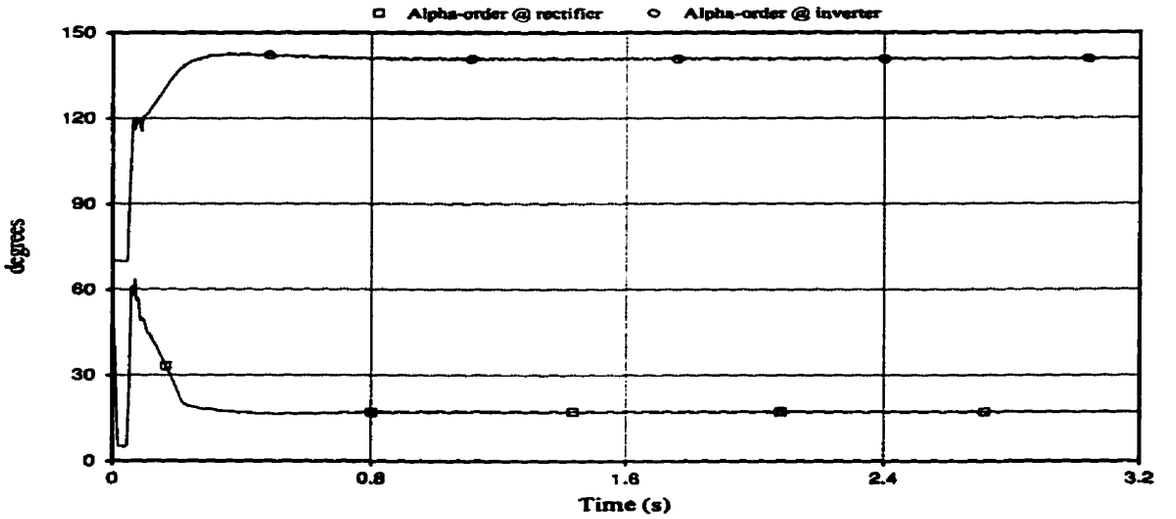

Fig. 7.8 - Firing Angles

Although the operation of the main system appears to be totally unaffected, it is worthwhile to examine some parameters in more details. Fig.7.9 shows the DC power at the inverter and the firing angles during the period after the cut-off fault has occurred.

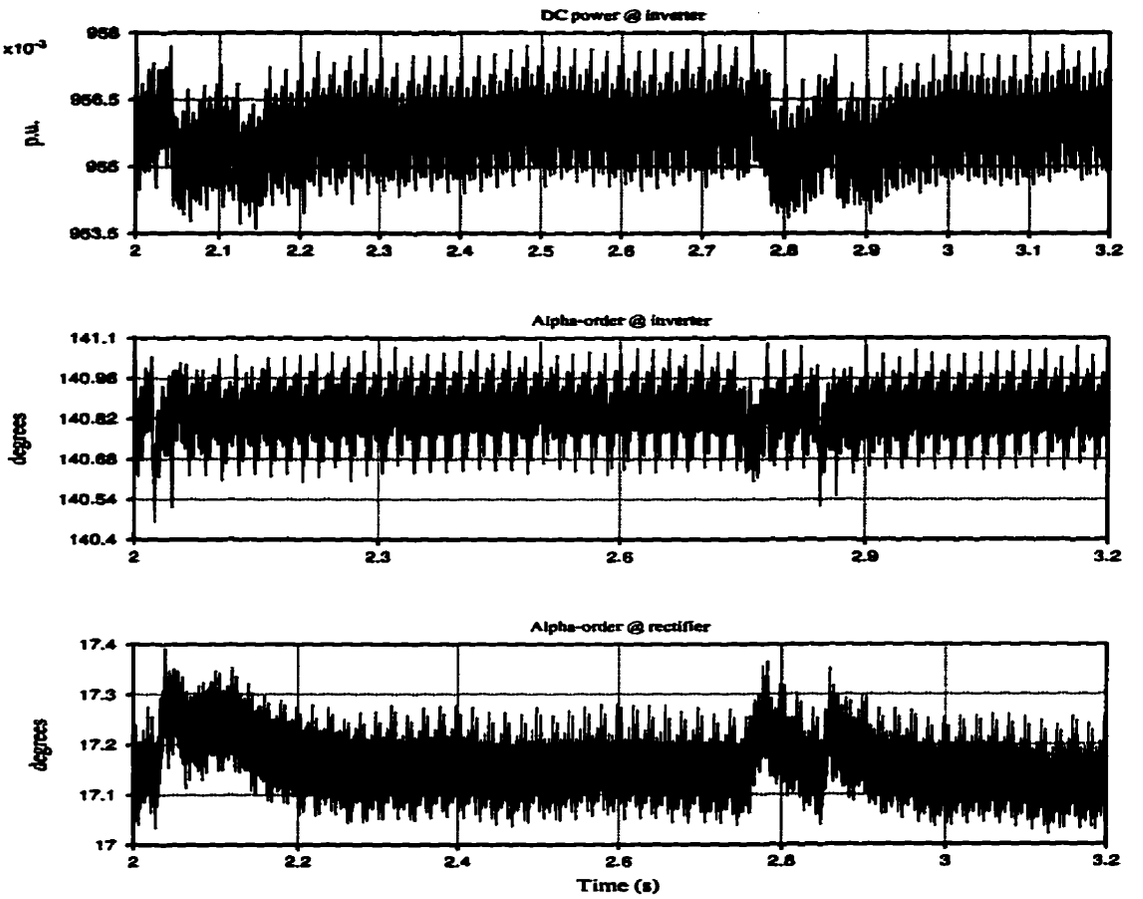

Fig. 7.9 - Main System's Variables in Detailed Mode

After the tap has been cut off from the main system at time =2.0 s, the DC power at the inverter shows a jump of around 0.0006 p.u. which corresponds to the 600 kW power rejected by the tapping station. Compensating action by the control system, through increasing the firing angles at both ends of the HVDC system, brings the power back to its pre-fault value. Clearing the fault at Time=2.1 causes an equal drop in the DC power at the inverter, until the consequent decrease in the firing angles brings the power back to its set level, again. At Time=2.7, when the load is increased to 100%, the DC power drops once more, but the

control system operation compensates this very quickly.

The results shown here prove that not only does a cut-off fault in the tapping station have no serious consequences for the main system, but also show that the control system associated with the main system is capable of keeping the operation balanced (i.e. the rectifier power to be equal to the requested power by the inverter plus the tapped power) without the need to get any control signals from the tapping station.

The cut-off fault is not applied on the primary winding of the transformer, because it is expected to be similar to a cut-off on the secondary.

7.4.2. Phase-to-ground Fault on the Transformer's Secondary

Similar to the previous case, the system is brought to the steady-state, and then, at full load, a phase-to-ground fault is applied on the secondary of the transformer. The chain of events are as follows:

- Time = 0.0: The main system is started,
- Time = 0.6: The tap's single-phase rectifier is activated,
- Time = 0.9: 33% of the load is applied on the tap,
- Time = 1.3: The load is increased to 66%,
- Time = 1.6: The load is increased to 100%,
- Time = 2.0: The fault is applied on the transformer winding,
- Time = 2.1: The fault has been cleared.

Unlike the previous case, the flow of power to the local load, as well as the flow of the DC power in the main system, has not been affected at all and all other parameters remain the same before and after the fault has occurred and cleared. This is because of the fact that the

secondary of the transformer is not grounded (only the secondary of the three-phase transformer, i.e. the wye winding on the local load side, has been grounded), so a phase-to-ground fault results in no abnormality. Fig. 7.10 shows the power tapped into the local load.

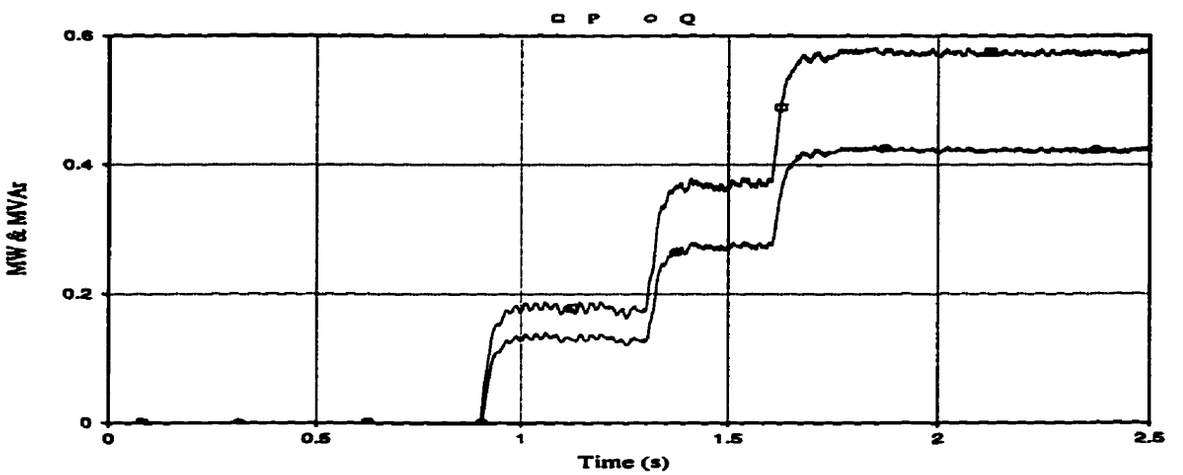

Fig. 7.10 - Local Load's Active and Reactive Powers

And Fig. 7.11 shows the DC power in the main system.

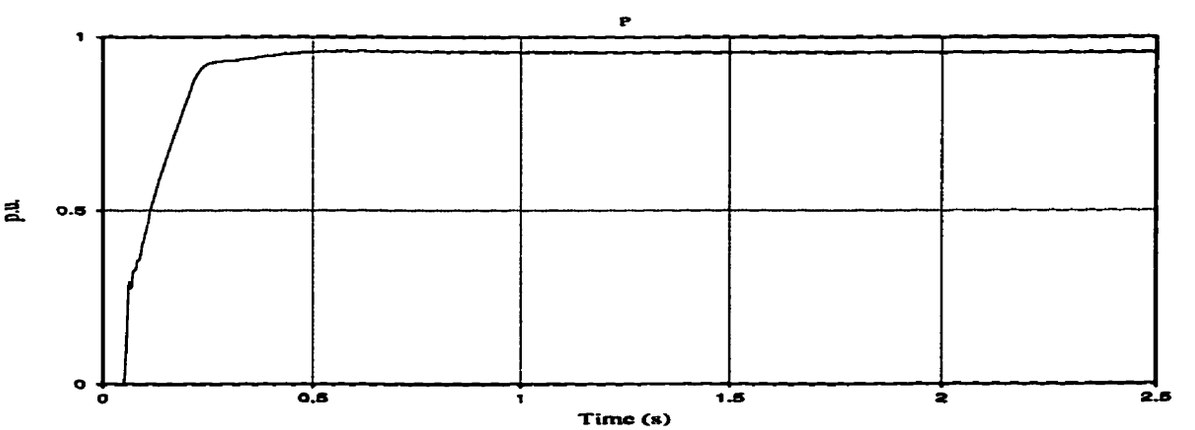

Fig. 7.11 - DC Power in the Main System

7.4.3. Phase-to-phase Fault on the Transformer's Secondary

The system is brought to the steady-state, and then, at full load, the short-circuit is applied on the secondary of the transformer. The chain of events are as follows:

- Time = 0.0: The main system is started,

- Time = 0.6: The tap's single-phase rectifier is activated,

- Time = 0.9: 33% of the load is applied on the tap,

- Time = 1.3: The load is increased to 66%,

- Time = 1.6: The load is increased to 100%,

- Time = 2.0: The short-circuit is applied, the DC link voltage starts to collapse,

- Time = 2.1: The short-circuit has been cleared, the DC link voltage starts to recover,

- Time = 2.3: The system is unable to recover fully, 33% load-shedding is performed,

- Time = 2.6: The system has stabilized with 66% load,

- Time = 2.8: The load is again increased to 100%,

- Time = 3.2: The system is working stably.

Fig. 7.12 shows the DC link voltage, the modulation index, and the local load's rms voltage.

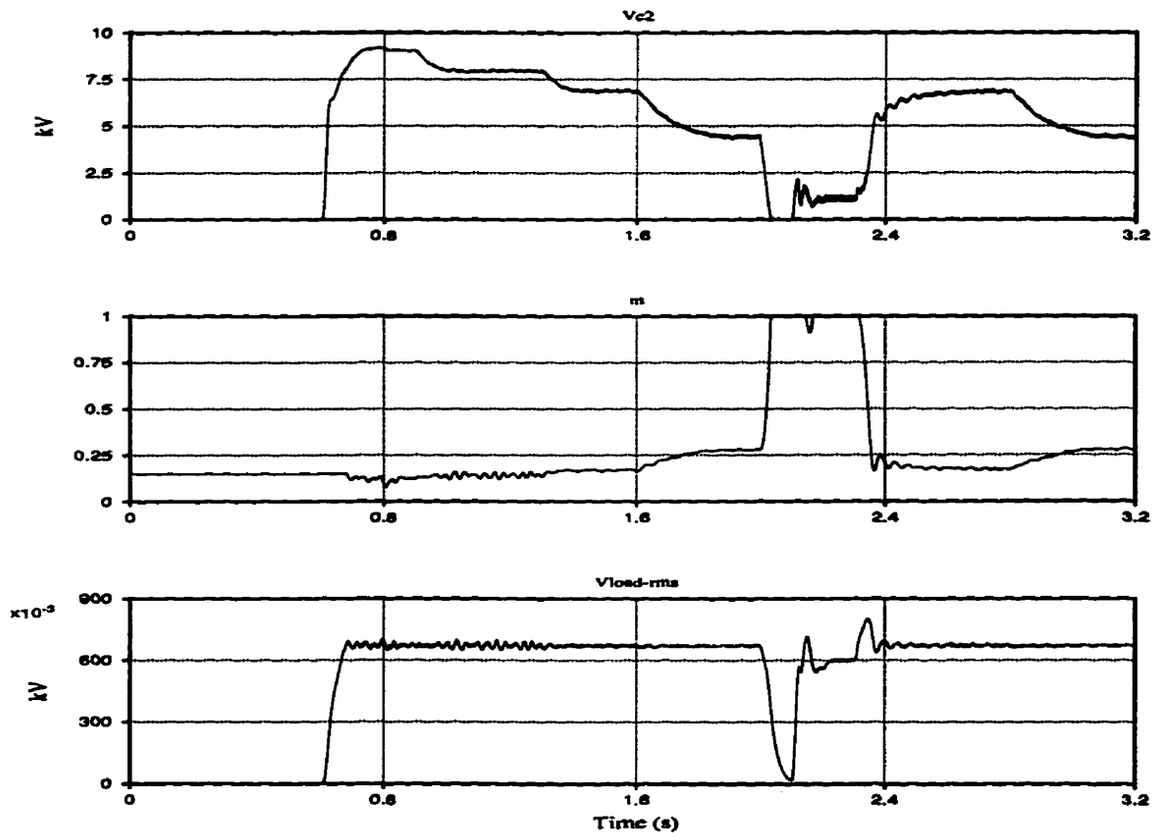

Fig. 7.12 - Tap's Variables

Fig. 7.13 shows the local load's active and reactive powers.

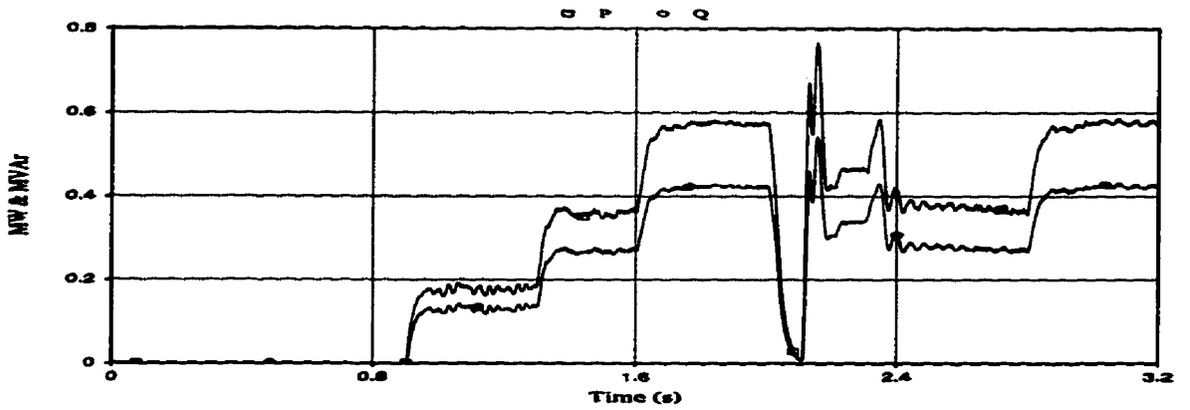

Fig. 7.13 - Local Load's Active and Reactive Powers

Fig. 7.14 shows the envelopes of the voltage across the capacitor C_1. Again, the peak voltage does not greatly surpass that of the no-load conditions.

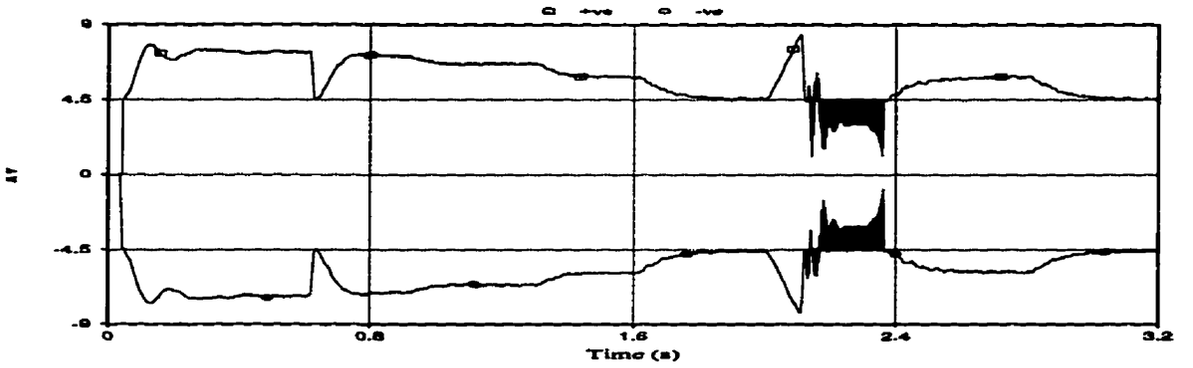

Fig. 7.14 - Envelopes of Vc1

Fig. 7.15 shows the DC power in the main system.

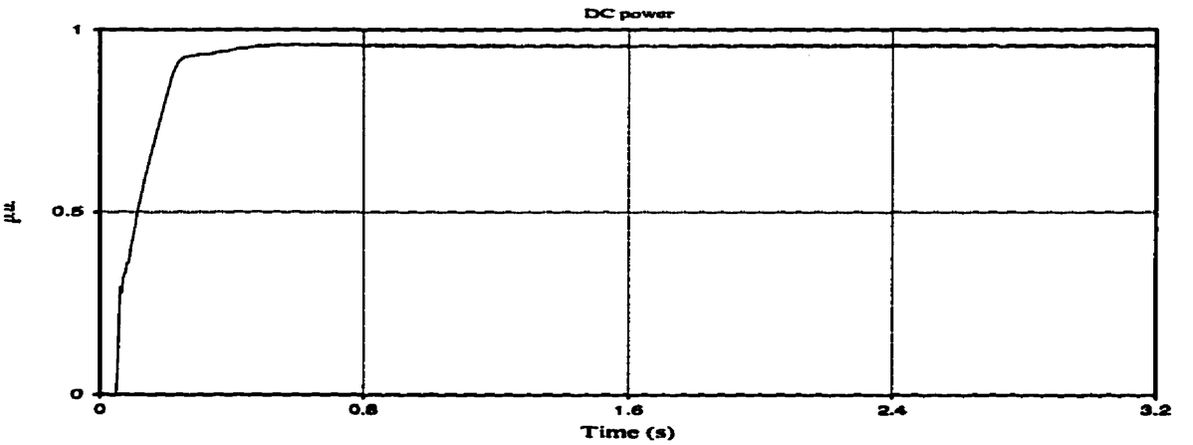

Fig. 7.15 - Main System's DC Power

The results shown here prove that a phase-to-phase (short-circuit) fault on the secondary winding of the single-phase transformer has no serious consequences for the main system's operation.

7.4.4. Phase-to-ground Fault on the Transformer's Primary

The single most serious fault is expected to be a phase-to-ground fault on the transformer's primary winding. This fault should have the effect of an ordinary line-to-ground fault on the HVDC system, but the tapping station may also be strained because of it. To examine the effects of such a fault, the system is brought to the steady-state, and then, at full load, a solid phase-to-ground fault is applied on the primary of the transformer. The chain of events are as follows:

- Time = 0.0: The main system is started,
- Time = 0.6: The tap's single-phase rectifier is activated,
- Time = 0.9: 33% of the load is applied on the tap,
- Time = 1.3: The load is increased to 66%,
- Time = 1.6: The load is increased to 100%,
- Time = 2.0: The phase-to-ground fault is applied, the DC line voltage collapses quickly, the DC line current is decreased to 0.55 p.u. (1.1 kA) by the control system,
- Time = 2.1: The fault has been cleared, the DC line voltage remains zero, the DC power transfer remains stopped, the DC line current remains at 1.1 kA,
- Time = 2.4: The system is not allowed to resume DC power transfer by the control system but the tapping station is working normally, due to its current-source nature.

Fig. 7.16 shows the DC link voltage, the modulation index, m, and the local load's rms

voltage.

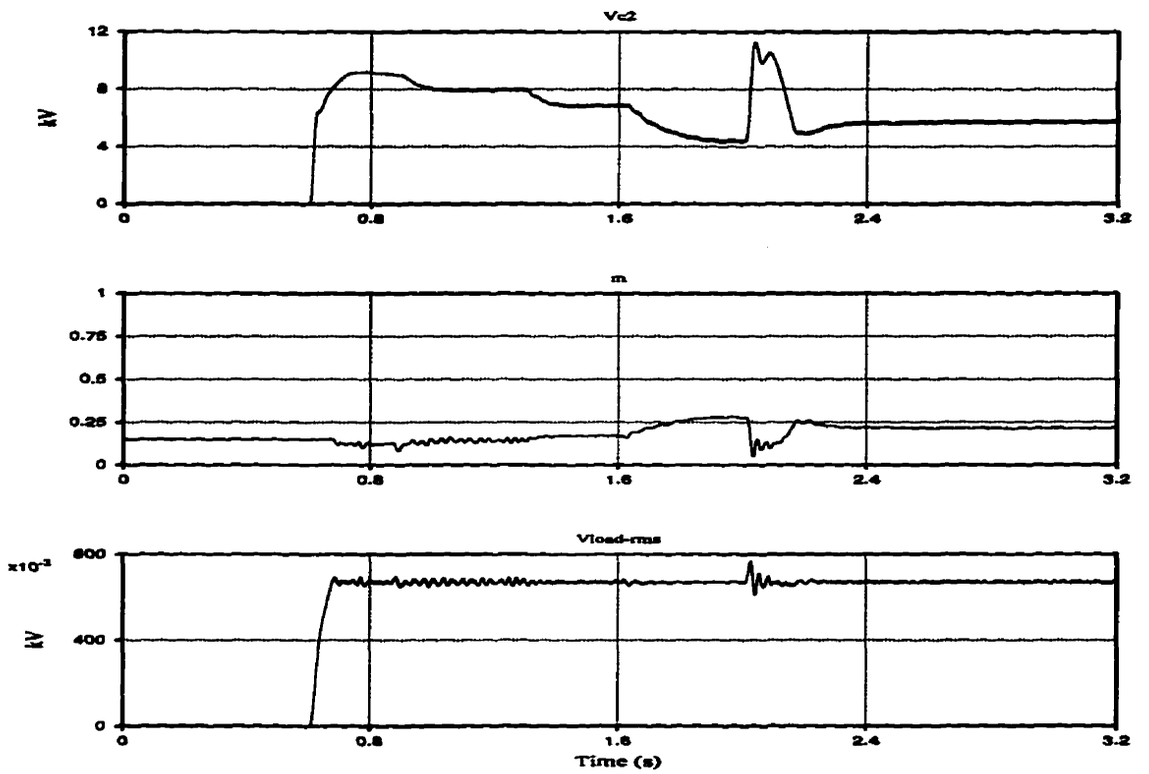

Fig. 7.16 - Tapping Station's Variables

Although the DC line voltage has collapsed after the fault, the flow of a 0.55 p.u. DC current in the DC line allows the tapping station to continue its operation, with minor disturbance, due to the fast reaction of the SPWM controller.

Fig. 7.17 shows the local load's active and reactive powers.

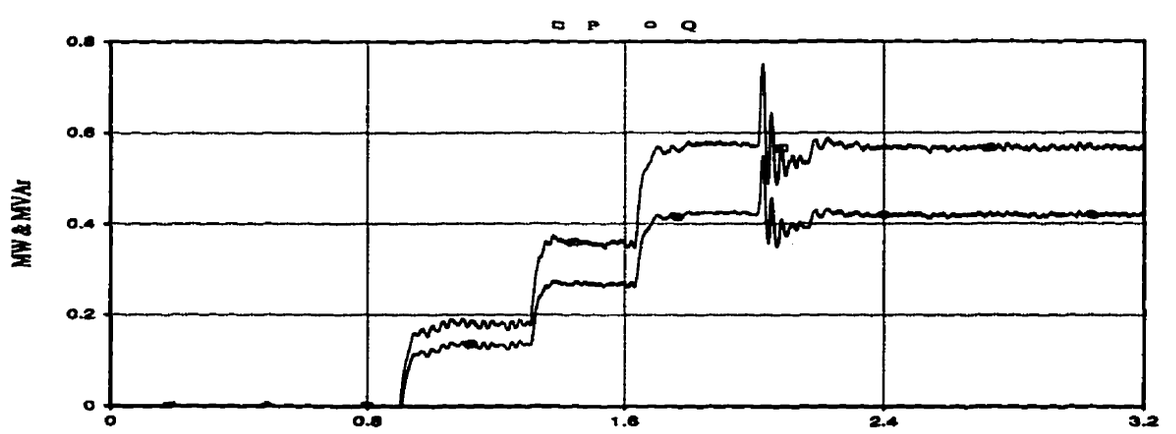

Fig. 7.17 - Local Load's Active and Reactive Powers

Fig. 7.18 Shows the envelopes of the voltage across the capacitor C_1.

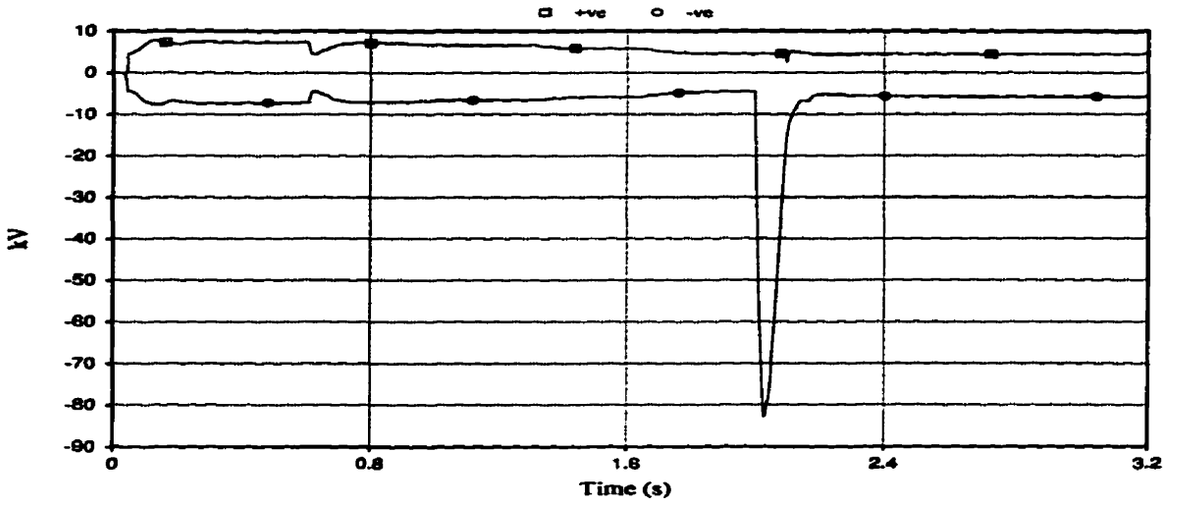

Fig. 7.18 - Envelopes of Vc1

Immediately after the fault, the negative envelope jumps to -82 kV, but starts to return to its pre-fault value very quickly. It takes 0.13 seconds before the voltage is at its pre-fault level. The reason for such a huge jump in the capacitor voltage can be explained as follows. Prior to the fault the voltage measurement is being performed between the two terminals of the transformer's primary winding, and therefore, the voltage observed is equal to the voltage generated across the capacitor C_1. After the fault, one terminal of the transformer winding is grounded, while the other is still at the line potential, and therefore, the observed voltage (the voltage experienced by capacitor C_1) will be the difference between the line potential and the ground. Of course, the line voltage is 500 kV prior to the fault, but the forced-retardation act performed by the rectifier control, through which the firing angle goes to around 90 degrees, brings this voltage back to zero very fast, and after that, the observed voltage is, once again, the saw-tooth voltage generated by the tap. This kind of over-voltage can be detrimental to both the capacitor and the transformer, if enough over-voltage protecting measures, e.g. a surge arrester, are not placed in parallel with the capacitor.

The jump in the primary's voltage causes a temporary rise in the secondary voltage, and consequently, on the intermediate DC link voltage. The SPWM controller, however, ensures a minimum effect on the local load's rms voltage, and thus, on the flow of power to the local load.

Fig. 7.19 shows the main system's variables.

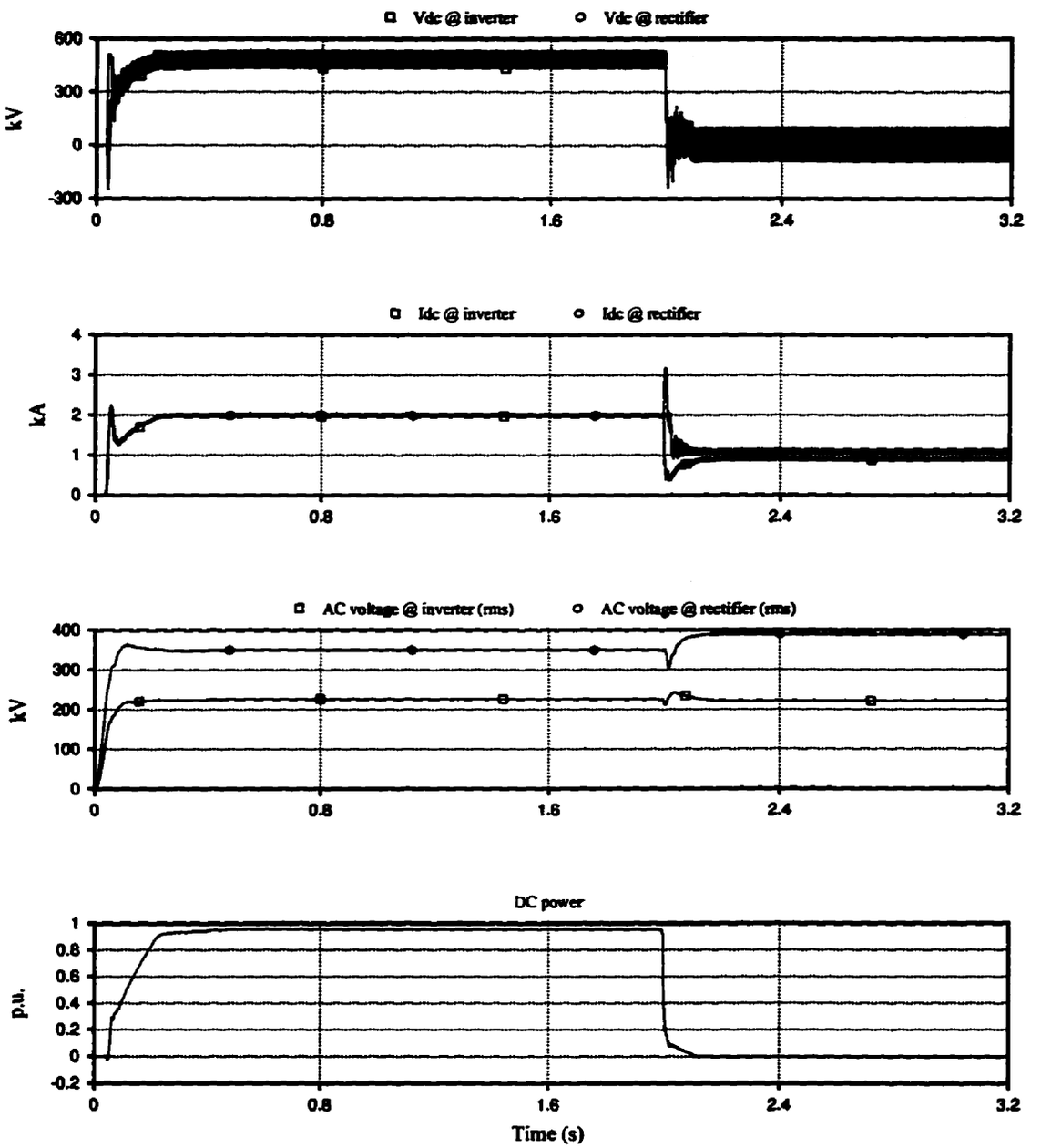

Fig. 7.19 - Main System's Variables

The DC voltage is forced to zero after the fault has occurred. The DC current is set at 1.1 kA, but the DC power flow is totally stopped, because of the zero DC voltage. As there is no Automatic Voltage Regulator (AVR) installed on the AC source of the study system, the AC rms voltage at the rectifier side has jumped because of the load-rejection phenomenon (the AC system is not an infinite bus, and has a SCR [3] of 2.5).

It is expected that the recovery of the main HVDC system, through gradual build-up of the DC voltage at the two ends, will not disturb the tapping station's performance, again, because of the current-source nature of the tap.

Fig. 7.20 shows the firing angles issued to the main system's converter by the control system.

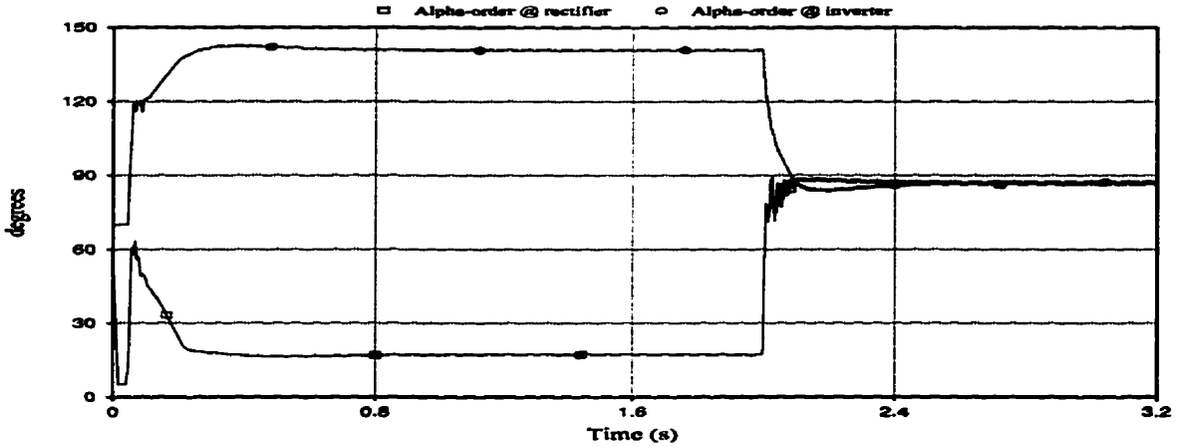

Fig. 7.20 - Main System's Firing Angles

The results shown here indicate that a phase-to-ground fault on the transformer's primary winding will have the same effect on the HVDC system as a normal line-to-ground fault. However, an increase in the number of such faults, because of the addition of the tapping station, is not expected, because of the high de-coupling provided by the air-core transformer.

7.5. Control Considerations

As mentioned in Chapter Two, the control regime for a small tapping station must be strictly

local. This is because of the fact that an integrated control system for the whole HVDC system, including the tapping station, necessitates more complex communication and control systems to be employed, which in turn, will lead to a higher fixed cost for the whole system. The high costs associated with such a complex communication system will probably overshadow the usefulness of the tapping station, and will probably make other alternatives, like local generation or AC transmission, more acceptable.

7.5.1. Varying DC Line Current

It was observed that the proposed scheme, along with its control regime, is capable of supplying a smooth flow of power to the local load for a wide range of DC line current, i.e. from 0.3 p.u. to 1.0 p.u. (with a base current of 2 kA). However, the normal operating range of the conventional HVDC transmission systems, includes DC currents from 0.1 p.u. to 1.0 p.u. Because of the proposed scheme's inability to supply the local load for the whole range of the DC line current, the configuration shown in Fig. 7.21 was studied.

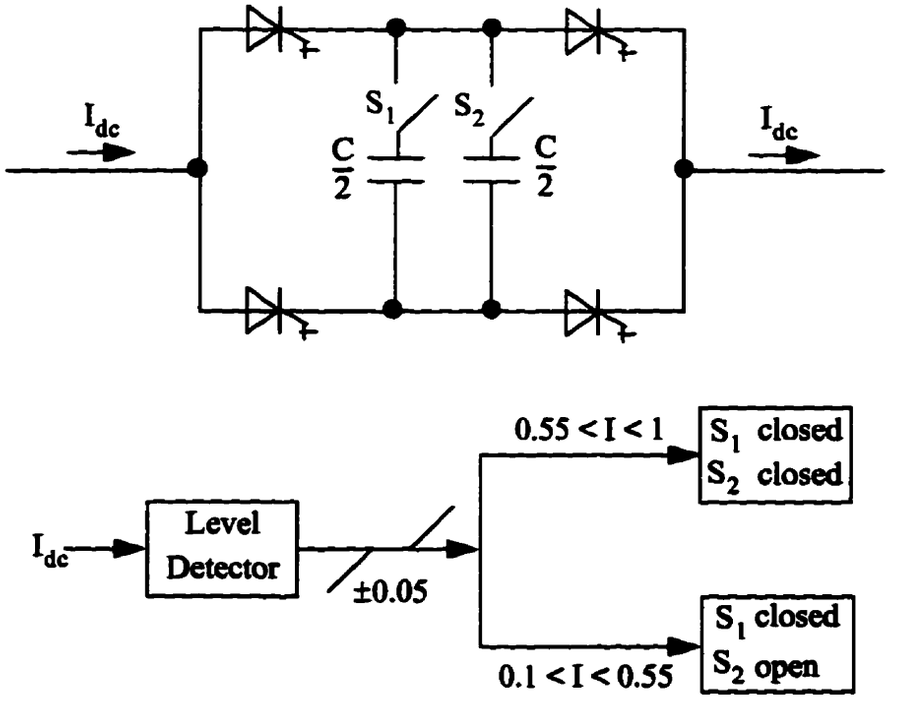

Fig. 7.21 - Multi-step Capacitance and its Controller

The idea is to use the full capacitance at higher levels of the DC current, and reducing the capacitance to 50% at lower currents, where based on equation (3.4) the low capacitance will lead to higher capacitor voltage. The multi-step capacitance is controlled through a controller, in which the DC current fluctuations smaller than 0.05 p.u. are unable to change the capacitance to avoid unnecessary oscillations around the boundary of the two current ranges.

The operation of the system with the multi-step capacitance was digitally simulated. The results, which are not presented here, showed an excessive amount of transients, the result of which is a total collapse of the V_{Tap}, and consequently, a full disruption in the flow of power to the local load (there is no effect on the operation of the main system). To remedy the problem of transients, the number of parallel capacitors were increased to three, each having a value of *C/3*. Still, the transients are much more sever than the tapping scheme can tolerate. An impractical case (from the economic point of view) of six parallel capacitors was also examined, without much improvement.

It is, therefore, concluded that the performance of the tapping station for the whole range of the DC line current, i.e. from 0.1 p.u. to 1.0 p.u., requires further investigation, or perhaps alternative initiatives similar to the unsuccessful multi-step capacitance. However as showed earlier, the tapping station and its control system has no difficulty for smooth transition of current from 0.3 p.u. to 1.0 p.u., or as showed in Section 7.4.4., in the case of a sudden jump in the current level due to a fault.

7.5.2. Varying DC Line Voltage

The power tapped through the proposed scheme, is totally independent of the DC line voltage, because of the current-source nature of the series tap. This means that the tapping

station does not need any information with regard to the DC line voltage set by the main converter stations. This was showed in Section 7.4.4.

Therefore, the requirement of the tapping station's control being totally local has been achieved. The main converters at the two ends of the HVDC line, however, must be able to take into consideration the drop of the DC voltage on the line, while setting the power and current orders at the rectifier end, and the voltage order at the inverter end. This arrangement seems quite possible through the existing control and communication system associated with the HVDC systems, as observed in Section 7.4.

7.6. DC Voltage Harmonic Content

As mentioned in Chapter Five, the imposed DC voltage drop on the HVDC line is rich in non-characteristic harmonics. Voltage harmonics, because of their unwanted effects on the system, including their interference with adjutant communication systems and their role in increasing the system losses, have to be strictly limited. For this reason, tuned and high-pass voltage filters are, as a matter of standard, installed on the DC side of the system.

Although there exists a universally accepted standard for the maximum allowable amount of voltage harmonics in AC systems, i.e. the IEEE Standard 519-1992 which calls for a Total Harmonic Distortion (THD) of less than 5%, such a universally accepted standard for DC systems has yet to be established. Nevertheless, based on the maximum allowable Telephone Interference Factor (TIF), different national standards and/or regulations call for different maximum allowable limits of the DC voltage distortion. These limits are usually around 1% (in the case of New Zealand) to 2% (in the case of Manitoba) of the DC voltage.

The Total Harmonic Distortion, with respect to the DC voltage, due to the first n harmonics

is found from the following relationship:

$$THD = \frac{\sqrt{\sum_{i=1}^{n} V_i^2}}{V_{dc}}, \qquad (7.1)$$

in which V_i is the magnitude of the *i*th harmonic.

Fig. 7.22 shows the absolute value of THD (i.e. the summation of the voltages has not been divided by the DC voltage) for the harmonic spectrum of V_{Tap} at a 0.6 kA DC current and full load (the harmonic spectrum is shown in Fig. 5.18).

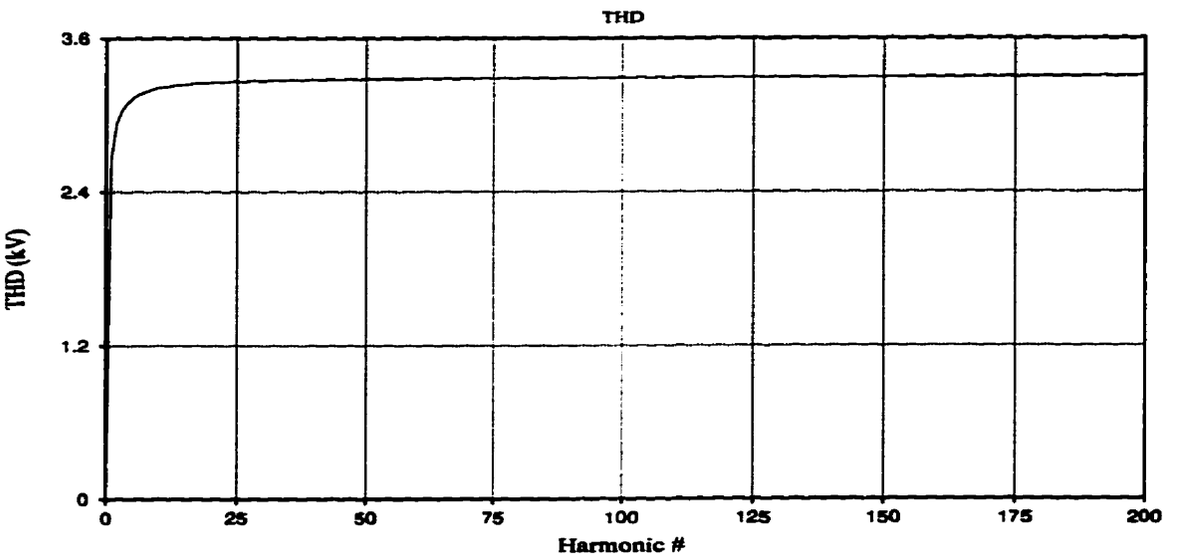

Fig. 7.22 - THD for Idc=0.6 kA

Obviously, the first 7-8 harmonics constitute the bulk of the voltage distortion, and the THD for the first 200 harmonics is equal to 3.28 kV. With a 500 kV DC voltage, this translates to a 0.66% THD which is probably acceptable in most of the conventional HVDC systems.

Fig. 7.23 shows the THD for the harmonic spectrum of V_{Tap} at a 2.0 kA DC current and full load (the harmonic spectrum is shown in Fig. 5.28). Since the DC line current is higher than the previous case, it takes a smaller imposed DC voltage to tap the same amount of

power to the local load, so the THD in this case is equal to 1.53 kV for the first 200 harmonics. This translates to a 0.31% THD on a 500 kV DC line, which seems reasonably small.

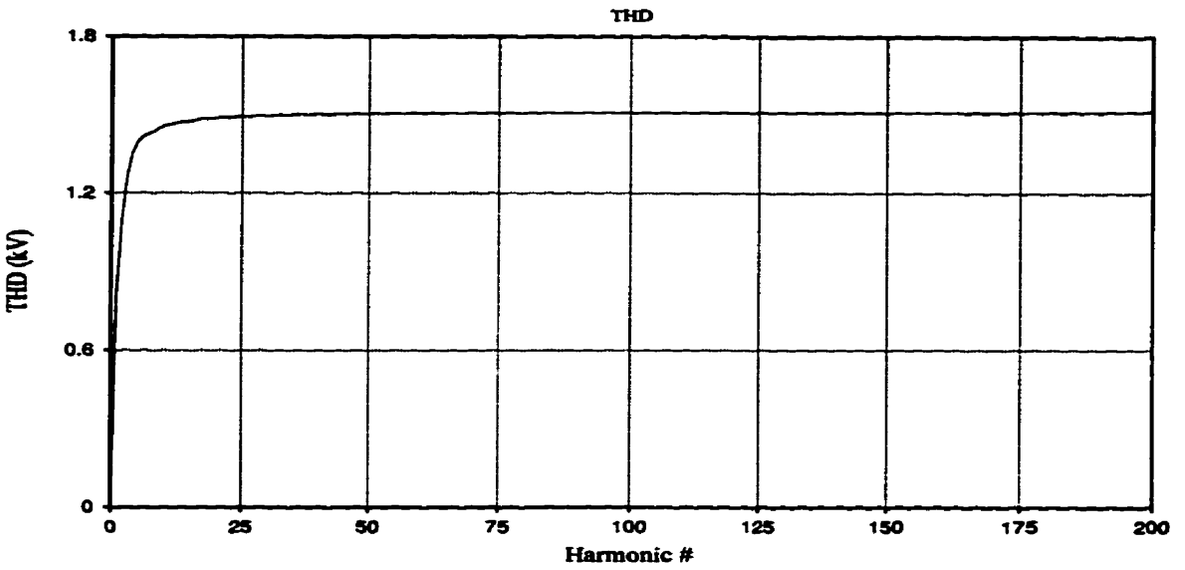

Fig. 7.23 - THD for Idc=2.0 kA

7.7. Additional Considerations Regarding Series and Parallel Taps

In Chapter Two, a brief introduction to the two categories of tapping stations, i.e. series and parallel taps, was presented. It was mentioned that for various reasons, including economical and operational reservations, series taps are most suited for supplying very small loads, while parallel taps seem to be more attractive in the cases where the load to be supplied is larger, and comparable with the main terminals' ratings. References [5] and [13] provide more detailed comparisons in this regard. Having studied different aspects associated with series taps, it is worthwhile to present a comparison between these two categories from two other angles, i.e. reliability and station power losses.

7.7.1. Series vs. Parallel Taps: Reliability

Reference [5] provides adequate information with regard to the issue of reliability assessment for power tapping stations. The authors of reference [5] believe that: "With

advanced converters and controls, small series taps having minimal reliance on communications and actions at the main stations should be possible without undue impact on overall reliability". Different fault analyses performed on the proposed series tap, and presented in the current Chapter, directly verify this assertion. On the other hand, a study done at Ontario Hydro in 1991, and reported by reference [5], which evaluated the reliability of a proposed +/- 500 kV HVDC connection between Manitoba and Ontario in the presence of two small reversible parallel taps showed that the additional taps increased the projected outage frequency of the whole HVDC system by a factor ranging from 1.5 o 1.8. This means that the increase in load meeting capability at the tap terminals is obtained at the expense of an increased frequency of momentary outages at all terminals on the affected pole for isolation of a faulty converter.

It can be argued that the proposed series scheme utilizes three independent converters, each one of which has its own control strategy, while a parallel tap uses only one converter, or in the case of a 12-pulse scheme, two identical converters in series. The larger number of converters in the series tap, according to this argument, means a higher frequency of converter outages/faults, and therefore the reliability seems to be higher for the parallel tap compared with the series tap.

To counter the above argument, two points need to be mentioned. First, two of the converters used in the series tap, i.e. the single-phase diode rectifier and the three-phase voltage-source inverter, have been in use for many years now, and are amongst the most standard power electronic items used. This means a high degree of reliability for these two converters. Secondly, even if the frequency of outage is higher in the series tap, it is safe to say that almost all the outages will only affect the local load, which by nature, is far less significant

than the main HVDC system. On the other hand, the majority of faults in a parallel tap, like commutation failure in the inverter because of high local fault current or because of high DC current diverted through the parallel branch, will interrupt the flow of power in the whole HVDC pole.

To summarize, while the series tap is not able to affect the reliability of the main HVDC system and its malfunction affects only the local load, the parallel alternative presents a far more serious threat to the reliability of the whole system.

7.7.2. Series vs. Parallel Taps: Power Losses

As it was mentioned in Chapter Two, there are cases of isolated loads in need to be connected to the nearby HVDC systems, where all other alternatives, like local generation or AC transmission lines, are much more costly. In such cases, the power losses associated with tapping stations are considered a very small price to pay and are not of an inhibitive magnitude. However, it is worthwhile to have a brief qualitative comparison between the two tapping alternatives with regard to power losses.

Traditionally, the nature of solid state devices used in power electronic applications, and the design of converters are such that the power losses in the converter are of a magnitude of around 2% of the power rating of the converter. To verify the accuracy of the above loss range, consider the single-phase bridge in the proposed scheme which is placed in series with the DC line. If in each branch two GTO thyristors are placed in series, as mentioned in Chapter Six, a total of 8 GTO thyristors will be present in the converter. At the full DC line current, i.e. 2 kA, the average (DC) current passing through each branch is equal to 1 kA. If the on-state voltage drop across the GTO thyristor is assumed to be equal to 2 V [15],

the total power losses in the series converter will be equal to:

$$P_{loss} = 8 \times 2 \times 1 = 16 \text{ kW}.$$

At a local power consumption of 600 kW, the losses amounts to 2.67% of the tapped power. Considering similar percentage of power loss for all the converters used in the series and parallel taps, it seems that the power losses in the series tap are higher than that of a parallel tap with the same power rating, because of the larger number of converters in the series alternative.

The above disadvantage for the series tap, however, is not relevant because it is based on the assumption that for a small load, both series and parallel taps are feasible. In practice, however, it seems that this assumption may not be acceptable, because, again, the cost of a low-power, high-voltage parallel tap, including the three-phase conventional transformer, is far higher than a series tap using an air-core transformer, thus making the power losses comparison irrelevant.

7.8. Summary of the Chapter

In this Chapter, some design, protection and control considerations associated with the proposed tapping station were addressed.

It was shown that the tapping station has no or very little negative impact on the operation of the main HVDC system. The control system required by the tapping station was shown to be independent of the main system's controls. Also, it was shown that the amount of voltage harmonics imposed on the DC line is not of an alarming magnitude. At the end, a comparison between series and parallel taps from the point of view of reliability and losses was presented.

Chapter Eight
Conclusion and Future Work

8.1. Conclusion

The present thesis deals with the issue of small power tapping from HVDC transmission systems.

First, in Chapter One, a brief review of HVDC transmission systems, including its history, principles of operation, its advantages/disadvantages compared to AC systems, and the selection criteria, was presented.

Then, in Chapter Two, the problem of small power tapping from HVDC transmission systems, the two different types of tapping configuration, and the previous work done in this field, was presented. It was shown that the ability to tap small amounts of power, i.e. power levels of between a few hundreds of kW to around 1 MW, from these systems into isolated loads located close to them, will further increase the attractiveness of the HVDC

systems, while providing a better prospect for economic and social development for such communities. The main economic and technical requirements for such tapping stations were also discussed.

In Chapter Three, a practical solution, based on the solid state devices with turn-off capabilities, i.e. GTO thyristors, currently available on the market, was proposed. The expected performance of the proposed scheme, as well as different alternatives for controlling different parts of the tapping station, were also discussed. It was discussed that one possible advantage of the proposed scheme is the use of a single-phase air-core transformer in the scheme. Detailed analysis of the transformer, however, was left for Chapter Six.

In Chapter Four, the proposed scheme along with the first group of possible control regimes, i.e. a controlled single-phase rectifier with the PPWM controller for the three-phase inverter, was simulated by the PSCAD/EMTDC digital simulation software package. The results of the simulation proved the technical feasibility of the proposed scheme, but the control regimes were found to be incapable of providing a reasonably good performance.

In Chapter Five, the proposed scheme along with the second group of possible control regimes, i.e. an un-controlled single-phase rectifier with the SPWM controller for the three-phase inverter, was simulated. The performance of the tapping station has improved, and the flow of power to the local loads for different conditions of the main HVDC system is reasonably satisfactory. It was shown that with a certain mode of control for the series tap, i.e. the variable frequency, ordinary thyristors can replace the GTO thyristors in the series tap.

Chapter Six is devoted to the theoretical analysis and digital simulation of the air-core

transformer. Using the classical electromagnetic theory, first, the relationships for the self- and mutual inductances of the air-core transformer were developed. A small prototype transformer built and studied in laboratory was used to successfully verify the theoretically found relationships. Also, the conventional transformer model in the PSCAD/EMTDC was found to be able to accurately simulate the performance of the air-core transformer. In the next step, the performance of the tapping station in conjunction with an air-core transformer with a diameter of 5 meters was simulated. It was shown that the tapping station is able to tap up to 600 kW from the HVDC system with satisfactory quality. It was however found that the transformer needs to be compensated through series capacitors, which will create voltages larger than what originally was expected across the transformer's windings, and also across the GTO thyristors in the series tap. The voltages, however, do not seem impossible to handle through the design of the air-core transformer, and through the use of two GTO thyristors in series.

The need of series capacitive compensation for the transformer, proves that the variable frequency control regime for the series tap has little practical merit, and the constant frequency regime must be used instead. This eliminates the possibility of using ordinary thyristors in the series tap, however.

The possible biomedical effects of the air-core transformer were also examined and it was shown that the transformer does not present significant health risks outside the HVDC system's right of way.

In Chapter Seven, some design, protection and control considerations associated with the proposed tapping station were addressed. Different possible faults on the single-phase transformer were studied, and it was shown that the tapping station has no or very little negative impact on the operation of the main HVDC system. The control system required

by the tapping station was shown to be independent of the main system's controls.

A proposal to enable the tapping station to operate within the full range of the DC line current, i.e. from 0.1 p.u. to 1.0 p.u., was also studied, but proved to be impractical. Other methods are needed to address this matter.

And finally, it was shown that the amount of voltage harmonics imposed on the DC line is not of an alarming magnitude.

8.2. Future Work

Although the technical feasibility of the proposed scheme was demonstrated through the present study, it is not expected that the electric power industry will implement this scheme, or similar schemes in the near future. This is because of the fact that, traditionally, HVDC systems play a major role in transferring large amounts of power in the electric networks, and any disturbance in these systems can greatly affect the reliability of the whole system, as well as the economical expectations of the utilities. For this reason, the utilities have to be as confident as possible that this kind of tapping schemes present no significant reliability risks to the main system. Besides the theoretical studies similar to the one presented in this work, building small prototype HVDC systems with tapping stations and performing real laboratory tests on them, will help to improve the existing understanding and knowledge about the small power tapping stations.

References

[1] M. A. Laughton and M. G. Say,"*Electrical Engineers' Reference Book*", 14th Edition, Butterworths, England, 1985.

[2] IEEE Transmission and Distribution Committee,"*HVDC Projects Listing*", January 1997.

[3] E. W. Kimbark,"*Direct Current Transmission*", vol. 1, John Wiley & Sons, Inc., 1971.

[4] D. E. Rodger,"*Canada's Remote Communities Seek Energy Efficiency*", Geos, Department of Energy, Mines, and Resources, Canada, Vol. 19, No. 1, pp. 16-22.

[5] IEEE-PES Task Force on Small HVDC Taps,"*Integration of Small Taps into (Existing) HVDC Links*", IEEE Transactions on Power Delivery, Vol. 10, No.3, July 1995, pp. 1699-1706.

[6] Manitoba HVDC Research Centre, "*Survey of Canadian Utilities for Information on the Electrical Supply of Isolated Communities*", Vol. 1, August 1993.

[7] V. Collet Billon, et al,"*From Design to Commissioning Tests of the Third Terminal of the Sardinia-Corsica-Italy HVDC Link*", IEEE Transactions on Power Delivery, Vol. 4, No.1, January 1989, pp. 794-799.

[8] E. Carpaneto, et al.,"*Small Power Tapping From HVDC Transmission Systems*", CIGRE, Proceedings of 31st Conference on High Voltage Electric Systems. Paris, 27 Aug. - 4 Sept. 1986, pp. 1-8.

[9] J. R. R. Ponte, et al,"*Small Series Converter Station Specification and Cost Evaluation*", IEE, Proceedings of 5th International Conference On AC And DC Power Transmission. London, 17-20 Sept. 1991, pp. 132-137.

[10] A. G. G. Lima, et al,"*HVMDC: A New Concept to feed Small Loads*", IEE, Proceedings of 5th International Conference On AC And DC Power Transmission. London, 17-20 Sept. 1991, pp. 120-125.

[11] H. M. Turanli, R. W. Menzies and D. A. Woodford,"*A Forced Commutated Inverter As A SmallTap On A DC Line*", IEEE Transactions on Power Electronics, vol. 4, No. 2, April 1989, pp. 187-193.

[12]J. P. Bowles, H. L. Nakra and B. Turner,"*A Small Series Tap On An HVDC Line*", IEEE, Transactions on Power Apparatus and Systems, vol. PAS-100, No. 2, Feb. 1981, pp. 857-862.

[13]A. Ekstrom and P. Lamell,"*HVDC Tapping Station: Power Tapping From A DC Transmission Line To A Local AC Network*", IEE, Proceedings of 5th International Conference On AC And DC Power Transmission. London, 17-20 Sept. 1991, pp. 126-131.

[14] Z. Zhao and M. R. Iravani,"*Application of GTO Voltage-source Inverter for Tapping HVDC Power*", IEE, Proceedings on Gener. Transm. Distrib., vol. 141, No. 1, January 1994, pp. 1926.

[15]"*GTO Thyristor Applications and Technical Data Book*", First Edition, 1992, Powerex Inc., Hills Street, Youngwood, Pennsylvania 15697.

[16] R. Dudley, A. Sarshar, K. Papp and A. Grisenti,"*Dry-type Air Core Reactors For HVDC Applications*", Proceedings of International Colloquium on HVDC and FACTS, September 18-19, 1995, Montreal, Canada.

[17] M. R. Spiegel, "*Mathematical Handbook of Formulas and Tables*" 32nd printing, Schaum's Outline Series, Mcgraw-Hill Book Company, 1994.

[18]Manitoba HVDC Research Center, *EMTDC User's Manual,* Version 3, 1988.

[19] C. W. Lander, "*Power Electronics*", Third Edition, McGraw-Hill Book Company, 1993.

[20]P. N. Enjeti et al.,"*Programmed PWM Techniques To Eliminate Harmonics: A Critical Evaluation*", IEEE Transactions on Industry Applications, vol. 26, no. 2, March/April 1990, pp. 302-316.

[21] M. Mohaddes, A. M. Gole and P. G. McLaren, "*Hardware Implementation of Neural Network Controlled Optimal PWM Inverter Using TMS320C30 Board*", Proceedings of IEEE's WES-

CANEX'97, June 26-27, 1997, Winnipeg, Manitoba, Canada, pp. 168-173

[22] E. Kreyszig, "*Advanced Engineering Mathematics*", Second Edition, John Wiley and Sons, 1967, pp. 476.

[23] K. Thorborg, "*Power Electronics*", Printice Hall, 1988.

[24] O. I. Elgerd, "*Electric Energy Systems Theory: An Introduction*", Second Edition, McGraw-Hill Book Company, 1983.

[25] C. Schauder et. al., "*TVA STATCON Project: Design, Installation and Commissioning*", CIGRE 1996 Session Papers, Group 14, HVDC Links and AC Power Electronic Equipment, Paper # 14-106.

[26] W. H. Hayt, Jr., *Engineering Electromagnetics*, McGraw-Hill Book Company, Fourth Edition, 1981.

[27] E. L. Carstensen, *Biomedical Effects of Transmission Line Fields*, Elsevier, 1987.

[28] M. Szechtman, et. al., "*First Benchmark Model for HVDC Control Studies*", Electra, Vol. 135, April 1991, pp. 55-73.

[29] O. B. Nayak, "*Dynamic Performance of Static and Synchronous Compensators at an Inverter Bus in a Very Weak AC System*", Ph.D. Thesis, University of Manitoba, 1993.